UNIVERSITEIT VAN PRETORIA
UNIVERSITY OF PRETORIA
YUNIBESITHI YA PRETORIA

THE INFLUENCE OF A MULTIPLE TUBE INLET CONDITION ON FULLY-DEVELOPED FRICTION FACTORS IN THE TRANSITIONAL FLOW REGIME.

By
Martin Joubert

Submitted in partial fulfilment of the requirements for a degree of

Master of Engineering

Department of Mechanical and Aeronautical Engineering
University of Pretoria
South Africa

ABSTRACT

THE INFLUENCE OF A MULTIPLE TUBE INLET CONDITION ON FULLY-DEVELOPED FRICTION FACTORS IN THE TRANSITIONAL FLOW REGIME

Author: Martin Joubert

Supervisor: Prof J.P. Meyer

Department: Mechanical and Aeronautical Engineering

Degree: Master of Engineering (Mechanical Engineering)

Concentrated solar power systems, such as parabolic trough heat exchangers, are being used more frequently in the energy sector. Engineers require accurate design information to optimise the effectiveness of these heat exchangers. Recent studies have shown that the transitional flow regime could potentially be the optimum region of operation, as it provides the best possible compromise between high heat transfer and low pressure drop. However, designers often choose to avoid the transitional flow region entirely, to evade the various uncertainties associated with this flow regime. Avoiding the transitional flow regime is not always possible, as changes in operating conditions, design constraints, and various heat transfer augmentation methods often result in the heat exchanger operating in the transitional flow regime. Although some research has been conducted on the effect of different inlet configurations on the pressure drop characteristics in the transitional flow regime, most of the work focused on single tubes, whereas the bulk of the heat exchangers available in industry would typically have bundles of tubes. The aim of this investigation is to experimentally obtain fully-developed pressure drop characteristics in the transitional flow regime, for different tube pitch ratios, under isothermal and diabatic conditions. An experimental setup was designed and built to house three tubes, spaced apart at different pitch ratios. A single tube heat exchanger was used for validation purposes, since reliable pressure drop correlations are readily available in various published journals. The multi-tube test section consisted of smooth stainless steel tubes, each with an inner diameter and length of 4 mm and 6 m, respectively. The study was performed for Reynolds numbers ranging from 1 000 to 7 000, at heat fluxes of 2 kW/m^2, 3 kW/m^2, and 4 kW/m^2, respectively. Transition effects were investigated for two tube pitch ratios, namely 1.25 and 1.5, based on the outer diameter of the tubes. It can be concluded that the presence of adjacent tubes had a significant effect under isothermal conditions, causing delayed and more abrupt transition from laminar to turbulent flow. This effect was more significant for the pitch spacing of 1.25 than for the pitch of 1.5. However, the disturbance caused at the inlet due to the presence of adjacent tubes seems to be damped out by buoyancy induced secondary flow effects with the addition of heat. This dampening effect becomes more significant for increasing heat fluxes.

Acknowledgements

The author would like to acknowledge to following people for their contributions to this project:

- Professor J.P. Meyer, for his role as supervisor, and whose comprehensive past research in the transitional flow regime helped make this project a success.
- Mr. Danie Gouws, for his technical advice and support throughout the manufacturing, and testing phases of the project.
- Mr. Matthew Pallent, fellow postgraduate student and researcher, whose support and technical ability proved to be invaluable throughout the entire project.
- Ms. M. Everts, for offering moral support and guidance, and placing her vast experience in research into the transitional flow regime at the authors disposal.
- Professor P.S. Els, whose technical advice and encouragement towards lateral thinking continues to inspire young engineering students at the University of Pretoria.
- Ms. Tersia Evans, for her role in the support and coordination of all postgraduate research students in the Clean Energy Research Group at the University of Pretoria.
- Mr R. Joubert and Mrs. H.M Joubert, for being supportive parents and for providing motivation to pursue my passion for the technical world.

Table of Contents

List of figures

List of tables

Nomenclature

Symbol	Description	Units
A	Area	m^2
C_p	Constant pressure specific heat	$J/kg.K$
D	Diameter	m
f	Darcy friction factor	
Gr	Grashof number	
Gz	Graetz number	
g	Gravitational acceleration	m/s^2
h	Heat transfer coefficient	W/m^2
k	Thermal conductivity	$W/m.K$
L	Length	M
$\dot{m}$	Mass flow rate	kg/s
m	Parameter used in correlations	
Nu	Nusselt number	
Pr	Prandtl number	
P	Pressure	Pa
R	Radius	m
Ra	Rayleigh number	
Re	Reynolds number	
T	Temperature	°C or K
V	Flow velocity	m/s

Greek letters

Symbol	Description	Units
α	Thermal diffusivity	m^2/s
β	Volume expansion	1/K
δ_t	Thermal boundary layer thickness	m
δ_h	Velocity boundary layer thickness	m
ρ	Density	kg/m^3
μ	Dynamic viscosity	$kg/m.s$
v	Kinematic viscosity	m^2/s
τ	Shear stress	Pa

Subscripts

Symbol	Description
b	Bulk
c	Critical
f	Fluid
h	Hydrodynamic
t	Thermal
w	Surface/wall
x	Local

Chapter 1: Introduction

1.1 Background

The vast energy demands of the planet, with a human population upwards of 7 billion, and the waning supply of fossil fuels resulted in the exploration of various sustainable alternative sources of energy. The parabolic trough concentrated solar power (CSP) system, an example of a system that is being used more extensively in the energy sector, is used to produce useful heat or electricity in a sustainable manner. The study and design of these heat exchangers require extensive knowledge of convective heat transfer characteristics, so that the overall effectiveness of these systems can be optimised.

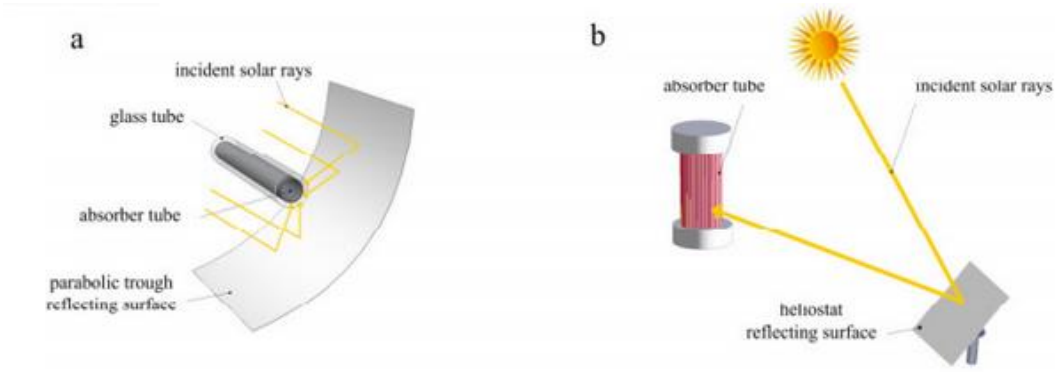

Figure 1: Schematic of two common types of concentrated solar dish systems (Chang, 2014). (a) Parabolic through collector. (b) Solar power tower system

When designing heat exchangers, engineers are forced to choose between the laminar and turbulent flow regime. Heat exchangers that operate in the laminar flow regime have low pressure drops and therefore require less pumping power to maintain flow, but unfortunately, the heat transfer coefficients associated with this flow regime are also quite low. Conversely, heat exchangers that operate in the turbulent flow regime have significantly higher heat transfer coefficients, at the cost of larger friction factors and therefore greater pumping power requirements and higher operational costs. It is therefore evident that the choice of flow regime will potentially have significant implications on the overall effectiveness of the heat exchanger.

A good design of heat exchangers should include considerations about how to increase the heat transfer coefficient and reduce the pressure drop simultaneously (Shokouhmand and Salimpour, 2007). Consequently, the transitional flow region, found between the laminar and turbulent regime, could potentially be the preferred choice of flow region, as it provides the best compromise between high heat transfer and low pressure drop (Meyer, 2014). Designers are, however, advised to avoid the transitional flow region entirely, to try and escape the various uncertainties and instabilities associated with this flow regime.

In an attempt to enhance the heat transferred to the fluid used in the receiver tube of the parabolic trough, different types of enhancement techniques are implemented, such as finned tubes, twisted tape mixers, or roughened inner tube surfaces. The resulting increase in pressure drop, caused by these augmentation devices, is corrected by reducing the mass flow rate in the

tubes, leading to the heat exchangers operating close to or in the transitional flow regime. Other factors, such as changes in operating conditions and various design constraints could also result in the flow moving into the transitional flow regime (Meyer and Olivier, 2014).

Osborne Reynolds introduced the concept of separate flow regimes as early as 1883. By injecting liquid dye into a stream of water flowing in a glass tube, he was able to distinguish between two different flow regimes he called “direct” and “sinuous”. These two regimes, later called laminar and turbulent flow, were investigated extensively in the following century. Laminar flow exists when the Reynolds number is less than 2 300, and flow is said to be fully turbulent when the Reynolds number exceeds 10 000 (ASHRAE, 2009). However, in most cases, flow is found to be fully turbulent at Reynolds numbers larger than 4 000 (Cengel and Ghajar, 2011).

Until fairly recently, no work has been done on the transitional region of flow that exists between the laminar and turbulent flow regimes. This transition from laminar to turbulent flow occurs at a Reynolds number of 2 300 for a smooth, horizontal tube with a rounded entrance (ASHRAE, 2009). However, the Reynolds number at which transition occurs also depends on surrounding disturbances, of which many are found in heat exchangers.

The behaviour of flow in the transitional flow region has been subject to investigation by mainly two research groups. These research groups are headed by Professor Afshin Ghajar from Oklahoma State University, and Professor Josua Meyer from the University of Pretoria, respectively.

Ghajar and his co-workers were the first to investigate the effects of disturbance caused by different inlet geometries on the heat transfer and pressure drop characteristics in the transitional flow regime. Their investigations, conducted for different ethylene-glycol and water mixtures, focused on fully developed flow in single tube heat exchangers.

The isothermal friction factors obtained from an isothermal investigation, conducted by Ghajar and Madon (1992), revealed that transition from laminar to turbulent flow was dependent on the inlet configuration, with smoother inlets causing a delay in transition.

A study, performed by Tam and Ghajar (1997), showed that diabatic friction factors in the laminar and transitional regime were higher than isothermal friction factors, due to the effects of secondary flow. The friction factors in the turbulent flow regime were found to remain unaffected by the addition of heat or changes in inlet configuration. Uniform heating proved to have a calming effect on the flow, resulting in transition being delayed for an increase in heat flux.

Tam *et al.* (2012) conducted an investigation into developing, and fully-developed, diabatic, and isothermal friction factors in the transitional flow regime. The authors developed correlations based on experimental data that could be used to predict pressure drop characteristics in the transitional flow regime.

A study of the influence of different inlet configurations on heat transfer characteristics, conducted by Ghajar and Tam (1994), confirmed that the onset of transition was influenced by inlet disturbances, with transition occurring first for the inlet that caused the most disturbance. The measured laminar heat transfer coefficients, which was much higher than the predicted theoretical values due to the effect of secondary flow, increased for an increase in heat flux.

The experiments conducted by Meyer and Olivier (2011) used the constant surface boundary condition to investigate the transitional flow regime. With water as a test fluid, the authors investigated the effect of different inlet configurations on transition in smooth, and enhanced tubes. The study confirmed that transition is independent of inlet disturbance, when heat is applied to the test section.

Meyer *et al.* (2013) investigated the effect of multi-walled carbon nanotubes, usually added to a fluid in an attempt to increase thermal conductivity and therefore augment heat transfer, on the Nusselt numbers and friction factors in the transitional flow regime. It was found that transition occurred earlier for increasing volume concentrations of multi-walled carbon nanotubes. Pressure drop measurements indicated that fluid viscosity increased by four times the amount of increase in thermal conductivity with the addition of these nanoparticles, which led to a significant increase in friction factor.

Ghajar and co-workers, as well as Meyer and co-workers investigated the effect of inlet configuration on pressure drop and heat transfer characteristics in the transitional flow regime. However, the studies were limited to single-tube heat exchangers only, whereas many heat exchangers used in industry typically have bundles of tubes. The effect of the pitch spacing of these tube bundles on pressure drop characteristics in the transitional flow regime has not been investigated.

1.2 The significance of tube pitch ratios

Concentrated solar power systems, such as parabolic trough heat exchangers, make use of shell-and-tube heat exchangers to produce steam. These heat exchangers consist of bundles of tubes joined together at the ends by tubesheets. These tubes are often spaced closely together to reduce the overall size of the heat exchanger, meaning adjacent tubes could potentially influence the flow field at the inlet of a specific tube. This could therefore influence the transitional isothermal and diabatic pressure drop characteristics of the tubes.

1.3 Problem statement

A fair amount of research has been conducted to investigate convective flow characteristics in the transitional flow regime. These investigations were mainly focused on the effect of different inlet geometries on single-tube heat exchangers. However, the effect of the pitch spacing of multi-tube heat exchangers on pressure drop characteristics in the transitional flow regime has not yet been investigated.

1.4 Aim

The purpose of this study was to determine the influence of the tube pitch of a multi-tube heat exchanger, consisting of three tubes, on fully-developed isothermal, and diabatic pressure drop characteristics in the transitional flow regime.

1.5 Objectives

The objectives of the investigation were:

- to build a calming section capable of serving as a square edge inlet for both the single- and multi-tube setup
- to modify an experimental setup to house both a single- and a multi-tube test section.
- to validate the experimental setup by comparing the results of a single-tube heat exchanger to correlations available in literature.
- to take pressure drop measurements over the fully-developed portion of a multi-tube heat exchanger, for a range of Reynolds numbers varying from 1 000 to 7 000.
- to investigate the effect of tube pitch on the start, end, and gradient of transition of isothermal and diabatic friction factors.

1.6 Scope of work

The purpose of this investigation was to determine the effect of tube pitch ratios on isothermal and diabatic friction factors, for Reynolds numbers ranging from approximately 1 000 to 7 000. This ensures that the entire transitional region is captured, as well as significant portions of the laminar and turbulent flow regimes. The multi-tube test section consisted of three smooth stainless steel circular tubes, with an inner diameter and length of 4 mm and 6 m, respectively. The effects of the two pitch ratios, equal to 1.25 and 1.5 times the tube outer diameter, were investigated whilst being heated at constant heat fluxes of 2 kW/m^2, 3 kW/m^2, and 4 kW/m^2. Water, with Prandtl numbers ranging from approximately 3 to 7, was used as the test fluid. The test section was connected to a modified experimental setup, used during previous transitional flow experiments.

1.7 Content of report

In Chapter 2, a literature survey is presented on the fundamental aspects relevant to convective heat transfer. Previous work conducted on the transitional flow regime, by Professor Ghajar and co-workers from the Oklahoma State University, and Professor Meyer and co-workers from the University of Pretoria, is also presented in this chapter. Chapter 3 contains details on the design of the experimental setup and the results of the uncertainty analysis. Chapter 4 covers the methods used to validate the experimental setup. Chapter 5 and 6 presents the isothermal and diabatic friction factor results, respectively, obtained from the experimental investigation. Chapter 7 summarises and concludes all the work presented in this document, whilst also providing some recommendations for possible future work.

Chapter 2:
Literature study

2.1 Introduction

This chapter aims to give an overview of some of the most indispensable concepts related to convective heat transfer and pressure drop in smooth tubes. Previous investigations into convective heat transfer in the transitional flow regime is also summarized in this chapter, as it lays the foundation for any future work to be performed.

2.2 Non-dimensional parameters

Dimensional analysis is often used to reduce the number and complexity of variables used to describe physical problems in engineering. This technique involves combining variables into groups of dimensionless numbers, which greatly reduces the number of experiments or simulations required to investigate the relationship between these individual variables. Some of the most common non-dimensional parameters used in convective flow problems are presented in this section.

2.2.1 Reynolds number

In 1883, Osborne Reynolds showed that transition between laminar and turbulent flow depends on surrounding disturbances such as surface roughness, surface geometry, flow velocity, surface temperature and the type of fluid (Cengel and Ghajar, 2011). He demonstrated that the flow regime depends mainly on the ratio of inertia ($\rho V^2/D$) and viscous ($\mu V/D^2$) forces. The Reynolds number, derived in order to quantify this ratio, is defined as follows (White, 2011):

$$Re = \frac{Inertia\ forces}{Viscous\ forces} = \frac{\rho V^2}{\mu\left(\frac{V}{D}\right)} = \frac{\rho VD}{\mu} \tag{2.1}$$

At low Reynolds numbers, characteristic of the laminar flow regime, viscous forces succeed in damping out random fluctuations in the fluid. However, at the higher Reynolds numbers associated with turbulent flow, inertial forces are much larger when compared to viscous forces, and thus cannot prevent the rapid fluctuations in the fluid.

2.2.2 Nusselt number

Convection is usually the dominant heat transfer mechanism in fluids, however, in some cases conduction can become significant. The Nusselt number, first introduced by German engineer Wilhelm Nusselt, is a dimensionless heat transfer coefficient that represents the ratio between the convective and conductive heat transfer mechanisms (Cengel and Ghajar, 2011). The Nusselt number, which represents the enhancement of heat transfer through a fluid due to fluid motion, would therefore be equal to one for the case of pure conductive heat transfer. The Nusselt number is defined as follows:

$$Nu = \frac{Convective\ heat\ transfer}{Conductive\ heat\ transfer} = \frac{hD}{k} \tag{2.2}$$

2.2.3 Prandtl number

The Prandtl number was first introduced by the German Physicist Ludwig Prandtl, who made significant contributions to boundary layer theory in the early 1900's. It describes the relative ability of a fluid to transport momentum and energy (Nellis and Sanford, 2009). The Prandtl number is defined as:

$$Pr = \frac{Molecular\ diffusivity\ of\ momentum}{Molecular\ diffusivity\ of\ heat} = \frac{\mu C_p}{k} = \frac{v}{\alpha} \tag{2.3}$$

Gasses, with Prandtl numbers of approximately 0.7, dissipate heat and momentum at the same rate and thus the thickness of the thermal and velocity boundary layers are the same. Fluids with small Prandtl numbers ($Pr \ll 1$), such as liquid metals, are highly conductive but inviscid. Consequently, heat diffuses more rapidly than momentum, resulting in the thermal boundary layer being much thicker than the velocity boundary layer. Fluids with large Prandtl numbers ($Pr \gg 1$), such as engine oil, are viscous and non-conductive. Such a fluid will transport momentum very well but not thermal energy, resulting in the velocity boundary layer being much greater than the thermal boundary layer.

2.2.4 Grashof number

The effect of natural convection can be quantified by the Grashof number, which represents the ratio of buoyancy forces to viscous forces acting on the fluid. The Grashof number provides the main criterion for determining the flow regime in natural convection (Cengel and Ghajar, 2011). The Grashof number is defined as:

$$Gr = \frac{g\beta(T_w - T_b)D^3}{v^2} \tag{2.4}$$

For natural convection, the square root of the Grashof number is analogous to the Reynolds number for forced convection (Nellis and Sanford, 2009). When natural and forced convection are present, the relative importance of each mode of heat transfer is determined by the value of the coefficient Gr/Re^2. When the value of this coefficient is much greater than unity ($Gr/Re^2 \gg 1$), inertia forces are negligible and natural convection effects dominate. Conversely, if the coefficient is much smaller than unity ($Gr/Re^2 \ll 1$), buoyancy forces are negligible and forced convection must be considered. In some cases, inertia and buoyancy forces are equally significant, resulting in the coefficient being approximately one ($Gr/Re^2 \approx 1$). In this case, commonly referred to as mixed convection, both natural and forced convection must be considered.

2.2.5 Rayleigh number

Buoyancy driven natural convection can become significant when heat is applied to a tube. In these cases, both natural and forced convection must be considered. The Rayleigh number, which is a product of the Grashof number and the Prandtl number, can be used as a criterion for determining whether the flow is dominated by mixed or forced convection.

$$Ra = GrPr = \frac{g\beta(T_w - T_b)D^3}{v^2} Pr = \frac{g\beta(T_w - T_b)D^3}{v\alpha} \tag{2.5}$$

2.2.6 Friction factor

Pressure drop is a quantity of significant importance when analysing tube flow, since it is directly related to the power requirements of the equipment used to maintain flow. The pressure drop occurs due to viscous effects and is considered to be an irreversible loss (Cengel and Ghajar, 2011).

$$\Delta P = f\frac{L}{D}\frac{\rho V^2}{2} \tag{2.6}$$

The Darcy friction factor, named after Henry Darcy, is used in the description of friction losses in pipe flow and can be defined as follows:

$$f = \frac{8\tau_w}{\rho V^2} \tag{2.7}$$

2.3 Classification of fluid flows

The concept of different flow regimes was first introduced by Osborne Reynolds in 1883. In his experiments with liquid dye, Reynolds was able to distinguish between two flow regimes, which he called “direct” and “sinuous”. These two flow regimes, later called laminar and turbulent flow, were studied extensively in the 19th and 20th century, resulting in many correlations for predicting heat transfer and pressure drop characteristics for flow in these regimes.

2.3.1 Laminar flow

Reynolds showed that a viscous fluid flowing at low velocities tends to move in a highly ordered and predictable fashion. This region, in which fluid flows in smooth layers, is known as the laminar flow regime. Heat exchangers that operate in the laminar flow regime have low pressure drops and therefore require less pumping power to maintain flow, but unfortunately, the heat transfer coefficients associated with this flow regime are also quite low

2.3.2 Turbulent flow

The liquid dye experiments performed in 1883 revealed that when the flow rate is increased beyond a critical point, various fluctuations in velocity can be observed. In this region, where flow behaviour tends to be more chaotic, is known as the turbulent flow regime. Heat exchangers that operate in the turbulent flow regime have significantly higher heat transfer coefficients, at the cost of larger friction factors and therefore greater pumping power requirements and higher operational costs.

2.3.3 Transitional flow

A third flow regime exists between the laminar and turbulent regimes. The transition from laminar to turbulent flow occurs gradually as flow starts to fluctuate between fully laminar and fully turbulent behaviour. This transition depends on various surrounding disturbances such as inlet configurations and surface roughness (Cengel and Ghajar, 2011). Only a few correlations are available in literature for predicting heat transfer and pressure drop

characteristics in the transitional flow regime. A summary of the work done in this flow regime is presented in Section 2.8.3 and Section 2.8.4.

2.4 Heat transfer fundamentals

The fundamentals of convective heat transfer relevant to this study and its underlying flow effects are presented in this section.

2.4.1 Thermal boundary conditions

There are different methods in which heat is transferred to the tubes of a heat exchanger. For this report, the uniform heat flux and uniform wall temperature boundary conditions will be studied carefully.

2.4.1.1 Uniform heat flux

The uniform heat flux boundary condition, shown in Figure 2a, is typically applied when heating wire is coiled around the perimeter of a tube, or in the case of a tube-in-tube heat exchanger with a low heat transfer coefficient (Cengel and Ghajar, 2011). For this thermal boundary condition, the bulk fluid temperature increases linearly along the length of the tube in the fully developed flow region.

2.4.1.2 Uniform wall temperature

The uniform wall temperature boundary condition, shown in Figure 2b, occurs as a tube is heated along its length by an isothermally condensing fluid, as is commonly found in the boilers used in power generation. This brings about a tube wall temperature that remains approximately constant along the entire length of the tube.

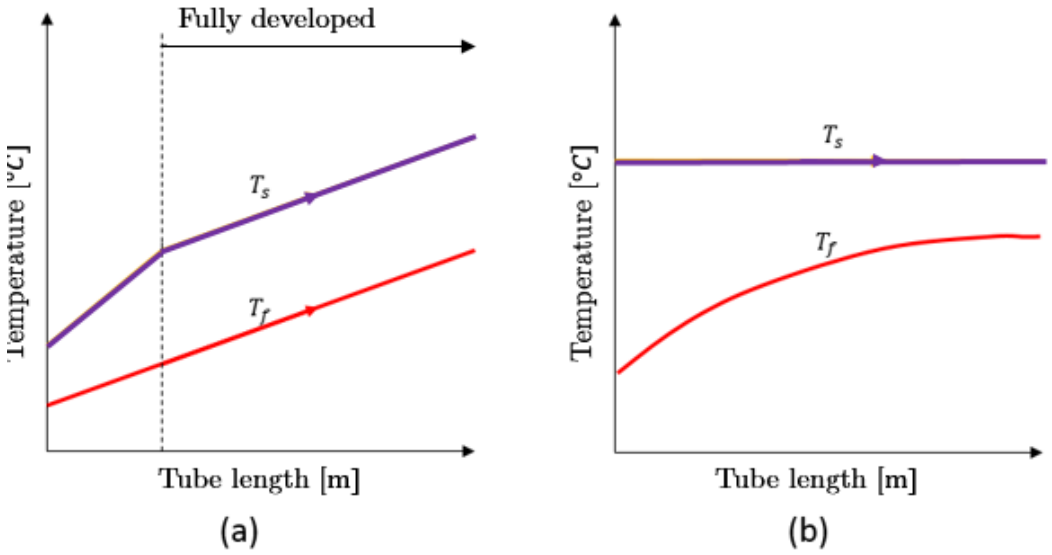

Figure 2: Temperature along the length of the tube: (a) The case of constant heat flux. (b) The case of constant wall temperature.

2.4.2 Secondary flow effects

In the case of internal convective heat transfer, a temperature gradient appears between the fluid adjacent to a heated tube wall and the fluid at the centre of a tube. This results in a higher fluid density at the centre of the tube than at the tube wall. This difference in density forces the fluid at the centre to circulate downwards, whilst the fluid at the wall circulates upwards, as shown in Figure 3.

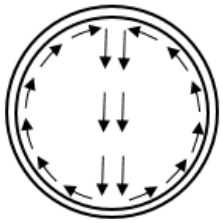

Figure 3: Secondary flow within the tube cross section.

This secondary flow, caused by natural convection, occurs along the entire length of the heat exchanger for a case of uniform heat transfer, because the temperature gradient between the wall and fluid exists throughout the length of the tube.

For the uniform wall temperature boundary condition, the secondary flow diminishes along the length of the tube, as the temperature gradient between the wall and fluid reduces. The convective heat transfer coefficient in a strong function of velocity. Consequently, heat transfer due to forced convection is usually significantly higher, compared to natural convection. Thus, natural convection is often neglected in convection heat transfer analyses. However, the error associated with making this assumption led to the implementation of the coefficient Gr/Re^2, which is used to determine the importance of natural convection in forced convection analyses. The ranges for specific convective heat transfer regimes is summarized in Table 1

Range	Flow regime
$\frac{Gr}{Re^2} < 0.1$	Forced convection negligible
$0.1 < \frac{Gr}{Re^2} < 10$	Mixed convection
$\frac{Gr}{Re^2} > 10$	Natural convection negligible

Table 1: Ranges for specific convective heat transfer regimes.

2.5 The entrance region

As shown in Figure 4 and Figure 5, the velocity and temperature profiles of a fluid flowing through a tube develops through various stages from the entrance region to the fully-developed

flow region. This section briefly summarises flow development, as experienced by a fluid flowing in a circular tube.

2.5.1 Thermal entry region

Consider a fluid, at a uniform temperature, entering a tube being heated or cooled. The resulting temperature gradient leads to the transfer of heat in the radial direction, between the tube wall and the adjacent fluid particles. Consequently, fluid at the tube wall and fluid at the tube centre will be at different temperatures, leading to the formation of a thermal boundary layer. The thickness of the thermal boundary layer increases along the tube length, in the direction of flow, until it reaches the centre of the tube. At this distance, thermally fully developed flow is achieved when the temperature profile has the same shape along the direction of flow. This distance, defined as the thermal entrance length, is calculated differently for laminar $(\delta_{t,laminar})$ and turbulent flow $(\delta_{t,turbulent})$, and is given by (Cengel and Ghajar, 2011):

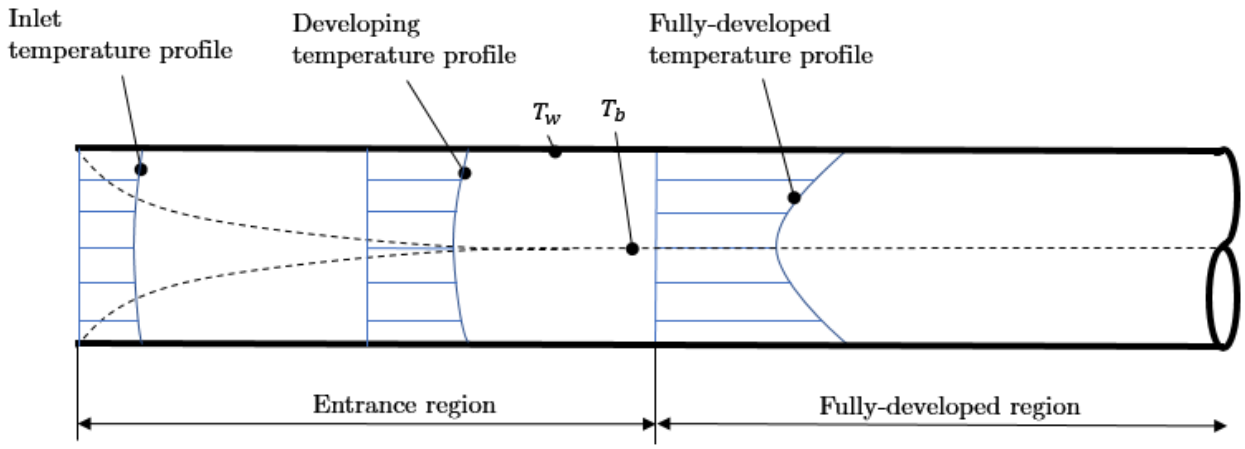

Figure 4: Thermal entry region.

$$\delta_{t,laminar} = 0.05RePrD \tag{2.10}$$

$$L_{t,turbulent} \approx 10D \tag{2.11}$$

2.5.2 Hydrodynamic entry region

When a fluid enters a tube at a uniform flow velocity, the fluid particles in contact with the tube wall comes to a complete stop, due to the no-slip condition. Due to the viscosity of the fluid, this layer in contact with the tube wall will start curbing the motion of the adjacent layers of fluid, thereby slowing them down gradually. The resulting velocity gradient leads to the formation of a viscous boundary layer, which grows along the length of the tube, until it reaches the centre and fills the entire tube. The distance from the entrance to the point where the boundary layer covers the entire tube is known as the hydrodynamic entry length, which is given by (Cengel and Ghajar, 2011):

$$\delta_{h,laminar} = 0.05ReD \tag{2.12}$$

$$L_{h,turbulent} \approx 10D \tag{2.13}$$

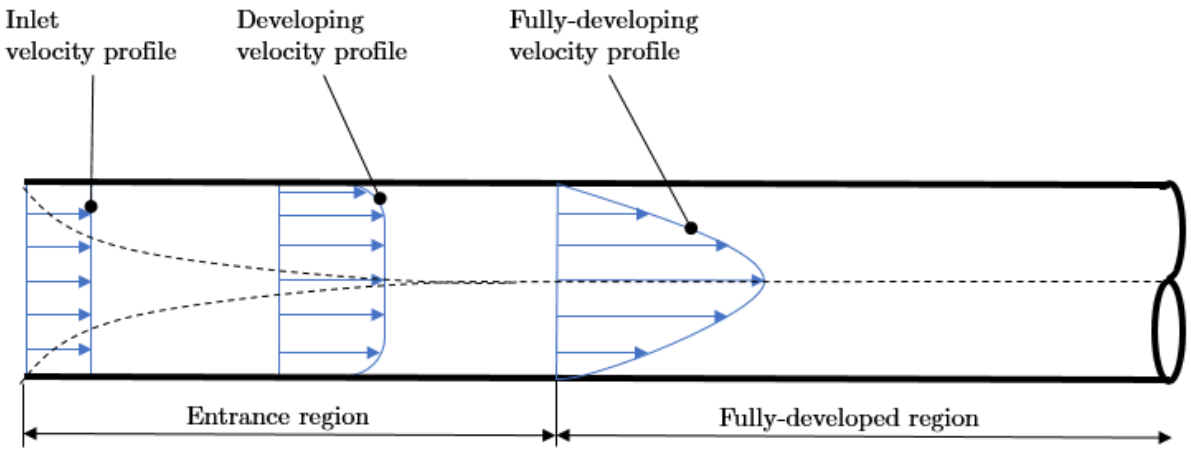

Figure 5: Hydrodynamic entry region.

2.6 Types of inlets

Transition from laminar to turbulent flow depends on surrounding disturbances (Meyer and Olivier, 2010). Certain types of inlets might typically cause such disturbances as the flow enters the tube. Four types of inlets were used in previous investigations, shown in Figure 6.

2.6.1 Square-edged inlet

This inlet, characterised by a sudden contraction in flow due to an abrupt change in cross sectional area, is often encountered in shell-and-tube heat exchangers.

2.6.2 Re-entrant inlet

This configuration is very similar to the square-edged inlet, as it also causes a sudden contraction in flow, however, the tube is extended approximately one tube diameter into the head of the inlet distributer. These inlets are often used to simulate the floating header of the shell-and-tube heat exchanger.

2.6.3 Bellmouth inlet

The bellmouth inlet is characterised by a smooth change in cross-sectional are and adopts a profile similar to the shape of a bell.

2.6.4 Hydrodynamically fully developed inlet

The fully developed inlet consists of a tube with the same diameter as the test section. This inlet ensures that a fully developed velocity profile is obtained at the entrance of the test section, since no change in cross-sectional area occurs.

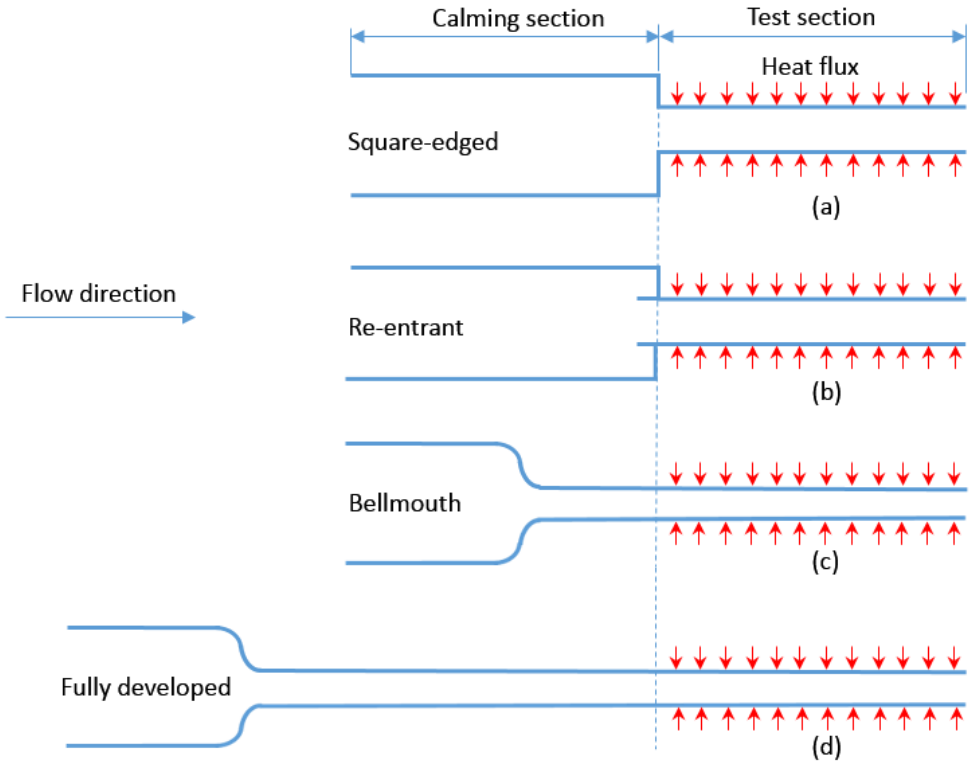

Figure 6: Schematic of the various inlet geometries used in the experimental work of Meyer and Olivier(2010): (a) Square-edged, (b) Re-entrant, (c) Bellmouth, (d) Fully developed inlet.

2.7 Shell-and-tube heat exchangers

The shell-and-tube heat exchanger is perhaps the most common heat exchanger found in the power generation industry, and are frequently used as direct steam generators in CSP systems. This exchanger consists of a bundle of round tubes, mounted in a cylindrical shell with a tube axis parallel to that shell (Sekulic and Shah, 2003). The tube bundles are held in place by header plates, often called tube sheets. The fluid on the tube-side of the heat exchanger never comes into direct contact with the fluid on the shell-side, and relies on heat transfer through the tube walls. Shell-and-tube heat exchanger design is usually split into shell-side design, and tube-side design. This document focuses specifically on the tube-side design of shell-and-tube heat exchangers.

Shell-and-tube heat exchangers are classified and constructed in accordance with the widely used Tubular Exchanger Manufacturers Association standards (TEMA, 1999). The design of shell-and-tube heat exchangers on the tube side involves the selection of tube sizes, the configuration in which the tubes are connected, and the spacing between adjacent tubes. Tube sheets, that hold together the bundles of tubes at the ends, must be designed to match the chosen tube configuration. The two most common tube-pitch configurations found in shell-and-tube heat exchangers are square, and triangular, as shown in Figure 7:

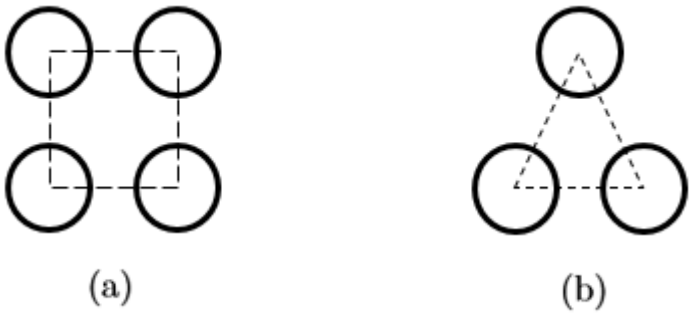

Figure 7: Schematic of different tube pitch configurations found in shell-and-tube heat exchangers.

The selecting of tube pitch, or spacing between adjacent tubes, are often seen as a trade-off between a close pitch for increased shell-side heat transfer and a more compact heat exchanger, and an open pitch for decreased shell-side "plugging" and ease of shell-side cleaning. To prevent leakage of the shell fluid at the tubesheet through a clearance between the tube hole and tube, the tube-to-tubesheet joints are made by the conventional rolling process (Sekulic and Shah, 2003), is shown in Figure 8:

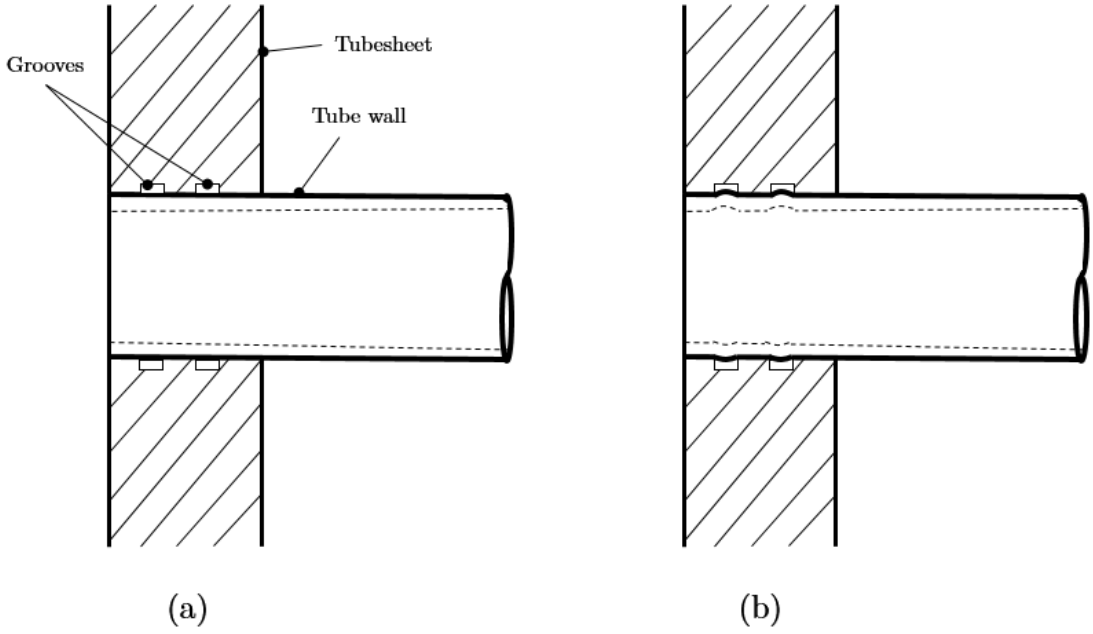

Figure 8: Schematic of a leak-free rolled joint between the tube and tube hole of a tubesheet. (a) before tube expansion. (b) after tube expansion

The tube pitch is usually specified as a value time the outer diameter of the tubes. The minimum tube pitch is restricted to 1.25, because the tubesheet may become too weak for proper rolling of the tubes, illustrated in Figure 8, which may result in leaky joints. Smaller pitch ratios are more difficult to clean mechanically, which leads to scale build up. The maximum tube pitch is usually not restricted to any specific value, however, larger tube pitch ratios do not offer any advantage other than easy mechanical cleaning, and increases the overall size of the heat exchangers. For this reason, the majority of heat exchangers have tube pitches ranging from 1.25 to 1.5 (Sekulic and Shah, 2003).

2.8 Previous work

The behaviour of flow in the transitional flow region has been subject to investigation by mainly two research groups. These research groups are headed by Professor Afshin Ghajar from Oklahoma State University, and Professor Josua Meyer from the University of Pretoria, respectively.

2.8.1 Pressure drop correlations

Table 2 presents some of the correlations for determining Darcy friction factors for flow in smooth tubes, where the pipe's surface roughness has no effect and the relative roughness is considered negligible ($\frac{\varepsilon}{D}$=0). This section is not intended as summary all the correlations

Author(s)	Proposed correlation	Flow condition
Isothermal friction factor		
Poiseuille (1840)	$f = \frac{64}{Re}$	Laminar fully-developed flow
Churchill (1977)	$\frac{2}{f} = 4\left(\frac{1}{[(8/Re)^{10} + (Re/36500)^{20}]^{1/2}} + [2.21 \times \ln(Re/7)]\right)^{1/5}$	Laminar, transitional, and turbulent fully-developed flow
Hrycak and Andruskiw (1974)	$f = 4(-3.1 \times 10^{-3} + 7.125 \times 10^{-6}Re - 9.7 \times 10^{-10}Re^2)$	Transitional fully-developed flow
Ghajar and Madon (1992)	$f = 4(-2.56 \times 10^{-3} + 2.49 \times 10^{-5}Re - 4.25 \times 10^{-9}Re^2)$ $f = 4(-9.88 \times 10^{-3} + 1.15 \times 10^{-5}Re - 1.29 \times 10^{-9}Re^2)$	Transitional fully-developed flow Square-edged Re-entrant
Petukhov (1970)	$f = (0.79ln(Re) - 1.64)^{-2}$	Turbulent fully-developed flow
Blasius (1913)	$f = 0.316Re^{-0.25}$	Turbulent fully-developed flow
Diabatic friction factor		
Deissler (1951)	$f = \frac{64}{Re}\left(\frac{\mu_b}{\mu_w}\right)^m$ $m = -0.58$	Laminar fully-developed flow
Test (1968)	$f = \frac{64}{Re}\frac{1}{0.89}\left(\frac{\mu_b}{\mu_w}\right)^m$ $m = 0.2$	Laminar fully-developed flow
Tam and Ghajar (1997)	$f = \frac{64}{Re}\left(\frac{\mu_b}{\mu_w}\right)^m$ $m = 1.65 - 0.13Pr^{0.84}Gr^{0.17}$	Laminar fully-developed flow
Tam and Ghajar (1997)	$f = 4\left[1 + \left(\frac{Re}{a}\right)^b\right]^C \left(\frac{\mu_b}{\mu_w}\right)^m$ $a = 4230, b = -0.16, c = -6.57, m = -1.13 - 0.396Gr^{0.16}Pr^{0.51}$ $a = 5840, b = -0.0145, c = -6.23, m = -1.1 - 0.46Gr^{-0.133}Pr^{0.41}$	Transitional fully-developed flow Square-edged Re-entrant
Allen and Eckert (1964)	$f = 0.316Re^{-0.25}\left(\frac{\mu_b}{\mu_w}\right)^{-0.25}$	Turbulent fully-developed flow

Table 2: Isothermal and diabatic friction factor correlations.

available in literature, instead it presents a few important friction factor correlations that was used in this study, to validate the experimental setup.

2.8.2 Work by Ghajar and co-workers

Professor Ashin Ghajar from Oklahoma State University and co-workers conducted investigations mainly focused on the effect of different inlet configurations on heat transfer and pressure drop characteristics in the transitional flow regime. The experiments, which made use of different concentrations of aqueous ethylene glycol mixtures, were performed to obtain correlations for diabatic and isothermal friction factors in the transitional flow regime, for three different inlet geometries. The studies that were performed to obtain heat transfer correlations will also receive some attention in this section, but since it is not the focus of this investigation, it will only be discussed briefly.

2.8.2.1 Pressure drop correlations

Ghadar and Madon (1992) performed an isothermal investigation with the purpose of obtaining fully developed friction factors across all flow regimes. The study was performed for three different inlet configurations, namely square-edged, re-entrant, and bellmouth. The study presented friction factors in the form of the skin friction coefficients, which refers to a fully developed friction factor, and apparent friction factors, which refers to the entrance region friction factor that considers pressure drop arising from both momentum flux due to flow development and shear stresses at the wall (Ghajar and Madon, 1992). Different correlations were obtained for each of the three inlet configurations. Transition was found to occur earlier for the inlets that cause greater disturbance. Transition occurred first for the re-entrant inlet, and last for the bellmouth inlet. The correlations obtained in this study are summarised in Table 2.

Tam and Ghajar (1997) conducted an investigation with the aim of developing correlations for the accurate prediction of isothermal and diabatic pressure drop characteristics across all flow regimes, for three different inlets. It was found that when a tube is heated uniformly, the resulting temperature variance in the radial, and axial direction lead to variations in the local fluid properties. This variable property effect was accounted for by making use of the property ratio method (Tam and Ghajar, 1997). The study confirmed that the range of Reynolds numbers values at which transitional flow exists is strongly inlet dependent. The diabatic study revealed that heating caused an increase in laminar and transitional friction factors, and furthermore, resulted in a delay in transition. The increase in friction factors when heating was applied in the laminar and transitional regime, were attributed to the effect of secondary flow which changes the velocity profile of the flow, leading to increased shear stresses. This claim was supported by the fact that the addition of heat did not affect the friction factors in the turbulent flow regime, where the effect of secondary flow is suppressed by the higher flow rates. The friction factors in the laminar and transitional regions decreased for an increase in heat flux. This was due to the temperature increase of the fluid near the tube wall, which decreases the fluid viscosity at this interface. Lastly, the authors proposed new laminar friction

factor correlations that would account for the secondary flow effects augmented by the application of heat. The correlations obtained in this study are summarised in Table 2.

Ghajar *et al.* (2010) performed an isothermal investigation of friction factors in the transitional flow regime using mini- and macro-tubes, with diameters ranging from 337 µm to 2083 µm. The authors found that the onset of transition was delayed for an increase in tube diameter and decrease in relative tube roughness. Furthermore, the Reynolds number range over which transition occurs became narrower with a decrease in tube diameter.

Tam *et al.* (2012) studied the effect of internal microfins, often used to augment heat transfer in smooth tubes, on fiction factors in the transitional flow regime. The authors found that the additional drag, resulting from the microfins, translated into higher friction factors in the laminar region. The use of microfins also led to an increase in the range of Reynolds numbers over which transition occurs. Increasing the spiral angle of the microfins led to a narrower transitional region, whilst also increasing friction factors significantly. The diabatic study confirmed that the start of transition is dependent on the inlet configuration and spiral angle of the microfins.

Tam and Ghajar (2013) performed a study to obtain accurate isothermal and diabatic friction factor correlations across all flow regimes, covering laminar, turbulent, and transitional regions. A variety of different heat fluxes, ranging from 4.3 - 8.9 kW/m^2, as well as three different inlet configurations were used in the investigation. The isothermal friction factors obtained from the investigation confirmed that flow transition is strongly inlet dependent, with transition occurring the earliest for the inlet that causes the most disturbance, namely the re-entrant inlet. Transition occurred last for the bellmouth inlet. It was found that heating had a significant influence on friction factors in the laminar flow regime. This effect was reduced in the transitional flow regime and negligible in the turbulent flow regime. The increase in friction factors, when heating was applied in the laminar and transitional regime, were attributed to the effect of secondary flow which changes the velocity profile of the flow, leading to increased shear stresses. The friction factors in the laminar and transitional regions were again found to decrease for an increase in heat flux. The authors explained that this was due to the temperature increase of the fluid near the tube wall, which decreases the fluid viscosity at this interface. The correlations obtained in this study are summarised in Table 2.

2.8.2.2 Heat transfer correlations

Ghajar and Tam (1994) completed a study with the purpose of obtaining heat transfer correlations across all flow regimes, for entrance and fully developed regions. The study considered both forced and mixed convection modes of heat transfer, whilst using three different inlet configurations. Nusselt number results obtained in the laminar region were significantly higher than the expected theoretical fully-developed prediction of 4.36. The authors explained that this was due to the effects of secondary flow, which is dominant in the laminar and lower transitional regions. The authors explained that a variation in physical properties along the length of the tube, due to the rise of bulk and wall temperature, could

account for the increased critical Reynolds numbers, when the tube is heated uniformly. The study found that the inlet configuration influenced the development of the heat transfer coefficients, causing transition to occur the earliest for the inlet that caused the greatest disturbance. The influence of secondary flow was found to be negligible in the turbulent region, as results in this region correlated well with theoretical forced convection predictions. The difference in inlet configurations were found to have a minor effect on heat transfer coefficients in the turbulent flow regime.

2.8.3 Work by Meyer and co-workers

Professor Josua P. Meyer, from the University of Pretoria, South Africa, performed various investigations into flow in the transitional region. His work, which involved using mainly water as a test fluid, is briefly summarised in this section.

2.8.3.1 Smooth tubes

The majority of the work conducted in the transitional flow regime made use of smooth tubes, as these tubes are the most common tube found in industry.

Pressure drop correlations

Meyer and Olivier (2010) measured the heat transfer coefficients and friction factors for a smooth tube-in-tube counterflow heat exchanger, operating in the transitional flow regime. In this study, the effects of the disturbances caused by four different inlets, namely square-edged, re-entrant, hydrodynamically fully-developed, and bellmouth were investigated. Isothermal friction factors showed that transition from laminar to turbulent flow had a strong dependence on the inlet configuration. Similar to investigations conducted by Ghajar, transition was found to occur the earliest for the inlet that caused the most disturbance, namely the re-entrant inlet.

The results obtained from the diabatic investigation showed that this dependence is, however, negligible when heating is introduced. This was due to the buoyancy-induced secondary flow suppressing the inlet disturbances. Laminar diabatic friction factors were found to be higher than the predicted theoretical values. The authors attributed this to the effects of natural convection, which influenced the boundary layer in such a way that the velocity profile is steeper near the wall surface, leading to higher shear stresses and therefore friction at the tube-wall interface.

Heat transfer correlations

Meyer and Olivier (2010) found that laminar Nusselt numbers were much higher than the predicted value of 4.36, due to mixing caused by buoyancy induced secondary flow effects. Heat transfer results confirmed that with the addition of heat, transition from laminar to turbulent flow is totally independent of inlet configuration.

2.8.3.2 Enhanced tubes

Meyer investigated the effects of various heat transfer augmentation methods, on the transition from laminar to turbulent flow. One such method involved increasing the heat transfer surface area by making use of fins, located inside the tube. This section briefly summarises his work on enhanced tubes.

Pressure drop correlations

The first study performed by Meyer and Olivier (2011) explored the effect of enhanced tubes on the isothermal pressure drop in the transitional flow regime. The isothermal friction factors obtained in the experiment showed that transition occurred much earlier for enhanced tubes than for smooth tubes. As for smooth tubes, transition from laminar to turbulent flow were found to be dependent on the type of inlet configuration used, with smoother inlets resulting in a delay in transition.

The isothermal friction factors obtained for enhanced tubes were found to be higher than for smooth tubes, in both the laminar and turbulent flow regimes. The authors attributed this to the increased relative surface roughness due to the fins, which led to increased drag. It was observed that a second, more predictable transition occurred between Reynolds numbers of 3 000 and 10 000 which lead to a rise in friction factor.

The second part of the study performed by Meyer and Olivier (2011) investigated the effect of heating on the friction factors of enhanced tubes. Results showed that the effects of inlet disturbance were once again negated by the buoyancy-induced secondary flow with the addition of heat. Diabatic friction factors obtained for enhanced tubes were much higher than the isothermal friction factors.

Heat transfer correlations

Heat transfer results in the laminar flow regime show a negative influence on the heat transfer process when using enhanced tubes. Fins inside the tube act as a barrier to prevent secondary flow in this regime, which prevents the fluid from mixing. The fins do not augment heat transfer at lower Reynolds numbers, since the flow rates are too low for the fins to induce a swirling motion.

Turbulent heat transfer coefficients showed a significant increase, due to the improved mixing effects of the spiralling motion induced by the fins. The authors also suggested that further increases can be attributed to the fins breaking up the viscous sub-layer. Enhanced tubes with greater helix angles had higher heat transfer coefficients, since the fins are more effective at inducing a swirling motion in the flow, leading to better mixing.

2.8.3.3 Multi-walled carbon nanotubes

Another way of augmenting heat transfer is to increase the thermal conductivity of the working fluid. By introducing multi-walled carbon nanotubes, the thermal conductivity of water is increased, which could potentially lead to a significant improvement in the thermal efficiency of the heat exchanger. Meyer *et al.* (2013) investigated the influence of multi-walled carbon

nanotubes on the heat transfer and pressure drop characteristics in the transitional flow regime. Three different volume concentrations of multi-walled carbon nanotubes were used in the study, namely 0.33%, 0.75%, and 1%. Pressure drops were found to increase for an increase in volume concentration, which can be attributed to the increase in viscosity of the fluid. (Meyer *et al.*, 2013). Furthermore, transition occurred earlier for an increase in concentration.

2.9 Summary and shortcomings of previous work

This chapter covered a few fundamental concepts relevant to convective heat transfer and pressure drop, such as different flow regimes and flow development. Some of the most important correlations for prediction pressure drop characteristics across all flow regimes were summarised in Table 2. These correlations will later be used to validate the experimental setup used to produce results in this investigation.

A short summary of shell-and-tube heat exchangers is presented in this Chapter. It was found that most of the tube bundles in shell-and-tube heat exchangers have pitch ratios within the range of 1.25 to 1.5, due to manufacturing and size restrictions.

A brief overview was presented on the previous work done in the transitional flow regime. Ghajar and co-workers used the constant heat flux boundary condition and focused on fully-developed flow using different ethylene–glycol mixtures as a test fluid. Meyer and co-workers used the constant wall temperature boundary condition for developing and fully-developed flow, whilst using water as a test fluid.

Ghajar and co-workers, as well as Meyer and co-workers investigated the effect of inlet geometries on the isothermal pressure drop characteristics in the transitional flow regime. The isothermal studies found that transition was delayed for inlets that cause less disturbance. Meyer and co-workers found that under diabatic conditions, inlet geometries had no effect on the transition from laminar to turbulent flow when a fluid with a low Prandtl number is used.

The studies investigating the transitional flow regime were focused on the effect of different types of inlet geometries, different heating methods, as well as surface roughness, in single tube heat exchangers. However, the effect of the pitch ratio of tube bundles in the transitional flow regime, commonly found in shell-and-tube heat exchangers, have not yet been determined.

2.10 Conclusion

Intensive research has been conducted in order to investigate characteristics of convective heat transfer in the transitional region. These studies include the effect of different types of inlet geometries, different heating methods, as well as surface roughness. However, all these studies were limited to single-tube heat exchangers. It was evident that this gap in literature had to be addressed, and a study focussing on multiple tubes spaced at different pitch ratios, specifically ranging from 1.25 to 1.5, was required in order to gain further understanding of the transition from laminar and turbulent flow in shell-and-tube heat exchangers.

Chapter 3:
Experimental process

3.1 Introduction

The aim of this chapter is to document the experimental work conducted in the investigation into pressure drop in smooth tubes with a multi-tube inlet configuration. This chapter provides an overview of some of the equipment and instrumentation used in the experimental setup, and summarises the experimental procedure followed. The methods used to process data into meaningful results are then briefly discussed, followed by a detailed uncertainty analysis.

3.2 Experimental setup

The system, shown schematically in Figure 9 and briefly described below, was designed and constructed to collect the data presented within this thesis. The experimental setup consisted of a closed loop system that circulated a test fluid through a test section, where measurements are taken, and back into a reservoir.

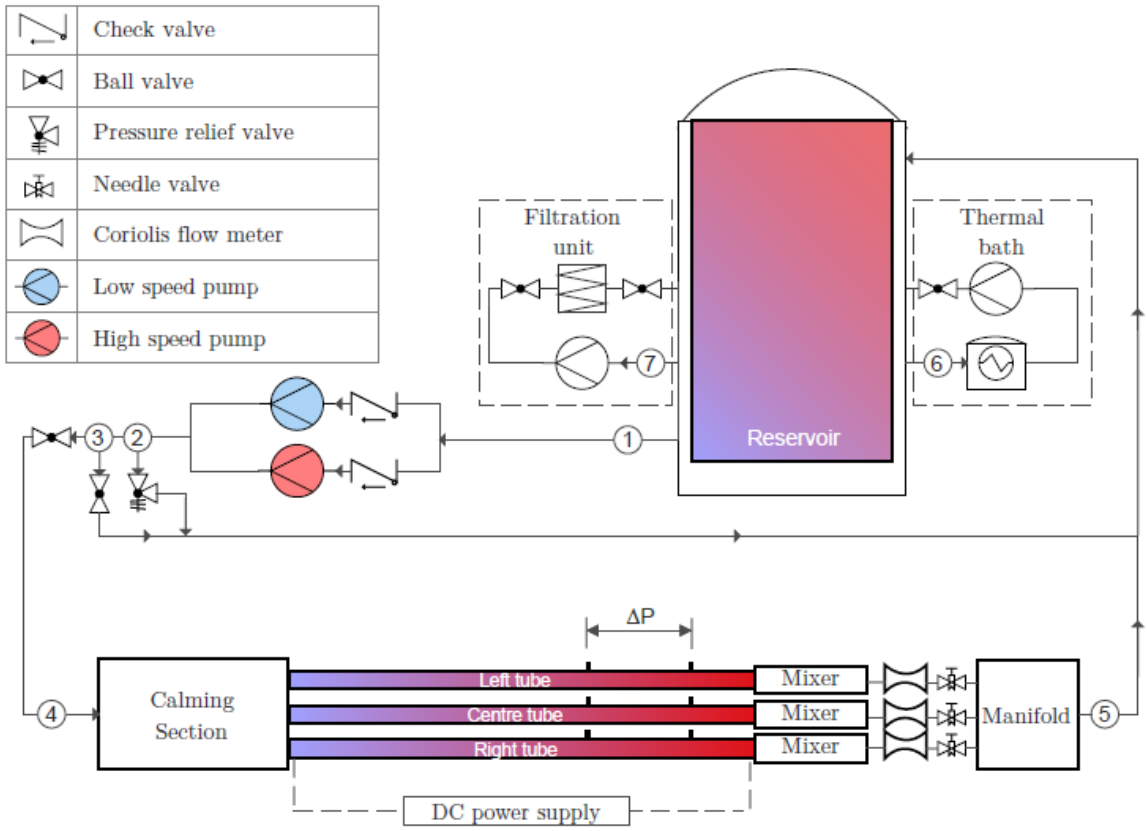

Figure 9: Experimental setup

1. The system circulated water from a reservoir, with a capacity of 260 litres, through a test section, by making use of either a low speed pump, or a high-speed pump. A variable speed gear pump was used as a low-speed pump, whilst a variable speed centrifugal pump was selected as the high-speed pump. Check valves were installed directly upstream of the two pumps, which allowed the user to select a pump by simply

switching it on. This configuration also allowed both pumps to be operated simultaneously.

2. A pressure relief valve was installed to protect the most fragile equipment, such as the pumps and the calming section. This would allow water to flow directly back to the reservoir if the pressure increased above a preselected threshold.
3. A bypass, located downstream of the pumps, allowed a fraction of the flow to be transported back to the reservoir without passing through the test section. This meant that the pumps must be operated at a much higher speed to achieve the desired flowrate within the test section. The increased pump speed, together with the artificial increase in backpressure at the pump head, greatly reduced the fluctuations in flow rate due.
4. The circulated test fluid then passed through the calming section and into the test section, where temperature, pressure, and flow rate measurements were taken. Needle valves located downstream of the flow meters allow for precise control of the flow resistance, and thus flow rate in each tube.
5. The flow from the three tubes were collected in the manifold and recirculated back into the reservoir.
6. A thermal bath, with a maximum cooling capacity of 900 W, was set to maintain a reservoir temperature close to the ambient temperature inside the climate-controlled lab, namely 21.8°C. Maintaining a constant inlet temperature equal to the ambient temperature ensures that all the heat transferred to the test fluid comes directly from the power supplies, and not the surroundings. Testing in a climate controlled environment allowed all experiments to be conducted at the same ambient conditions, throughout the year.
7. The water in the reservoir was pumped through a filtration cycle continuously, to remove algae, limescale build up, and any other solid particles left over from the manufacturing process.

3.3 Calming section

The calming section was manufactured out of a PVC pipe with an inner diameter of 232 mm and a length of 1.2 m. The design, based on the work of Ghajar and Madon (1992), used various stages of fine wire meshing and perforated screens, as shown in Figure 10, to ensure that a uniform velocity profile is achieved at the inlet of the test section. Pulsations produced by the pump, as well as asymmetric flow caused by partially closed ball valves located upstream of the test section, were damped out in the calming section. Air drawn into circulation accumulates in the calming section due to the large contraction ratio. This prevents air from passing through the test section, where it could influence pressure drop measurements. The accumulated air can then be removed through the bleed valves incorporated in the design. A PT100 temperature probe was placed in the calming section to measure the temperature of the fluid entering the test section.

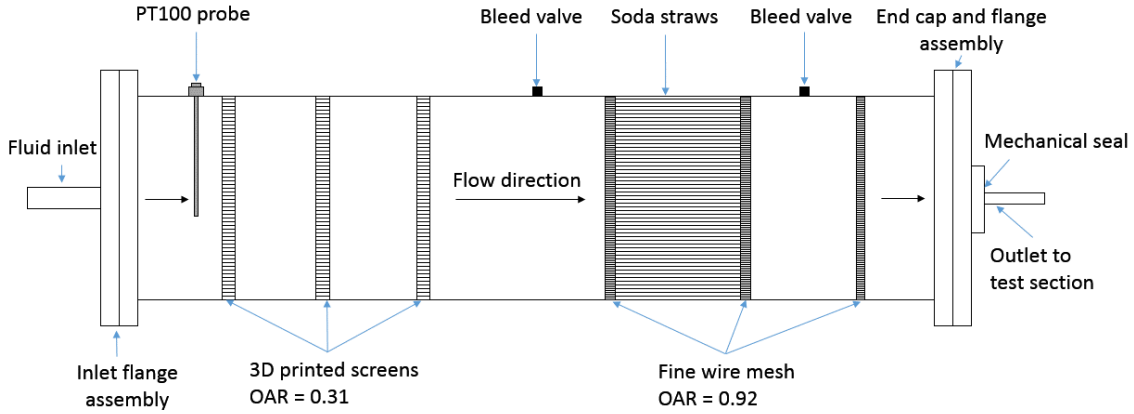

Figure 10: Schematic representation of the calming section

The end caps and flanges of the calming section were moulded out of casting epoxy, and turned down to specification on a lathe. Holes were drilled into the end cap for the two different pitch ratios, as shown in Figure 11, by using a milling machine. No redrilling of bolt holes were necessary since the same mould was used to produce the two mating parts. The stainless steel tubes were slid into the end cap and fixed into position with a mechanical seal. An endoscope was used to ensure that the tubes were flush with the face of the endcap, producing a square edge inlet.

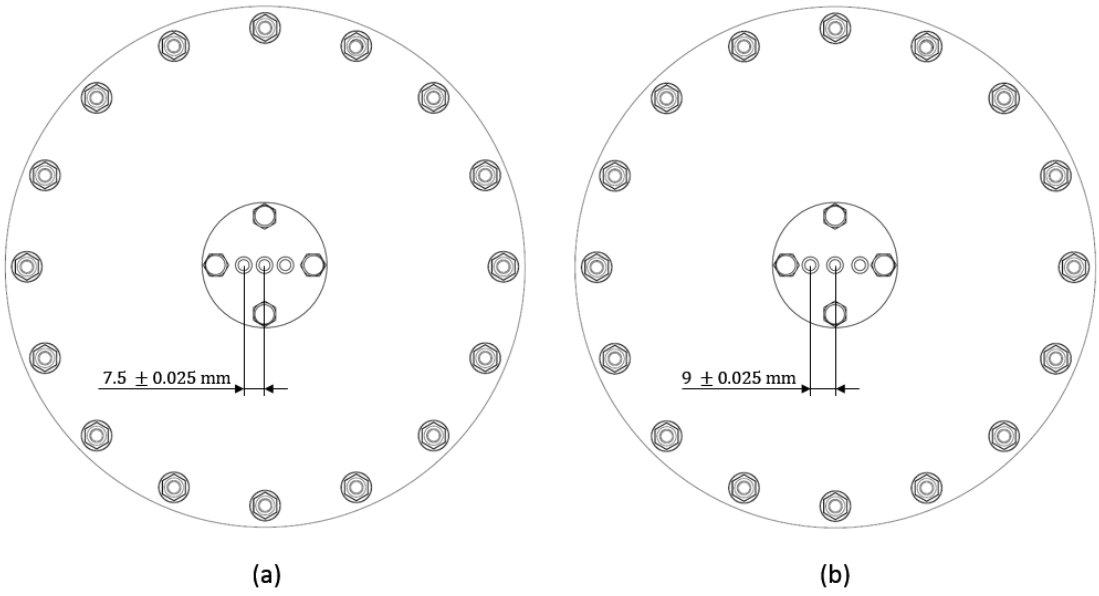

Figure 11: Schematic of the endcaps used to join the multi-tube test section to the calming section

3.4 Test section

The single and multi-tube test sections were manufactured from seamless, 316L stainless steel tubes, with a length of 6.0 m (±1 mm). The inner and outer diameter of the tubes were 4 mm

and 6mm, respectively, with tolerances on the outer diameter and wall thickness given as ±0.076 mm. The surface roughness of the tubes used in the study were considered to be too low to have an effect and relative roughness of the tubes were therefore negligible ($\frac{\varepsilon}{D}=0$).

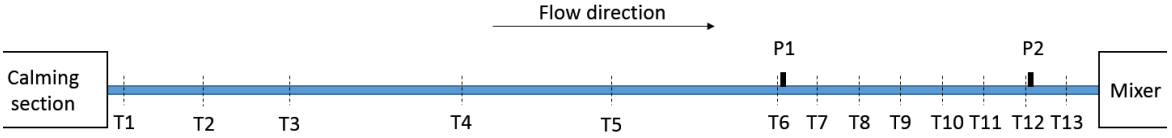

Figure 12: Schematic representation of the test section, showing thermocouple and pressure tap locations.

	Distance[mm]
Thermocouple station 1	105
Thermocouple station 2	584
Thermocouple station 3	1105
Thermocouple station 4	2146
Thermocouple station 5	3050
Thermocouple station 6	4050
Pressure tap 1	4060
Thermocouple station 7	4300
Thermocouple station 8	4550
Thermocouple station 9	4800
Thermocouple station 10	5050
Thermocouple station 11	5300
Thermocouple station 12	5550
Pressure tap 2	5560
Thermocouple station 13	5800

(a)

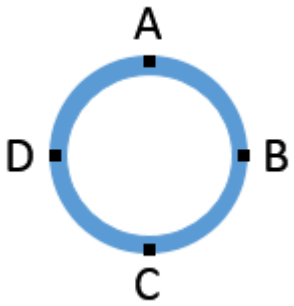

(b)

Figure 13: (a) Summary of thermocouple and pressure tap station positions in millimetres. (b) Cross-section of a thermocouple station

The three tubes of the multi-tube test section were held apart at a uniform distance, equal to that of the pitch ratio, by making use of 3D printed spacers positioned at 0.5 m intervals. This helped to equalize the flow resistance across each tube, meaning that any flow maldistribution that occurred would be the result of flow effects caused by the multi-tube inlet condition.

In this study, the three tubes of the multi-tube test section will be referred to as “Left tube”, “Centre tube”, and “Right tube”, with the directions given from the point of view of an observer at the calming section, looking in the direction of the flow as shown in Figure 9. Furthermore, the single-tube setup will be referred to as a “Single tube”, in figures and graphs.

The 316L stainless steel tubes has an electrical resistivity of 74 μΩcm (at 20°C). This value is temperature dependent, and is expected to increase as temperature of the tube increases. Using a multi-meter, the resistance of the tube was measured to be 0.282 Ω at the lab temperature of 21.8°C.

By passing current directly through the tube, uniform heat fluxes could be maintained with Elektro-Automatic PS90 40-60 power supplies. Direct current power supplies were chosen, since alternating current power would produce a phenomenon called “Skin effect”, which would result in a non-uniform distribution of current across the cross section of the tube, with a

maximum current density expected at the outer radius of the tube. This would result in the cross section of the tube not being heated uniformly. The tubes were coated with Kapton film to prevent electrical continuity between adjacent tubes, which would otherwise result in an electrical short.

Pressure taps were silver-soldered onto the tubes at distances of 4.06 m and 5.56 m from the inlet, well outside of the predicted theoretical 3.3 m flow development length, calculated using Equation 2.10 and 2.12 for forced convection. These pressure taps were used to determine fully-developed friction factors for Reynolds numbers ranging from 1 000 to 7 000.

To measure the wall temperature needed for various diabatic friction factor correlations, thirteen thermocouple stations, consisting of three thermocouples each, were placed along the length of each tube, as shown in Figure 12 and Figure 13. The test section was insulated with 155 mm of Armaflex insulation, with a thermal conductivity of 0.034 W/mK. The maximum heat loss, predicted with the one-dimensional heat conduction equation, was found to be less than 3%. Figure 13 shows the location of each thermocouple and pressure tap, relative to the inlet of the tubes. The test section is represented schematically in Figure 12.

3.5 Mixer

Heating the test section uniformly creates temperature gradients between the tube wall and tube centre, as shown in Figure 4. This makes measuring the bulk fluid temperature at the outlet of the tube challenging, especially at lower Reynolds numbers. Bakker (2000) proposed a method using 5 alternating baffle plates, spaced 90° apart, to break up the thermal boundary layer. This thoroughly mixes the test fluid, resulting in a zero-temperature gradient in the radial direction. The baffle plates, manufactured out of copper plates measuring 8 mm wide and 16 mm long, were inserted into an acetal mixing block, shown in Figure 14. The mixing block redirects the fluid after it has been mixed, to flow over and along the PT100 sensor. This exposes a larger area of the PT100 probe to the test fluid, eliminates stagnant recirculation zones, and reduces measurement error and the thermal lag of the system. The mixing blocks were machined out of acetal plastic and were heavily insulated to minimize the amount of heat lost to the environment. A bleed valve was installed to ensure that the PT100 probe was completely submerged in the test fluid.

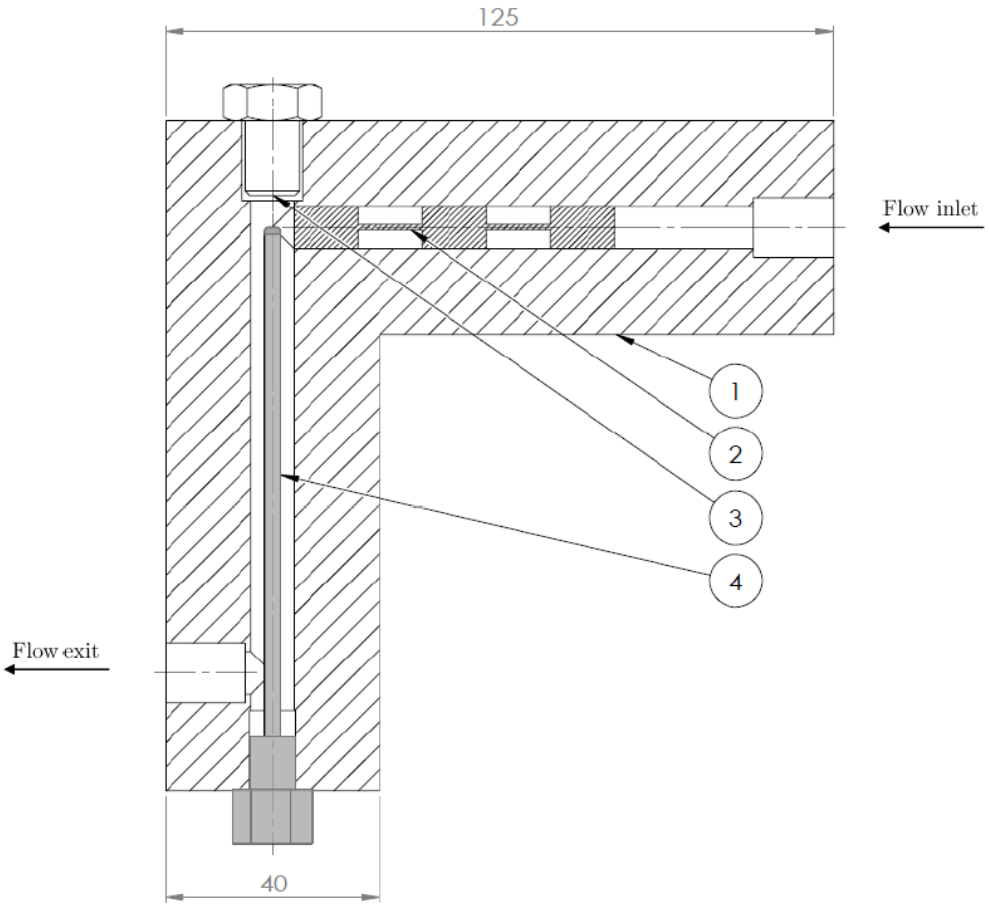

Figure 14: Mixing block with PT100 sensor used to measure bulk fluid temperature downstream of each tube. All dimensions in mm. (1) Acetal block. (2) Baffle plates. (3) Bleed valve. (4) PT100 probe

3.6 Manifold

A manifold, with a diameter of 240 mm, was installed downstream of the needle valves. The manifold collects the flow from the multiple tube test section and delivers it into the return line of the reservoir. Unifying the flow in a manner similar to the rear header of a shell-and-tube heat exchanger helps balance the flow resistance in each tube, resulting in a more accurate distribution of mass flow across the three tubes. If necessary, further variations in flow resistance can be corrected using needle valves installed directly upstream of the manifold.

3.7 Lab instrumentation and equipment

3.7.1 Pressure transducers

Friction factor results were obtained by taking differential pressure measurements over a length of 1.5 m in the fully developed portion of each test section, by using Validyne DP15 variable reluctance pressure transducers.

Pressure taps, positioned in the fully developed portion of the tube, as shown in Figure 12, were drilled to a diameter of 0.4 mm. Rayle (1949) concluded that an orifice, drilled to 10% of the inner diameter of the test section, would not influence the boundary layer significantly, and would have a negligible effect on the dynamic head.

The holes were drilled at 30 000 RPM to minimize the size of the burrs forming inside the tube. A 4mm braided steel cable, wrapped in heat shrink, was then used to remove any burrs resulting from the drilling process, as failure to do so could give errors in the range of 15 to 20% of the dynamic head (Rayle, 1949).

The variable reluctance sensors function by measuring displacement on interchangeable diaphragms through the resulting change in impedance of the two sensing coils. Diaphragms with different full scale values were used. The small diaphragm, with a full-scale value of 8.6 kPa, was used for Reynolds numbers ranging from 1 000 to 4 400, while the large diaphragm, with a full-scale value of 22 kPa, was used for all Reynolds numbers larger than 4 400. The accuracy of the diaphragms is 0.25% of the full-scale value, which translates to 21.5 Pa and 55 Pa respectively.

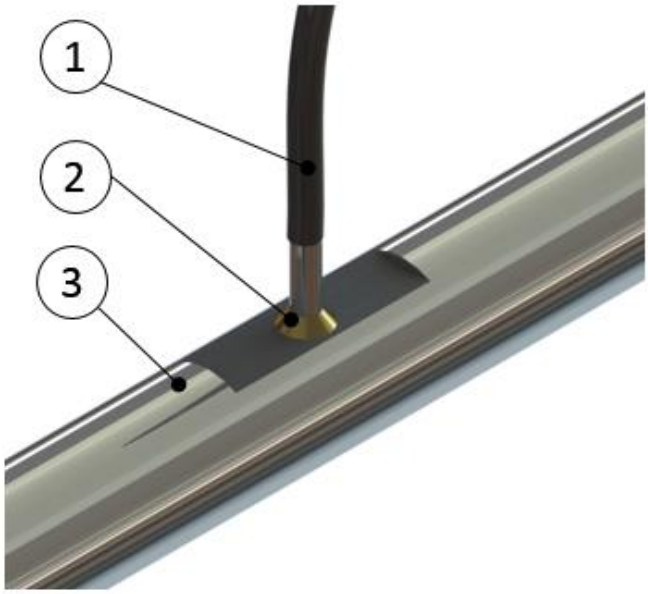

Figure 15: 3D model of a pressure tap station: (1) Plastic pneumatic hose connected to the pressure transducer, glued onto stainless steel capillary tube. (2) Stainless steel capillary tube silver-soldered onto the test section. (3) Stainless steel test section

The diaphragms were calibrated with a water column, by connecting a Beta T-140 manometer in parallel with the DP15 sensor. The manometer had a full-scale value of 50 kPa and an accuracy of 50 Pa. The pressure calibration process is discussed in detail in Appendix A.

3.7.2 PT100 probes

Four PT100 probes were used to measure bulk fluid temperatures. One probe was placed in the calming section to measure inlet temperature, whilst the remaining probes were placed in the mixer blocks located downstream of the test section. The PT100 probes were calibrated in a thermal bath, using a DigiCal probe as reference with an accuracy of 0.03°C. The calibration process is described in Appendix A.

3.7.3 Thermocouples

Wall viscosity values are required in order to plot some of the diabatic friction factor correlations available in literature. Thermocouple stations were spaced along the length of the tube, shown in Figure 12, to measure wall temperature at various points and determine the wall viscosities. Each station had a T-type thermocouple positioned at the top and bottom of the tube (Position A and C in Figure 13 c). Due to spatial limitations, the third thermocouple was placed on either the left, or right side of the tube (Position B or D in Figure 13 c), alternating along the length of the test section.

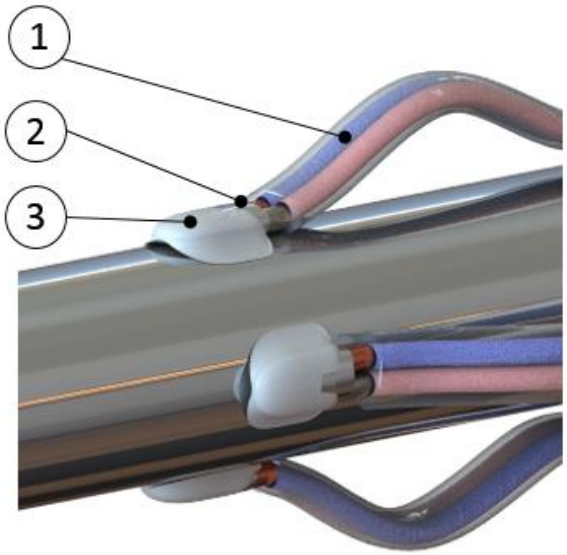

Figure 16: 3D model of a thermocouple station, showing all three thermocouples: (1) T-type thermocouple wire. (2) Tin soldered connection between the copper and constantan cores of the thermocouple. (3) Thermally conductive epoxy, with a thermal conductivity of 9 W/mK*, used to attach thermocouples to the stainless steel tube.*

The thermocouples were glued into 0.5 mm deep indentations, drilled 90° apart on the tube circumference. The stations were measured, marked and drilled using a 3D printed jig, which ensured that all the holes are drilled to the same depth. The Arctic Alumina thermal adhesive that was used had a thermal conductivity of 9 W/mK and a curing time of 5 minutes.

3.7.4 Flow meters

Three identical Coriolis flow meters, placed downstream of the test section, were used to measure the mass flow rate of the test fluid flowing in each tube. The flow meters were factory calibrated, and had an accuracy equal to 0.05% of the full-scale value of 1.36 kg/min.

3.7.5 Power supplies

Three Elektro-Automatic PS90 40-60 power supplies, capable of delivering a maximum current and voltage of 60A and 40V respectively, were used to maintain constant heat flux boundary conditions of 2 kW/m^2, 3 kW/m^2 and 4 kW/m^2, through direct current heating.

The terminals of the power supply were connected to the stainless steel tubes using brass lugs to ensure a secure electrical connection could be maintained, as shown in Figure 17. The tubes, as well as the connectors, were coated with Kapton film to prevent electrical continuity between adjacent tubes, which would otherwise result in an electrical short.

During testing, the electrical resistivity of the tubes would change as the temperature increased. This meant that input currents and voltages had to be adjusted constantly, to ensure that the desired heat flux is achieved. The power provided to each test section were logged and averaged, to account for small variations during testing.

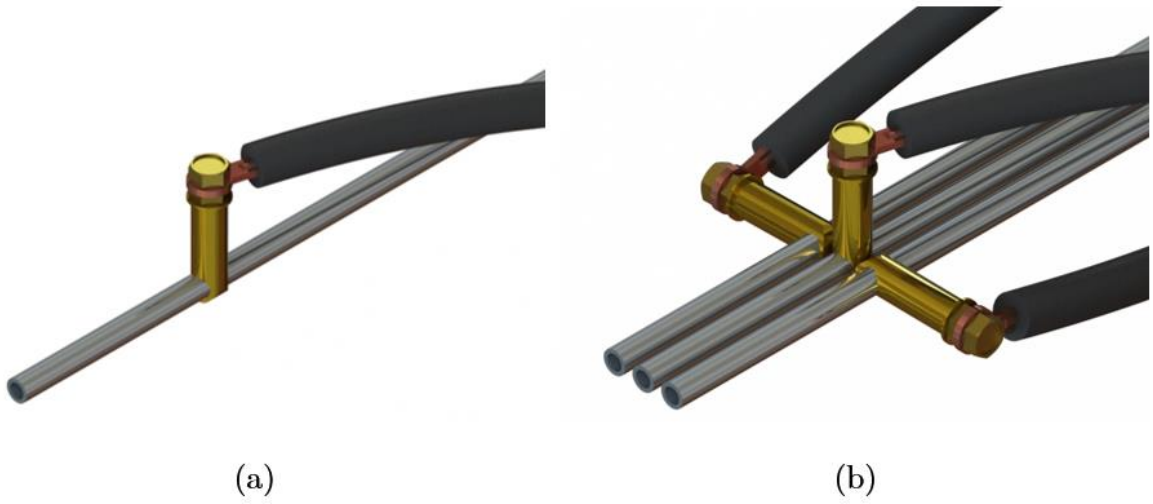

Figure 17: 3D model of the lugs used to connect the power supplies to the stainless steel tubes: (a) Single tube configuration. (b) Multitube configuration with lugs spaced 90° apart.

3.8 Experimental procedure

Using water as a test fluid, experiments were conducted for Reynolds numbers ranging from 1 000 to 7 000, ensuring that the laminar, transitional, and turbulent flow regimes were captured. Since the effects of hysteresis are negligible in the transitional flow regime (Meyer and Olivier, 2010), experiments were conducted for decreasing Reynolds numbers only. This helped to minimize the amount of residual heat stored in the insulation which could negatively influence turbulent results.

The setup was turned on and the pumps were set to operate at a very high speed. The desired mass flow rates were then achieved by adjusting the supply and bypass valves. Any minor corrections that were required were made by adjusting the voltage supplied to the pump. A high pumping speed was maintained throughout to investigation, to reduce flow pulsations.

Mass flow rates, pressure drop and temperatures were plotted in real time and monitored to determine when steady state conditions were reached. Steady state conditions were achieved approximately an hour after initial start-up. Thereafter, the tiny decremental changes made to mass flow rate meant a significant decrease in time required to reach steady state, roughly 20 minutes.

The three different heat fluxes were achieved by setting the supply voltage and current on the power supplies. Small adjustments were continuously made to the supply voltage and current to maintain the desired heat flux, as the electrical resistance of the tubes increased with increasing temperatures.

Once steady state conditions were achieved, a sample consisting of 200 points were taken at a frequency of 10 Hz. In the transitional region, the sample size was increased to 1 000 points, to better average out the severe fluctuations associated with this regime. The sample points were then averaged to obtain a single data point which was then used in calculations. The process was repeated for decreasing Reynolds number increments of 200 in the turbulent regime, 50 in the transitional regime, and 100 in the laminar flow regime.

3.9 Data reduction

This chapter deals with the different methods used to obtain the desired quantities from the raw data collected from experiments. A heat balance is performed using measured inlet, exit and wall temperatures, whilst the pressure drop measured across the test section was used to obtain friction factors.

3.9.1 Heat balance and bulk fluid temperature

Wall temperature measurements were taken at various positions along the test section, by making use of T-type thermocouple stations. Inlet and exit flow temperatures were measured using PT-100 probes located at the entrance of the calming section, and at the outlet of the mixer.

Firstly, a heat balance is performed by comparing the heat transfer rate of the water to the electrical input power. The heat transfer rate of the water can be calculated from:

$$\dot{Q}_{water} = \dot{m} C_p (T_e - T_i) \tag{3.1}$$

The electrical input power is governed by the voltage and current provided by the power supplies:

$$\dot{Q}_{electric} = VI \tag{3.2}$$

Losses in the system can easily be calculated by completing a simple energy balance:

$$Losses[\%] = \frac{\dot{Q}_{electric} - \dot{Q}_{water}}{\dot{Q}_{electric}} \times 100 \tag{3.3}$$

The average energy balance over all the measurements taken was less than 3%. A maximum energy loss of 5% occurred at a Reynolds number of 1019 and a heat flux of 4 kW/m^2. The uniform heat flux boundary condition causes the fluid temperature to increase linearly along the length of the tube. The bulk fluid temperature, at which the fluid properties used in the study are to be determined, are calculated by taking the average of the inlet temperature

(measured by the PT100 probe located in the calming section) and the outlet temperature (measured by the PT100 probes located in the mixing blocks):

$$T_b = \frac{T_{f,11} + T_{f,12}}{2} \tag{3.4}$$

The average surface temperature, needed for diabatic friction factor correlations, was determined using the trapezoidal rule:

$$T_w = \frac{1}{L}\int_0^L T_w(x)dx \tag{3.5}$$

However, the tube wall temperature at a given position $T_w(x)$ was measured 0.5 mm into the tube wall. The temperature drop over the remaining 0.5 mm thickness of the tube wall must be determined from the product of the thermal resistance and the heat transfer rate:

$$\Delta T = \dot{Q} R_{tube} \tag{3.6}$$

Where the tube resistance R_{tube} is calculated from:

$$R_{tube} = \frac{\ln(\frac{d_o}{d_i})}{2\pi L k} \tag{3.7}$$

3.9.2 Reynolds number and friction factor

The Reynolds number was determined using a bulk temperature calculated half way between the two pressure taps:

$$Re = \frac{4\dot{m}}{\mu D_i \pi} \tag{3.8}$$

Using the pressure drop measured across the pressure taps and using fluid properties determined at the bulk fluid temperature, the friction factor can be determined from:

$$f = \frac{2D_i \Delta P}{\rho V^2 L} = \frac{\rho \Delta P D^5 \pi^2}{8\dot{m}^2 L} \tag{3.9}$$

3.10 Uncertainty

The uncertainties of the experiment were calculated according the method proposed by Dunn (2010). Firstly, the accuracies of all the instruments used were listed, followed by a study of the geometrical accuracy of the stainless steel test sections. These accuracies were then used to determine the uncertainty of Reynolds numbers and friction factors, presented in Chapter 5 and Chapter 6, calculated for a 95% confidence interval.

3.10.1 Instrument accuracy

The accuracy of the lab equipment used to investigate the influence of inlet pitch ratio on friction factors in the transitional flow regime is addressed in the order in which they were discussed in Section 3.7.

3.10.1.1 Pressure transducers

Differential pressure measurements were taken over 1.5m in the fully developed portion of each test section, by using Validyne DP15 variable reluctance pressure transducers. The variable reluctance sensors function by measuring displacement on interchangeable diaphragms through the resulting change in impedance of the two sensing coils.

A low- and a high-pressure diaphragm was used with maximum full scale values of 8.6 kPa and 22 kPa, respectively. The diaphragms were calibrated with a water column, by connecting a Beta T-140 manometer in parallel with the DP15 sensor. The manometer had a full-scale value of 50 kPa and an accuracy of 50 Pa. A linear regression analysis, as presented by Dunn (2010), was performed to determine the uncertainty associated with each diaphragm.

Diaphragm full-scale	Pressure range	Uncertainty range
8.6 kPa	0 – 8.5 kPa	25.2 – 25.8 Pa
22 kPa	8 – 20 kPa	26.2 – 29.2 Pa

Table 3: Summary of the uncertainty for each pressure diaphragm, calculated using linear regression analysis as proposed by Dunn (2010).

3.10.1.2 PT100 probes

Four PT100 probes were used to measure bulk fluid temperatures. One probe was placed in the calming section to measure inlet temperature, whilst the remaining probes were placed in the mixer blocks located downstream of the test section. The PT100 probes were calibrated in a thermal bath, using a DigiCal probe as reference with an accuracy of $0.03°C$. A linear regression analysis, as presented by Dunn (2010), was performed to determine the uncertainty associated with each PT100 probe.

Position	Uncertainty range [$°C$]
Inlet probe	0.1002
Left tube outlet probe	0.1002
Centre tube outlet probe	0.1003
Right tube outlet probe	0.1004

Table 4: Summary of the uncertainty for each PT100 sensor, calculated using linear regression analysis as proposed by Dunn (2010).

3.10.1.3 Coriolis flow meters

Three identical Coriolis flow meters, placed downstream of the test section, were used to measure the mass flow rate of the test fluid flowing in each tube. The flow meters were factory calibrated, and had an accuracy equal to 0.05% of the full-scale value of 1.36 kg/min, which translates to an accuracy of 6.8×10^{-4} kg/min.

3.10.1.4 Power supplies

Three Elektro-Automatic PS90 40-60 power supplies were used to maintain constant heat flux boundary conditions through direct current heating. The manufacturer specified an accuracy of 0.2% of the nominal value of current or voltage.

3.10.2 Geometrical accuracy

3.10.2.1 Tube length

The length of the stainless steel tubes was determined using a tape measure to within an accuracy of 1 mm.

3.10.2.2 Tube diameter

The inner and outer diameter of the instrumentation grade stainless steel tubes were 4 mm and 6mm, respectively, with accuracy on the outer diameter and wall thickness given as ±0.076 mm, in the specification certificate.

3.10.3 Fluid properties

The thermo-physical properties of water, used as a working fluid in this study, were calculated from tables presented by Sengers and Watson (1986), who proposed improved international formulations for viscosity and thermal conductivity of water which has been adopted by the International Association of the Properties of Steam. The uncertainties associated with these properties, for temperatures ranging from 0-100°C and pressures from 0.1 - 1 MPa are summarized in Table 5:

Property	Dynamic Viscosity	Density	Thermal conductivity	Specific heat	Prandtl number
Symbol [units]	μ [Pa · s]	ρ[kg/m^3]	k[W/m · K]	C_p [J/kg · K]	Pr
Uncertainty	1%	0.004%	2%	0.04%	2.3%

Table 5: Uncertainties associated with fluid properties.

3.10.4 Calculated uncertainties

3.10.4.1 Reynolds number

To determine the uncertainty associated with the Reynolds number, the uncertainties of the mass flow rate, inner diameter, and the dynamic viscosity of the working fluid must be determined.

The uncertainty of the mass flow rate was determined from the sensor bias, as supplied by the manufacturers of the flow meter, and the sensor precision, which was obtained by multiplying Student's t-variable with the standard deviation of a 200-point sample measurement. These two values are then substituted into Equation 3.10 to determine the uncertainty associated with mass flow rate.

$$\delta m = \left(b_i^2 + p_i^2\right)^{0.5} \tag{3.10}$$

The Reynolds number was calculated from:

$$Re = \frac{4\dot{m}}{\mu D_i \pi} \tag{3.11}$$

Whereby the uncertainty of the Reynolds number was calculated using:

$$\delta Re = \frac{4}{\pi}\left[\left(\frac{1}{\mu D_i}\delta\dot{m}\right)^2 + \left(-\frac{\dot{m}}{\mu D_i^2}\delta D\right)^2 + \left(-\frac{\dot{m}}{\mu^2 D}\delta\mu\right)^2\right]^{0.5} \tag{3.12}$$

The calculated Reynolds number uncertainties were plotted against Reynolds number in Figure 18 and Figure 19. Furthermore, the Reynolds number uncertainties for the different flow regimes were summarized in Table 6 and Table 7 for the pitch of 1.25 and 1.5, respectively.

Heat flux	Flow regime	Left tube	Centre tube	Right tube
0 kW/m²	Laminar	1.06%-1.20%	1.07%-1.23%	1.07%-1.21%
	Turbulent	1.03%-1.04%	1.03%-1.05%	1.03%-1.04%
2 kW/m²	Laminar	1.07%-1.21%	1.08%-1.26%	1.07%-1.23%
	Turbulent	1.03%-1.05%	1.03%-1.05%	1.03%-1.05%
3 kW/m²	Laminar	1.08%-1.30%	1.08%-1.30%	1.07%-1.33%
	Turbulent	1.03%-1.05%	1.03%-1.05%	1.03%-1.05%
4 kW/m²	Laminar	1.08%-1.24%	1.09%-1.29%	1.09%-1.26%
	Turbulent	1.03%-1.05%	1.03%-1.05%	1.03%-1.05%

Table 6: Uncertainties of Reynolds numbers of the multi-tube test section with a pitch of 1.25.

Heat flux	Flow regime	Left tube	Centre tube	Right tube
0 kW/m²	Laminar	1.06%-1.15%	1.06%-1.17%	1.06%-1.18%
	Turbulent	1.03%-1.06%	1.03%-1.06%	1.03%-1.06%
2 kW/m²	Laminar	1.07%-1.21%	1.07%-1.23%	1.08%-1.25%
	Turbulent	1.03%-1.05%	1.03%-1.05%	1.03%-1.05%
3 kW/m²	Laminar	1.08%-1.27%	1.08%-1.33%	1.08%-1.29%
	Turbulent	1.03%-1.05%	1.03%-1.04%	1.03%-1.05%
4 kW/m²	Laminar	1.09%-1.31%	1.10%-1.33%	1.08%-1.33%
	Turbulent	1.03%-1.05%	1.03%-1.06%	1.03%-1.05%

Table 7: Uncertainties of Reynolds numbers of the multi-tube test section with a pitch of 1.5.

From Figures 16 and 17, and Tables 6 and 7, it was concluded that the uncertainty of Reynolds number is not a function of temperature, as it does not increase for increasing heat fluxes. Reynolds number uncertainties remained below 1.4% for all heat fluxes and pitch ratios. A clear spike in uncertainty was evident in the transitional flow regime, caused by the fluctuations in mass flow rate, which leads to higher standard deviations, and ultimately, higher uncertainties.

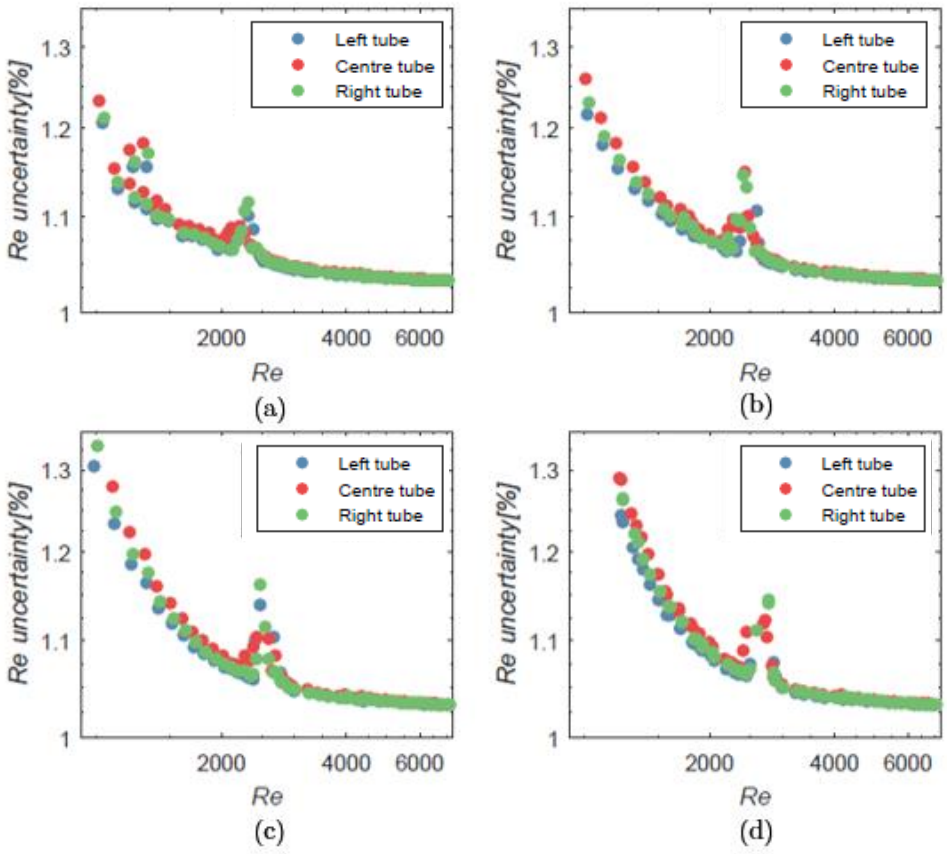

*Figure 18: Reynolds number uncertainties for the multi-tube test section with a pitch of 1.25: (a) Isothermal case (b)*2 kW/m^2 *heat flux(c)* 3 kW/m^2 *heat flux (d)* 4 kW/m^2 *heat flux.*

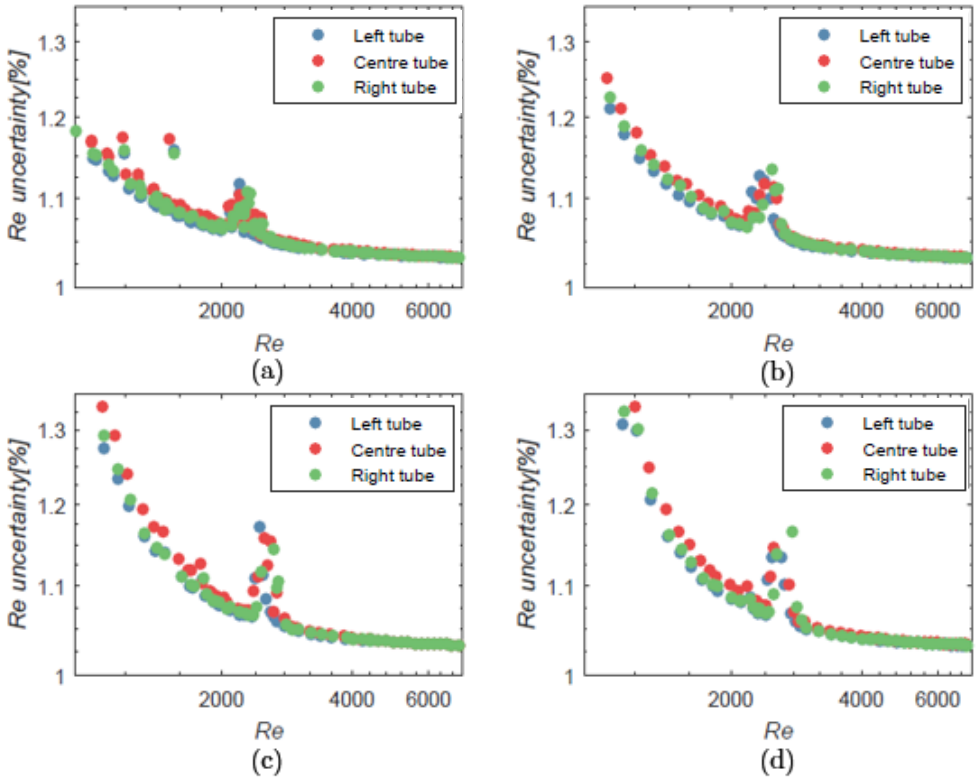

*Figure 19: Reynolds number uncertainties for the multi-tube test section with a pitch of 1.5: (a) Isothermal case (b)*2 kW/m^2 *heat flux(c)* 3 kW/m^2 *heat flux (d)* 4 kW/m^2 *heat flux.*

3.10.4.4 Friction factor

The uncertainty of the friction factor is dependent on the uncertainty of the fluid density, diameter of the test section, mass flow rate, measured pressure drop and the distance over which it is measured. Friction factor can be determined from Equation 3.13:

$$f = \frac{\rho \Delta P D^5 \pi^2}{8 \dot{m}^2 L} \tag{3.13}$$

Which means the uncertainty associated with the friction factor is determined from:

$$\delta f = \frac{\pi^2}{8}\left[\left(\frac{\Delta P D^5}{\dot{m}^2 L}\delta\rho\right)^2 + \left(\frac{\rho D^5}{\dot{m}^2 L}\delta\Delta P\right)^2 + \left(\frac{5\rho\Delta P D^4}{\dot{m}^2 L}\delta \mathrm{D}\right)^2 + \left(-\frac{2\rho\Delta P D^5}{\dot{m}^3 L}\delta\dot{m}\right)^2 + \left(-\frac{\rho\Delta P D^5}{\dot{m}^2 L^2}\delta L\right)^2\right]^{0.5} \tag{3.14}$$

The calculated friction factor uncertainties were plotted against Reynolds number in Figure 18 and Figure 19. Furthermore, the friction factor uncertainties for the different flow regimes are summarized in Table 6 and Table 7 for the pitch of 1.25 and 1.5, respectively.

Heat flux	Flow regime	Left tube	Centre tube	Right tube
0 kW/m²	Laminar	9.58%-10.43%	9.29%-10.07%	9.29%-10.03%
	Turbulent	9.30%-9.36%	9.01%-9.07%	9.01%-9.02%
2 kW/m²	Laminar	9.76%-11.84%	9.43%-11.33%	9.40%-11.12%
	Turbulent	9.30%-9.36%	9.01%-9.07%	9.01%-9.06%
3 kW/m²	Laminar	9.78%-12.33%	9.48%-13.42%	9.43%-12.99%
	Turbulent	9.30%-9.38%	9.01%-9.09%	9.01%-9.08%
4 kW/m²	Laminar	9.97%-13.87%	9.65%-12.70%	9.66%-12.48%
	Turbulent	9.30%-9.37%	9.01%-9.08%	9.01%-9.08%

Table 8: Uncertainties of friction factors for the multi-tube test section with a pitch of 1.25.

Heat flux	Flow regime	Left tube	Centre tube	Right tube
0 kW/m²	Laminar	9.52%-10.31%	9.25%-10.12%	9.25%-10.15%
	Turbulent	9.30%-9.35%	9.01%-9.06%	9.01%-9.06%
2 kW/m²	Laminar	9.79%-12.38%	9.33%-11.24%	9.44%-11.03%
	Turbulent	9.30%-9.35%	9.01%-9.06%	9.01%-9.06%
3 kW/m²	Laminar	9.82%-13.18%	9.60%-12.72%	9.56%-12.64%
	Turbulent	9.30%-9.41%	9.01%-9.06%	9.01%-9.07%
4 kW/m²	Laminar	10.03%-17.88%	9.70%-15.54%	9.63%-15.54%
	Turbulent	9.30%-9.39%	9.01%-9.08%	9.01%-9.08%

Table 9: Uncertainties of friction factors for the multi-tube test section with a pitch of 1.5.

The uncertainty associated with friction factor increases for increasing heat fluxes. A sensitivity study revealed that the third term of Equation 3.14, which accounts for the uncertainty of the tube diameter, is responsible for 93% of the total friction factor uncertainty. Uncertainties increased for decreasing Reynolds numbers, due to the inaccuracies associated with measuring lower pressures.

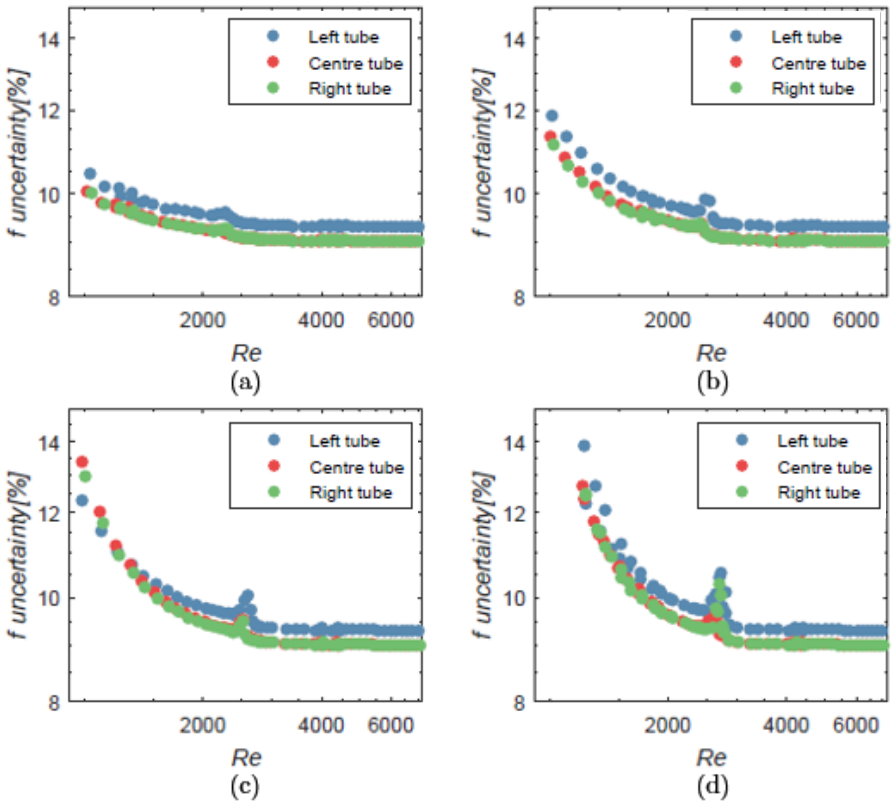

Figure 20: Friction factor uncertainties for the multi-tube test section with a pitch of 1.25: (a) Isothermal case (b) 2 kW/m^2 *heat flux(c)* 3 kW/m^2 *heat flux (d)* 4 kW/m^2 *heat flux.*

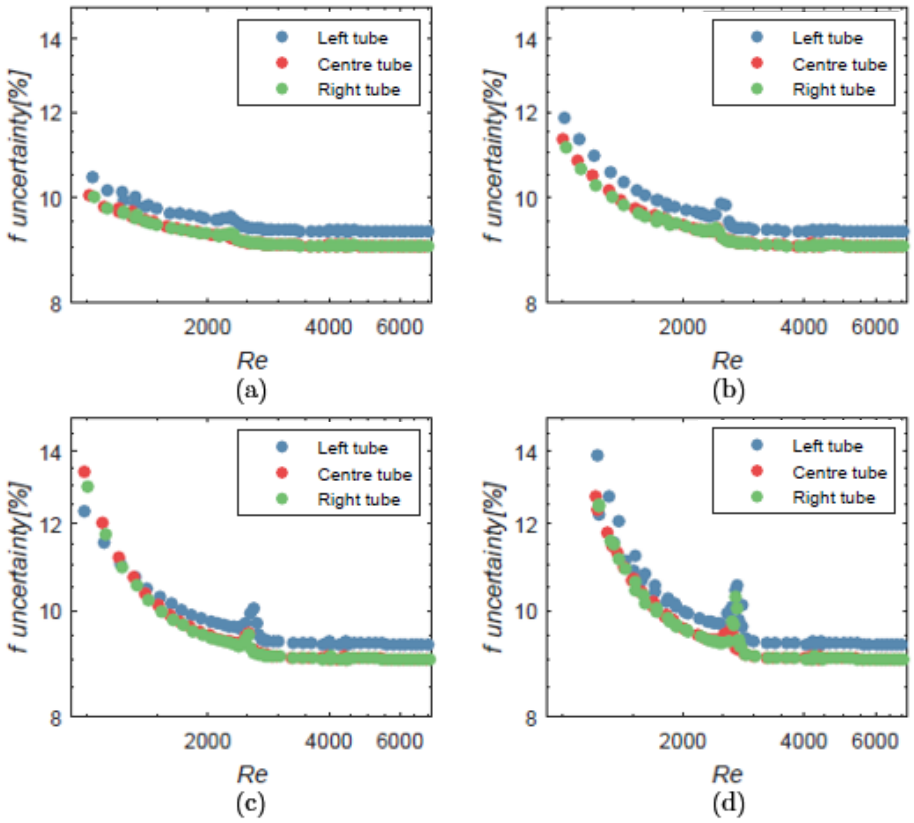

Figure 21: Friction factor uncertainties for the multi-tube test section with a pitch of 1.5: (a) Isothermal case (b) 2 kW/m^2 *heat flux(c)* 3 kW/m^2 *heat flux (d)* 4 kW/m^2 *heat flux.*

3.11 Conclusion

The purpose of this chapter was to document the experimental work conducted in the investigation into pressure drop in smooth tubes with a multi-tube inlet configuration. An overview was given of the experimental plant built to accommodate both the single-tube and multi-tube test setup.

A calming section, based on the work of Tam and Ghajar (1994), was built to dampen out any pulsations created by the pump and to ensure a uniform inlet velocity profile is achieved for each tube. Both the single-tube and multi-tube setup consisted of seamless stainless steel tubes with an inner diameter of 4 mm and a length of 6 m. The tubes were slid into the calming section and fixed into position using a mechanical seal. An endoscope was used to ensure that the tubes were flush with the endcap, producing a square edge inlet.

The single-tube test section was used to validate the experimental setup, and was later used as a reference when comparing the effect of different tube pitch ratios. The multi-tube test section was used to test two different pitch ratios based on the outer diameter of the tubes, namely 1.25 and 1.5. These two pitch ratios were chosen as they represent the lower and upper limit of the range of pitch ratios most commonly used in shell-and-tube heat exchangers.

Using water as a test fluid, experiments were conducted for Reynolds numbers ranging from 1 000 to 7 000, ensuring that the laminar, transitional, and turbulent flow regimes are captured. Tests were repeated for three uniform heat fluxes, with 2 kW/m^2, 3 kW/m^2, and 4 kW/m^2 being applied to the tubes using direct current heating. The inlet temperature was measured using a PT100 probe in the calming section and outlet temperatures were measured in mixing blocks located at the outlet of each tube. The test section was insulated between the two points where temperatures are measured to ensure minimal losses to the environment. Differential pressure was measured across two pressure taps in the fully developed portion of the test sections using variable reluctance pressure transducers with interchangeable diaphragms.

The methods used to process data into meaningful results were then briefly discussed, followed by a detailed uncertainty analysis based on the work presented by Dunn (2010). The uncertainty associated with Reynolds numbers did not increase for increasing heat fluxes, and remained below 1.4% for all heat fluxes and pitch ratios, which means that critical Reynolds numbers can be predicted very accurately. However, the uncertainties of friction factors were found to increase sharply, for increasing heat fluxes. A sensitivity study revealed that the uncertainty of the tube diameter is responsible for 93% of the total friction factor uncertainty. Even though instrument grade tubes, manufactured to extremely fine tolerances, were used, the small diameter required to achieve fully-developed flow across all flow regimes lead to friction factor uncertainties of 9%-14%. This was due to the relatively large ratio of tube tolerance to tube diameter.

Chapter 4: Validation

4.1 Introduction

The experimental setup must be verified to ensure that the study produces reliable results. A single tube heat exchanger was built for validation purposes, since reliable pressure drop correlations are readily available in various published journals. The reliability of pressure drop data was affirmed by plotting friction factors as a function of Reynolds numbers and then comparing them to the correlations in Table 2.

4.2 Isothermal friction factors

Initially, measurements were taken without the addition of heat, to eliminate buoyancy and viscosity variations. As discussed in Section 3.4, pressure drop measurements were taken across the last third of the test section, where fully developed flow was expected for the laminar, transitional, and turbulent flow regimes. Outlet effects were avoided by placing the last pressure tap sufficiently far away from the outlet of the test section. Fully developed isothermal friction factors were validated by considering 77 data points, for Reynolds numbers ranging from 1 000 to 7 000, to ensure that the entire transitional region was captured. With transition expected to occur at a Reynolds number of roughly 2 300, the chosen range ensured that a large portion of the laminar, as well as the turbulent regime was recorded in the study. The isothermal friction factors are shown in Figure 22.

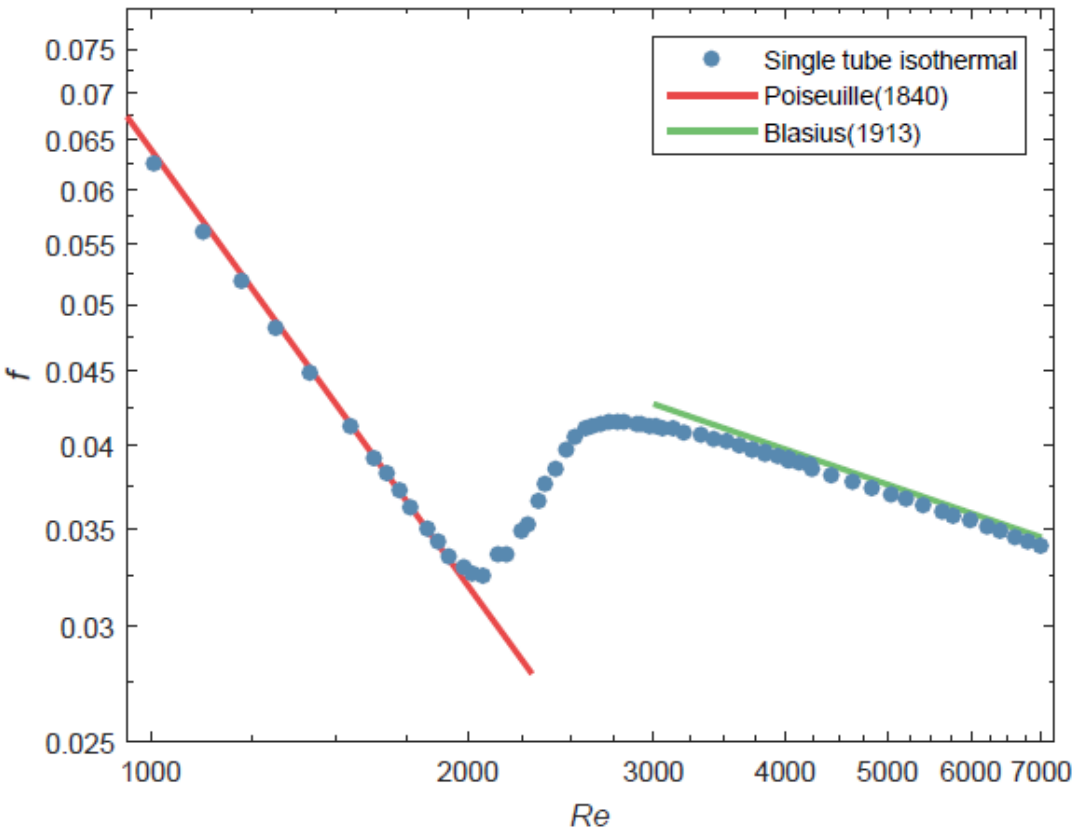

Figure 22: Single tube isothermal friction factors for Reynolds numbers ranging from 1 000-7 000.

The laminar results, which consisted of 17 points within the Reynolds number range of 1 000 to 2 100, were compared to the Poiseuille (1840) correlation, valid for fully developed flow. With the entry lengths expected to range from 1.4 m to 3.36 m this regime, fully developed flow was achieved for all laminar Reynolds numbers since pressure was measured at distances of 4 m and 5.5 m from the inlet. The results in the laminar region deviated from the theoretical values by an average of 1.7%, with the maximum deviation of 1.8% occurring at a Reynolds number of 1 006.

The turbulent measurements, consisting of 34 points within the Reynolds number range of 3 500 to 7 000, were compared to the Blasius (1913) equation, valid for isothermal fully developed turbulent flow. For turbulent flow, entry lengths are independent of Reynolds number and are considerably shorter than that of the laminar region. Thus, fully developed flow was achieved for all measurements in the turbulent flow regime. On average, the turbulent friction factors were within 1.3% of the Blasius correlation, with a maximum deviation of 2.1% occurring at a Reynolds number of 3 517.

4.3 Diabatic friction factors

Fully developed diabatic friction factors were validated by considering 82 data points, for decreasing Reynolds numbers ranging from 7 000 to 1 000. The chosen range includes the laminar, transitional, and turbulent flow regimes. Pressure drop measurements were taken for decreasing Reynolds numbers to minimize the amount of residual heat stored in the insulation. The test section was heated uniformly by applying a constant heat flux of 3 kW/m^2. The results, summarized in Figure 23, were then compared to the Poiseuille (1840) and Allen and Eckert (1964) correlations presented in Section 2.8, as well as the experimental results of Mulock-Houwer (2015).

The diabatic laminar results, which consisted of 13 points within the Reynolds number range of 1 000 to 2 300, were compared to the Poiseuille (1840) correlation. Diabatic friction factors in the laminar region followed the slope of this correlation and decreased linearly for increasing Reynolds numbers. The start of transition was significantly delayed by the addition of the 3 kW/m^2 heat flux, with transition occurring at a Reynolds number of 2 353, compared to a critical Reynolds number of 2 067 for the isothermal case. This supported the findings of previous studies summarized in Section 2.8, which concluded that heating tends to delay the start of transition.

In the laminar region, diabatic friction factor results deviated from the Poiseuille (1840) correlation by an average of 2.0%, with the maximum deviation of 2.4% occurring at a Reynolds number of 1 374. These deviations were somewhat larger than those of the isothermal study, and showed a slight downward shift of friction factors with the addition of heat. This is supported by previous studies conducted Tam *et al.* (2013) and Meyer and Olivier (2011) that showed that an increase in heat flux resulted in a decrease in friction factor in the laminar flow regime, because of secondary flow effects.

The diabatic turbulent measurements, consisting of 32 points within the Reynolds number range of 3 200 to 7 000, were compared to the modified Blasius equation, as presented by Allen and Eckert (1964). This correlation accounts for the difference in viscosity between the tube wall and the centre of the tube, brought about by the resulting temperature gradient, when the tube is heated uniformly. On average, the turbulent diabatic friction factors were within 1.5% of the Allen and Eckert (1964) correlation, with a maximum deviation of 3.3% occurring at a Reynolds number of 3 310. The experimental results for the laminar, transitional, and turbulent flow regimes correlated very well with the results obtained by Murlock-Houwer (2016), which also used a constant heat flux of 3 kW/m^2.

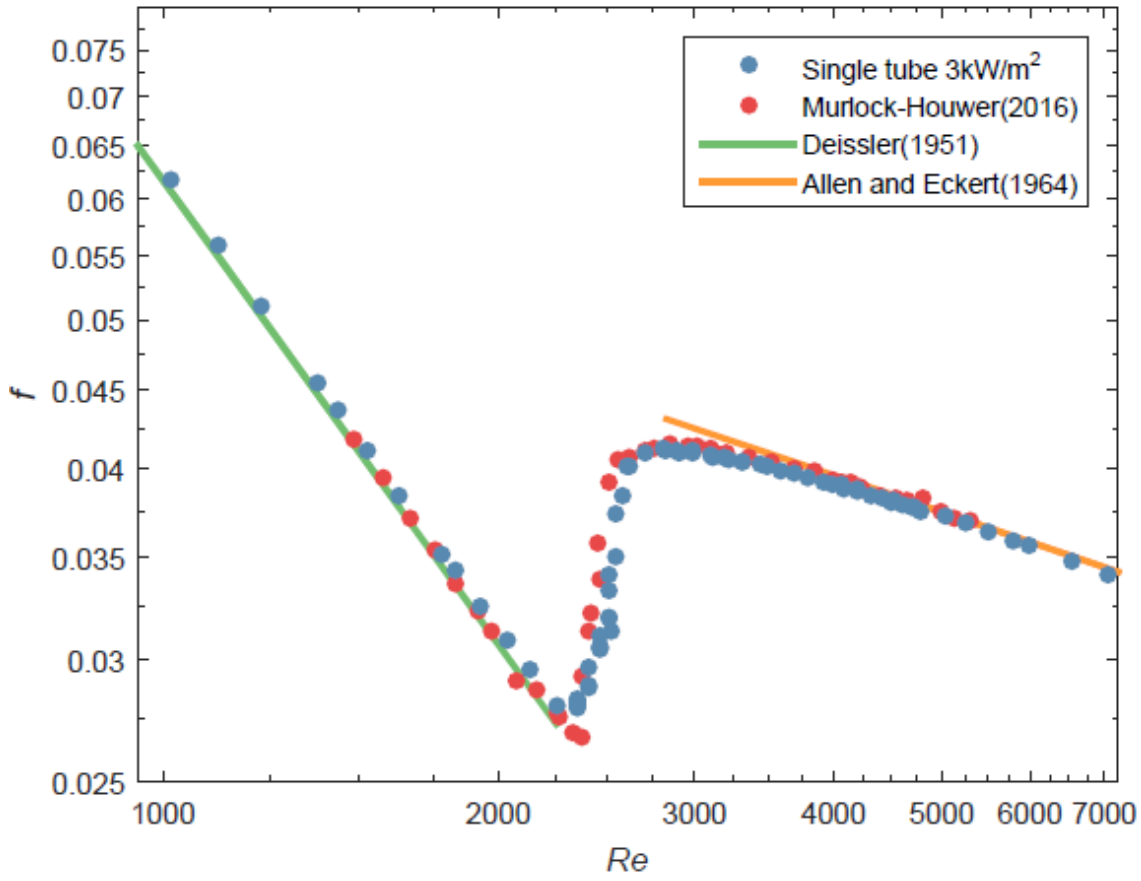

Figure 23: Single tube diabatic friction factors for Reynolds numbers ranging from 1 000 to 7 000, with a constant heat flux of 3 kW/m^2.

4.4 Conclusion

The experimental setup and data reduction methods were verified in this chapter. A single tube heat exchanger was used for validation, since reliable pressure drop correlations are readily available in literature. The pressure drop was measured across the last third of the test section to ensure that fully developed friction factors were measured for the laminar, transitional, and turbulent flow regimes. Outlet effects were avoided by placing the last pressure tap more than 100 diameters upstream of the tube exit.

Isothermal friction factors were validated first and were found to correlate well with literature in both the laminar and turbulent flow regimes. The results in the laminar region deviated from the Poiseuille (1840) correlation by an average of 1.7%, while the results in the turbulent regime were within 1.3% of the Blasius correlation. The onset of transition occurred at a Reynolds number of 2 067.

The diabatic friction factors were validated by taking pressure drop measurements for decreasing Reynolds numbers, whilst the test section was being heated uniformly with a constant heat flux of 3 kW/m^2. The diabatic friction factor results showed a delay in the start of transition when compared to that of the isothermal results, with transition only starting at a Reynolds number of 2 353. In the laminar and transitional flow regimes, the addition of heat resulted in lower friction factors, due to buoyancy effects associated with secondary flow. The diabatic friction factors in the laminar region deviated from the Poiseuille (1840) correlation by an average of 2.0%, while the results in the turbulent flow regime were within 1.5% of the Allen and Eckert (1964) correlation.

The experimental results for the laminar, transitional, and turbulent flow regimes were almost identical to the results obtained by Mulock-Houwer (2016), who also used a constant heat flux of 3 kW/m^2. Transition occured at a Reynolds number of 2 353 compared to a critical Reynolds number of 2 380 found by Mulock-Houwer (2016).

It was therefore reasonable to conclude that the experimental tools and procedures used to produce data are reliable, and will yield accurate measurements for different heat fluxes and mass flow rates. Using similar equipment and processes to produce the multi-tube results, presented in Chapters 5 and 6, would therefore most probably yield reliable results.

Chapter 5:
Isothermal friction factor results

5.1 Introduction

The conditions of the single-tube study, used for validation purposes in Chapter 4, were replicated for the multi-tube setup to investigate the effect of the pitch ratio between adjacent tubes on isothermal friction factors in the transitional flow regime. For this study, three identical stainless steel tubes with square-edged inlets, as presented in Chapter 3, were spaced horizontally at a pitch of 1.25 times the outer diameter of the tubes, or 7.5 mm. Fully developed pressure drop measurements were taken for Reynolds numbers ranging from 1 000 to 7 000, without the addition of heat, to eliminate buoyancy and viscosity variations. The horizontal tube pitch spacing was then changed to 1.5 times the tube outer diameter, or 9 mm, and the measurements were repeated. In this chapter, isothermal friction factor data recorded for the two different pitch ratios are presented as a function of Reynolds number, and plotted against the single tube data from Chapter 4.

5.2 Isothermal friction factors for a pitch of 1.25

The isothermal friction factors determined for the multi-tube test section with a pitch of 1.25, or a centre-to-centre spacing of 7.5 mm, are summarised in Figure 24. Also included in this figure, are the single tube results used for validation purposes in Chapter 4. The multi-tube results are presented per the convention established in Figure 9, regarding the notation of left tube, centre tube, and right tube.

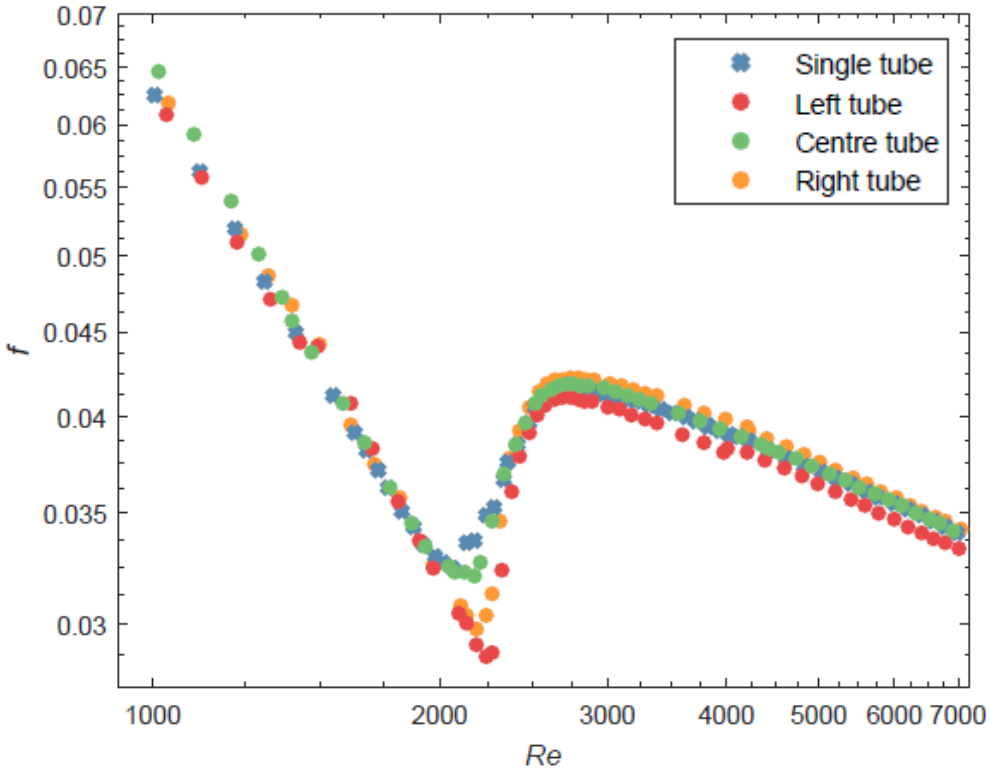

Figure 24: Multi-tube isothermal friction factors as a function of Reynolds number, for a horizontal pitch of 1.25, compared to the isothermal friction factor results for the single tube test section.

5.2.1 Laminar isothermal friction factors for a pitch of 1.25

From Figure 24, it is evident that the measurements within the Reynolds number range of 1 000 to 2 000 are laminar, as friction factors decreased for increasing Reynolds numbers, for both the single-tube and multi-tube data. This region was analysed further in order to investigate the influence of the pitch on laminar isothermal friction factors.

The multi-tube data in this regime correlated well with the single-tube data collected for validation purposes, with all data points falling well within the friction factor uncertainty of 9.3%. Closer inspection revealed that the left tube deviated from the single tube data by an average of +2.2%, with a maximum deviation of -5.6% occurring at a Reynolds number of 1 998. The right tube deviated by an average of +2.1%, with a maximum deviation of +5.7% occurring at a Reynolds number of 1 428.

The centre tube results correlated the best out of the three tubes, when compared to the single-tube data, with an average deviation of +1.5% and a maximum deviation of +4.9% occurring at a Reynolds number of 1 015.

5.2.2 Turbulent isothermal friction factors for a pitch of 1.25

Measurements for Reynolds numbers between 3 600 and 7 000 were considered to be turbulent for the purpose of this discussion. The turbulent isothermal friction factors for the multi-tube setup correlated well with the single-tube results. The data collected for the centre tube were nearly identical to that of the single-tube setup, with an average deviation of +0.3% and a maximum deviation of +0.4% occurring at a Reynolds number of 4 147. Isothermal friction factors collected for the left and right tube deviated slightly more, with the left tube deviating with an average of -2.2% and a maximum of -2.9% at a Reynolds number of 4 386. The right tube deviated from the single-tube results by an average of +1.3% and a maximum of +2.5% at a Reynolds number of 4 500.

5.2.3 Transitional isothermal friction factors for a pitch of 1.25

The isothermal friction factors that fall within the transitional flow regime are plotted in Figure 25, for both the single-tube and multi-tube setup. The start of transition is characterized by a sharp increase in friction factor, as the flow rate is increased and flow moves out of the laminar region. The critical Reynolds number, or the point at which transition starts, is highlighted in Figure 25 for both the single-tube and multi-tube setup.

As discussed in Chapter 4, transition occurred at a Reynolds number of 2 067 for the single-tube test section. The centre tube of the multi-tube setup closely followed the behaviour of the single tube, with transition occurring slightly later, at a critical Reynolds number of 2119. The left and right tubes of the multi-tube setup experienced a significant delay in transition when compared to the single tube, with critical Reynolds numbers of 2 236 and 2 189, respectively.

A trend line was added to the transitional friction factors of each tube, to highlight the gradient of transition. From this, it is evident that the three tubes of the multi-tube setup experienced a sharper transition than the single tube setup. The gradient of transition of the centre tube was only slightly sharper than that of the single tube and much less steep than the left and right tube. The left and right tube of the multi-tube setup had identical gradients.

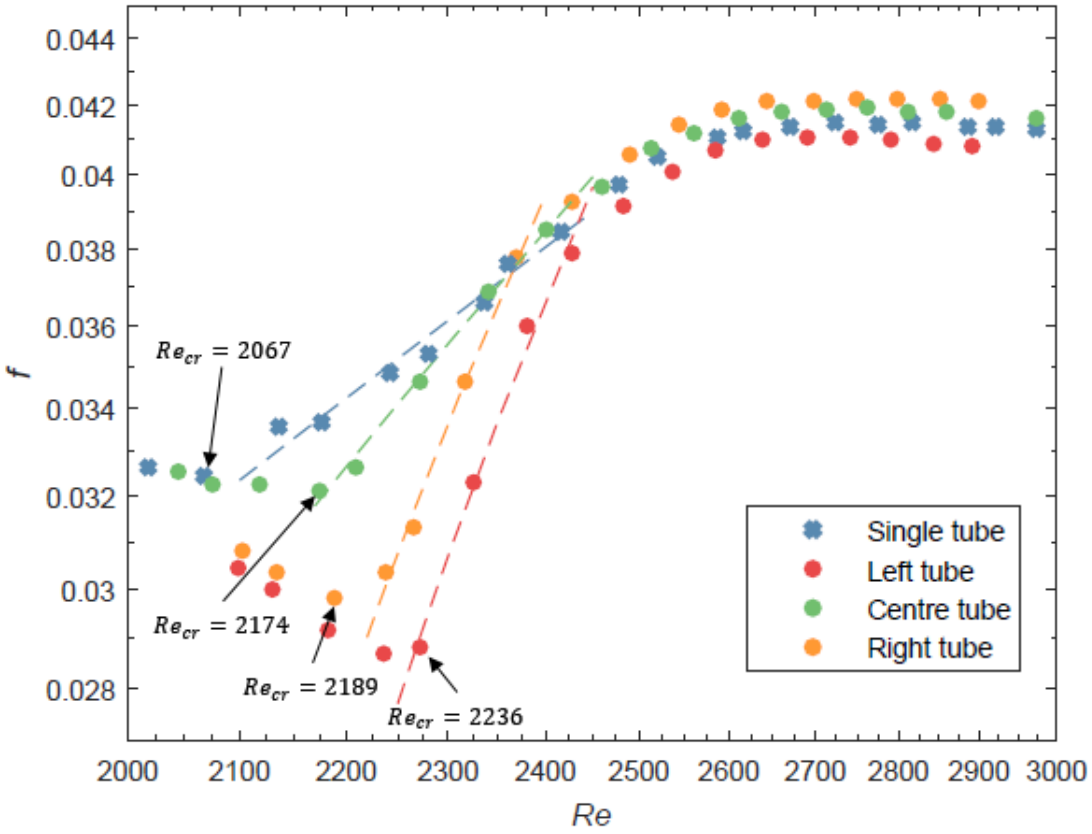

Figure 25: Multi-tube isothermal friction factors in the transitional flow regime, as a function of Reynolds number, for a horizontal pitch of 1.25, compared to the isothermal friction factor results for the single tube test section.

5.3 Isothermal friction factors for pitch of 1.5

The isothermal friction factors determined for the multi-tube test section with a pitch of 1.5, or a centre-to-centre spacing of 9 mm, are summarised in Figure 26. Included in this figure, are the single tube results of Chapter 4.

5.3.1 Laminar isothermal friction factors for pitch of 1.5

The measurements that fell between Reynolds numbers of 1 000 and 2 000 were considered to be fully laminar. Once again, the multi-tube data in the laminar regime correlated well with the single tube results presented in Chapter 4.

The centre tube deviated from the single tube data by an average of -1.8%, with a maximum deviation of -3.2% occurring at a Reynolds number of 1 933. The left tube had an average deviation of +2.9%, and a maximum deviation of +4.8%, which occurred at a Reynolds number

of 1 025. The right tube correlated to within an average of -1.3% of the single tube results, with a maximum deviation of -3.0% occurring at a Reynolds number of 1 971.

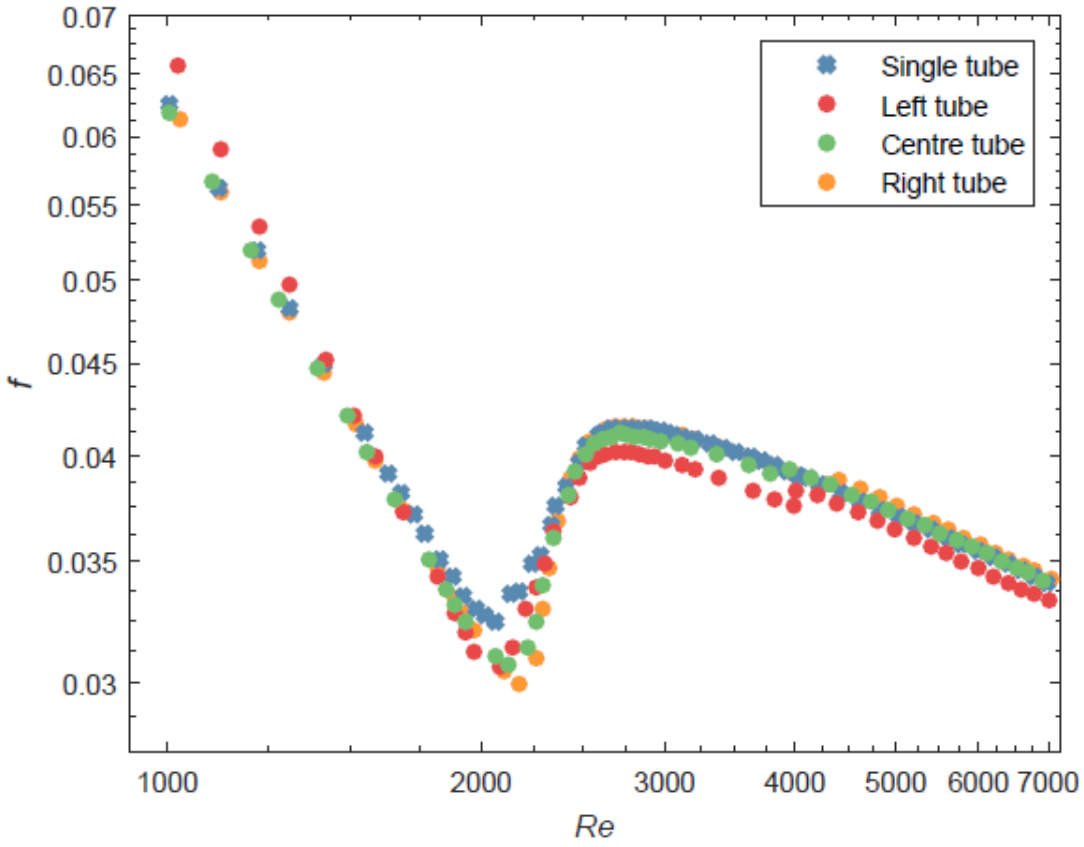

Figure 26: Multi-tube isothermal friction factors as a function of Reynolds number, for a horizontal pitch of 1.5, compared to the isothermal friction factor results for the single tube test section.

5.3.2 Turbulent isothermal friction factors for pitch of 1.5

The same range of Reynolds numbers were chosen for the turbulent analysis, namely 3 600 to 7 000. The turbulent isothermal friction factors for the multi-tube setup correlated well with single tube data. The centre tube data barely deviated from the single tube results, with an average deviation of +0.44%, and a maximum deviation of +1.3% at a Reynolds number of 3 609. The right tube deviated from the single tube data by an average of +0.90%, with a maximum deviation of +2.5% occurring at a Reynolds number of 4 018. Once again, the isothermal friction factors collected for the left tube deviated slightly more than the rest, with an average deviation of -2.4% and a maximum deviation of -4.2%, at a Reynolds number of 3 641.

5.3.3 Transitional isothermal friction factors for pitch of 1.5

The isothermal friction factors that fall within the transitional flow regime are plotted in Figure 27, for both the single-tube and multi-tube setup, and the critical Reynolds numbers are indicated for comparative purposes.

The multi-tube setup, with a pitch of 1.5, closely followed the transitional behaviour of single tube. All three tubes of the multi tube setup again experienced a delay in transition when compared to the single tube results. However, this delay was a lot less significant for the test section with a larger pitch. The centre tube experienced the onset of transition at a Reynolds number of 2 129, whilst the left and right tubes had critical Reynolds numbers of 2 086 and 2 176, respectively.

Trend lines were added to the transitional friction factors of each tube, to better investigate the gradient of transition. Even though the multi-tube setup, with a pitch of 1.5, experienced a slightly sharper transition when compared to the single tube, the difference in transition gradient was not as evident as with the smaller pitch, as summarized in Table 10.

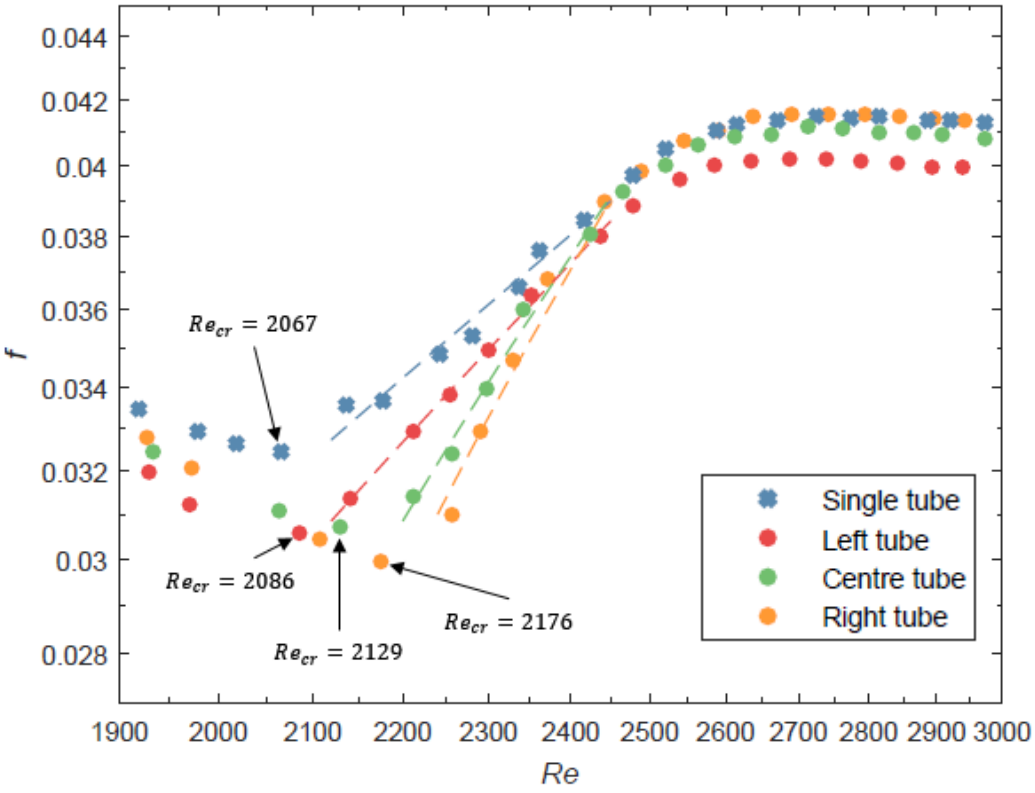

Figure 27: Multi-tube isothermal friction factors, in the transitional flow regime, for a horizontal pitch of 1.5, compared to the isothermal friction factor results for the single-tube test section.

5.4 Summary and conclusion of isothermal friction factor results

This chapter discussed the results from an investigation into the effect of the horizontal pitch ratio between tubes on isothermal friction factors in the transitional flow regime. For this study, three identical stainless steel tubes with square-edged inlets, as presented in Chapter 3, were spaced horizontally at pitches of 1.25 and 1.5 times the outer diameter of the tubes. Isothermal friction factor data were produced from fully developed pressure drop measurements, taken for Reynolds numbers ranging from 1 000 to 7 000. The results for the two different pitch ratios were plotted against Reynolds numbers, and compared against isothermal friction factor data from the single-tube setup, used for validation purposes in Chapter 4.

5.4.1 Laminar and turbulent results

The results that fall within the laminar, and turbulent flow regimes are summarized in Table 10. The laminar data produced for all three tubes of the multi-tube setup correlated well with the single tube data, for both the 1.25 and 1.5 pitch ratio. The turbulent results for the two pitch ratios also showed very little difference, when compared to that of the single tube setup. A sudden jump in friction factor can be observed in the data collected for each tube, at a Reynolds number of roughly 4000. This abrupt change can be attributed to the changing of diaphragms in the variable reluctance pressure transducer. At this point, the low-pressure diaphragm is exchanged for a high-pressure diaphragm, resulting in reduced measurement accuracy, which is dependent on the full-scale pressure value of each diaphragm. Both the laminar and the turbulent results fell within the calculated friction factor uncertainty of roughly 9.2%. From the results shown in Figure 24 and Figure 26, as well as the summary presented in Table 10, it is evident that both the laminar and turbulent isothermal friction factors are hardly influenced by the different inlet pitch ratios, since the results are nearly identical to that of the single tube. This coincides with the findings of Meyer (2010) and Ghajar and Tam (1994).

	Deviation in friction factors					
	Pitch 1.25			Pitch 1.5		
	Left tube	Centre tube	Right tube	Left tube	Centre tube	Right tube
Laminar	+2.33%	+1.54%	+2.15%	+2.94%	-1.81%	-1.28%
Turbulent	+2.19%	+0.26%	-1.33%	-2.41%	+0.44%	+0.90%

Table 10: Comparison of the average deviation of laminar and turbulent isothermal friction factors for the multi-tube test setup, for pitch ratios of 1.25 and 1.5, compared to the single-tube setup.

5.4.2 Transitional results

The isothermal friction factor results for the three tubes of the multi-tube setup, shown in Figure 25 and Figure 27, exhibits a significant delay in transition, compared to the singe-tube setup. The delay in transition from laminar to turbulent flow experienced by the multi-tube setup, was more significant for the pitch of 1.25, where the tubes are spaced closer together, than for the pitch of 1.5. The three tubes of the multi-tube setup also underwent a more abrupt transition from laminar to turbulent flow, leading to sharper transition gradients. The test section with a pitch of 1.25 experienced a sharper transition than the setup where the tubes were spaced further apart, at a pitch of 1.5. The end of transition appeared to remain largely unaffected for both tube inlet pitch ratios, as transition ended in a relatively small band of Reynolds numbers, close to that of the single tube.

Setup configuration		Start of transition	End of transition	Transition gradient
Single tube		Re = 2 067	Re = 3 059	1.9×10^{-5}
Pitch 1.25	Left tube	Re = 2 236	Re = 3 093	5.9×10^{-5}
	Centre tube	Re = 2 174	Re = 3 060	2.9×10^{-5}
	Right tube	Re = 2 189	Re = 3 103	5.8×10^{-5}
Pitch 1.5	Left tube	Re = 2 086	Re = 3 113	2.3×10^{-5}
	Centre tube	Re = 2 129	Re = 3 083	3.3×10^{-5}
	Right tube	Re = 2 176	Re = 3 118	3.8×10^{-5}

Table 11: Comparison of critical Reynolds numbers and transitional gradients for the single-tube setup, and the multi-tube setup with pitch ratios of 1.25 and 1.5.

Chapter 6:
Diabatic friction factor results

6.1 Introduction

Each of the three tubes used for the isothermal study were connected to its own power supply, and heated via direct current. For this diabatic study, pitch ratios of 1.25 and 1.5, based on the outer diameter of the tubes, were investigated by taking fully developed pressure drop measurements for Reynolds numbers ranging from 1 000 to 7 000, with uniform heat fluxes of 2 kW/m^2, 3 kW/m^2, and 4 kW/m^2 being applied over the entire test section. In this chapter, diabatic friction factor results, recorded for the two different pitch ratios, are presented as a function of Reynolds number and plotted against the single tube data from Chapter 4. The maximum and average deviation of the multi-tube data, compared to the single tube data, were then calculated for the laminar and turbulent regions, in order to investigate the influence of the pitch spacing on the diabatic friction factors in these flow regimes. Critical Reynolds numbers and transition gradients are then determined to investigate the effect of inlet pitch spacing on diabatic friction factors in the transitional flow regime. A summary of diabatic friction factor results are then presented, so that the necessary conclusions can be drawn.

6.2 Diabatic friction factors for a uniform heat flux of 2 kW/m^2

The multi-tube diabatic friction factors for a constant heat flux of 2 kW/m^2 are presented per the convention shown in Figure 9. Included in the figures are results for the single-tube test section heated uniformly with the same heat flux of 2 kW/m^2.

6.2.1 Diabatic friction factors for a pitch of 1.25

The results for the multi-tube setup, spaced horizontally at a pitch of 1.25 times the outer diameter, or 7.5 mm, heated uniformly at a heat flux of 2 kW/m^2, are shown in Figure 28.

6.2.1.1 Laminar diabatic friction factors for the pitch of 1.25

The measurements that fell between Reynolds numbers of 1 000 and 2 000 were considered to be fully laminar. The multi-tube data in the laminar regime correlated well with the single-tube results for the same heat flux. The centre tube deviated from the single tube data by an average of -1.6%, and a maximum deviation of -3.7%, which occurred at a Reynolds number of 1 811. The right tube correlated to within an average of +2.6% of the single tube results, with a maximum deviation of +4.0% occurring at a Reynolds number of 1 851. As with the isothermal results, the left tube had a significantly larger average deviation, of -8.4%, and a maximum deviation of -9.5% occurring at a Reynolds number of 1 205. This indicates that minor geometrical differences could be present in the left tube, such as small variations in pressure tap holes, tube diameter irregularities, or spacing differences between pressure taps.

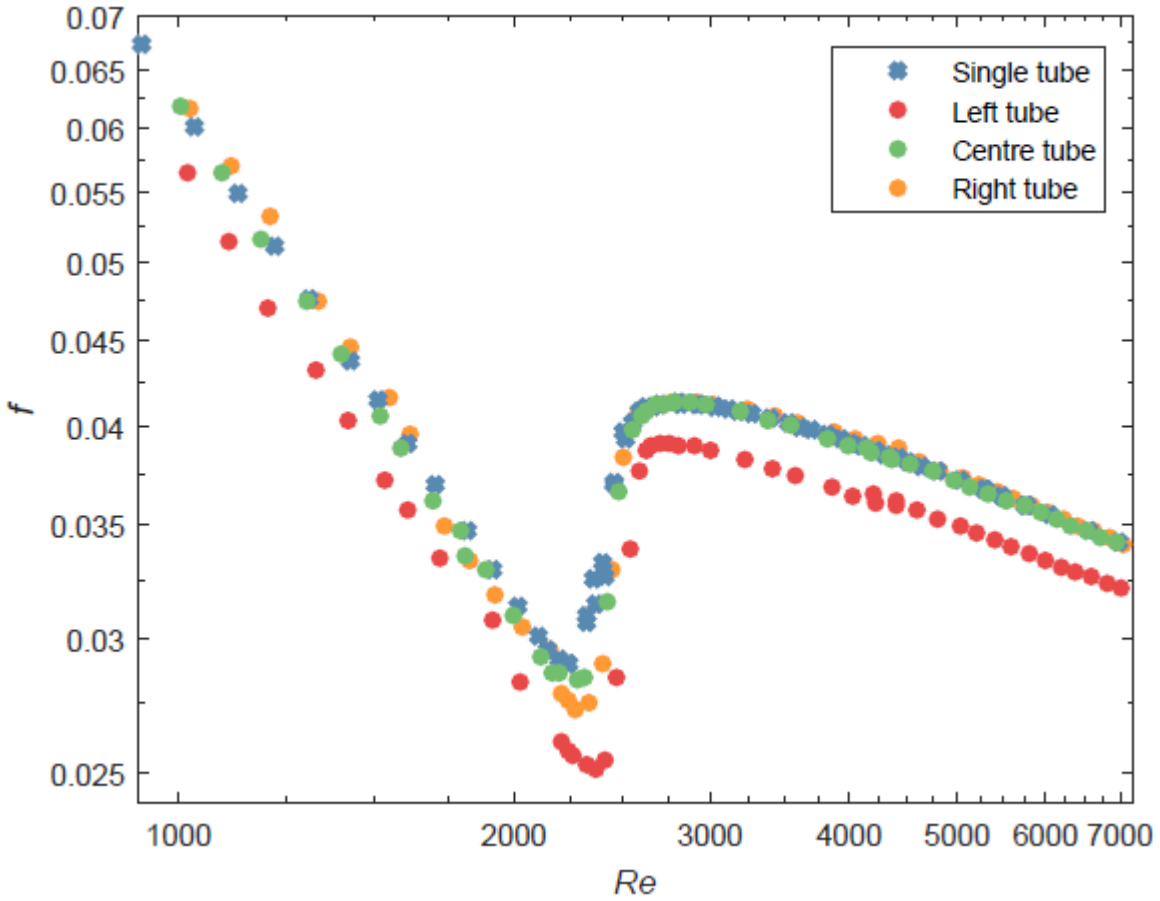

Figure 28: Multi-tube diabatic friction factors as a function of Reynolds number, for a horizontal pitch of 1.25 and a heat flux of 2 kW/m^2*, compared to the diabatic friction factor results for the single-tube test section heated at* 2 kW/m^2*.*

6.2.1.2 Turbulent diabatic friction factors for the pitch of 1.25

As with the isothermal study, Reynolds numbers ranging from 3 600 to 7 000 were chosen for the turbulent analysis. Once again, the diabatic friction factors collected for the left tube deviated slightly more than the rest, with an average deviation of -6.6% and a maximum deviation of -7.4%, at a Reynolds number of 4 036. From Figure 28, it is evident that the centre and right tubes had an almost insignificant deviation from the single tube data. The centre tube had an average deviation of -0.3%, and a maximum deviation of -0.6%, which occurred at a Reynolds number of 4 193. The right tube correlated to within an average of +0.4% of the single tube results, with a maximum deviation of +1.4% occurring at a Reynolds number of 4 433.

6.2.1.3 Transitional diabatic friction factors for the pitch of 1.25

The diabatic friction factors, for a heat flux of 2 kW/m^2 and a pitch of 1.25, that fall within the transitional flow regime are plotted in Figure 29, for both the single-tube and multi-tube setup. The critical Reynolds numbers, or the point at which transition starts, are also highlighted in Figure 29. Transition occurred at a Reynolds number of 2 235 for the single-tube test section.

The three tubes of the multi-tube setup experienced a significant delay in transition, when compared to the single tube, with transition occurring at Reynolds numbers of 2 315, 2 330, and 2 416 for the centre, right, and left tubes respectively.

Transition gradients, illustrated by the trend lines plotted through transitional friction factors, showed that a sharper transition was once again experienced by the tubes of the multi-tube test section. However, the difference in transition gradients was perhaps not as pronounced as with the isothermal study.

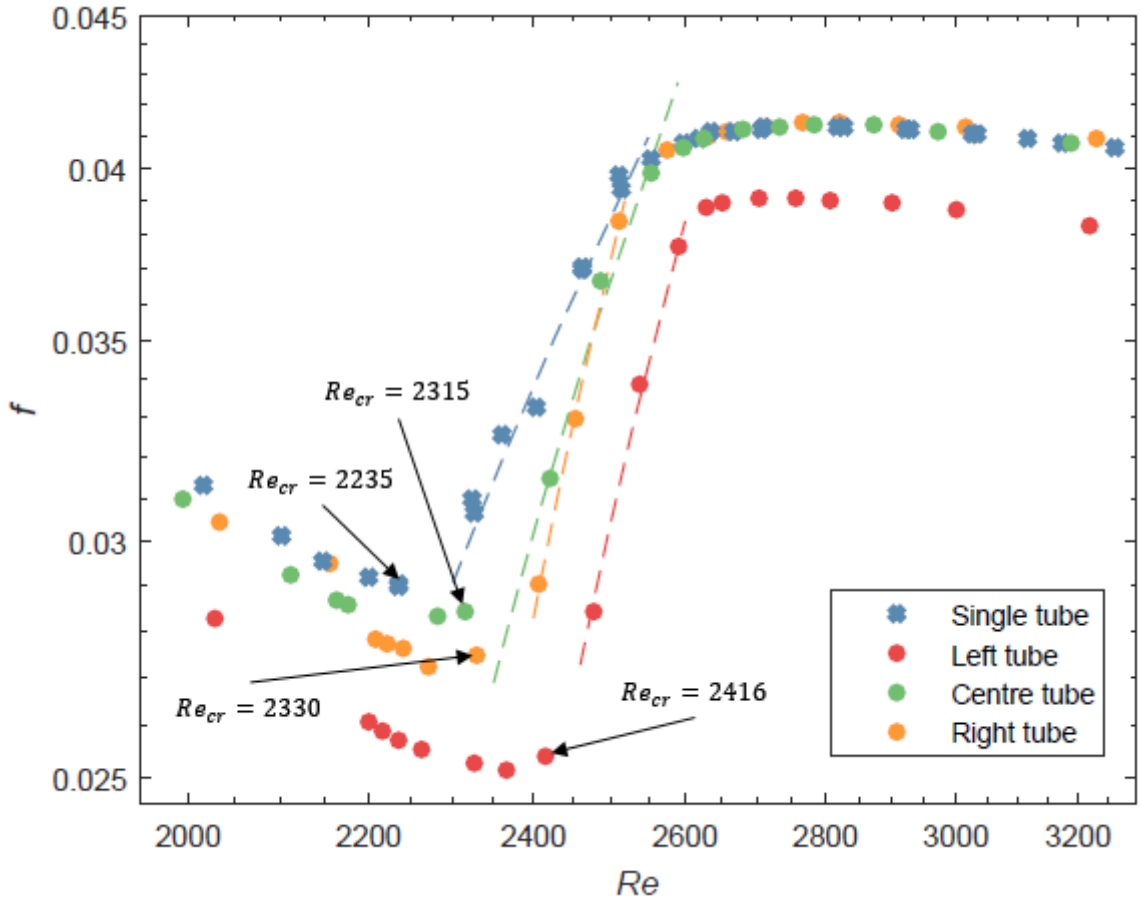

Figure 29: Multi-tube diabatic friction factors in the transitional flow regime, as a function of Reynolds number, for a horizontal pitch of 1.25 and a heat flux of 2 kW/m^2*, compared to the diabatic friction factor results for the single-tube test section heated at* 2 kW/m^2.

6.2.2 Diabatic friction factors for a pitch of 1.5

The results for the multi-tube setup, spaced horizontally at a pitch of 1.5 times the outer diameter, or 9 mm, heated uniformly at a heat flux of 2 kW/m^2, are shown in Figure 30.

6.2.2.1 Laminar diabatic friction factors for the pitch of 1.5

The fully laminar multi-tube measurements for Reynolds numbers between 1 000 and 2 000 were evaluated and compared to single-tube results. The left tube data once again stood out from the rest, with average deviations equal to -7.9%, when comparted to single tube results. A maximum deviation of -9.4% occurred at a Reynolds number of 1 906. The centre tube

correlated better, with an average deviation of -2.1%, and a maximum deviation of -3.5%, which occurred at a Reynolds number of 1 873. The right tube correlated to within an average of -1.7% of the single tube results, with a maximum deviation of -5.2% occurring at a Reynolds number of 1 119. The variations in the left tube results once again points to possible geometrical differences in the tube.

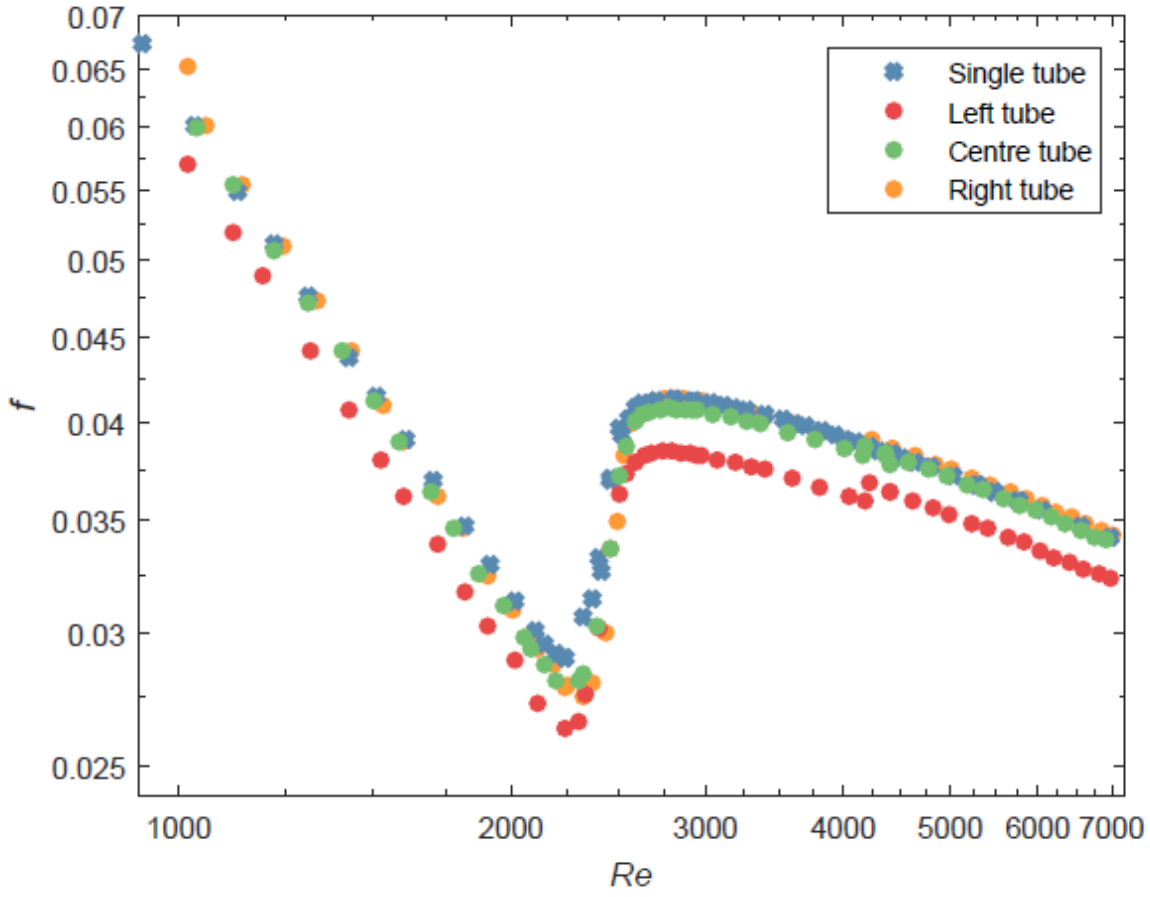

Figure 30:Multi-tube diabatic friction factors as a function of Reynolds number, for a horizontal pitch of 1.5 and a heat flux of 2 kW/m^2*, compared to the diabatic friction factor results for the single-tube test section heated at* 2 kW/m^2*.*

6.2.2.2 Turbulent diabatic friction factors for the pitch of 1.5

Measurements for Reynolds numbers between 3 600 and 7 000 were considered to be turbulent for the purpose of this discussion. The data collected for right and centre tubes were nearly identical to that of single-tube setup. The centre tube had an average deviation of -0.7% and a maximum deviation of -1.5% occurring at a Reynolds number of 3 767, whilst the right tube correlated to within an average of +0.6% of the single tube results, with a maximum deviation of +1% occurring at a Reynolds number of 4 245. The left tube deviated from the single tube data by an average of -6.2%, with a maximum deviation of -8.2% occurring at a Reynolds number of 4 445.

6.2.2.3 Transitional diabatic friction factors for the pitch of 1.5

The diabatic friction factors, for a heat flux of 2 kW/m^2 and a pitch of 1.5, that fall within the transitional flow regime, are plotted in Figure 31 for both the single-tube and multi-tube setup. The critical Reynolds numbers, or the point at which transition starts, are indicated for comparative purposes. As previously mentioned, transition occurred at a Reynolds number of 2 235 for the single-tube test section heated uniformly with a heat flux of 2 kW/m^2. The three tubes of the multi-tube setup experienced a delay in transition, when compared to the single tube, with transition occurring at Reynolds numbers of 2 276, 2 326, and 2 300 for the centre, right, and left tubes respectively. The delay in transition experienced by the setup with a pitch of 1.5 was not as significant as with a pitch of 1.25.

Transitional gradients, illustrated by the trend lines plotted through transitional friction factors, experienced by the multi-tube setup with a pitch of 1.5 are very similar to that of the single tube, indicating that the pitch of 1.5 has less of an influence than the pitch of 1.25, pertaining to the sharpness of transition.

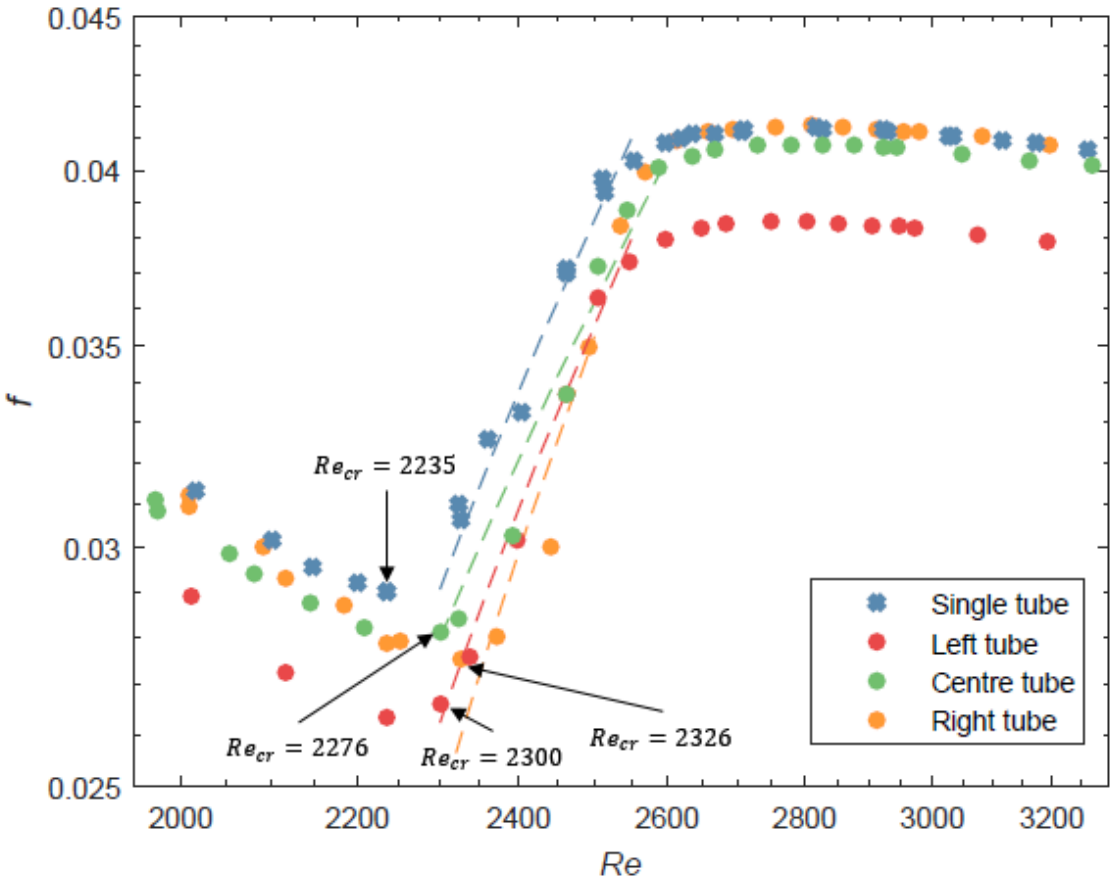

Figure 31: Multi-tube diabatic friction factors in the transitional flow regime, as a function of Reynolds number, for a horizontal pitch of 1.5 and a heat flux of 2 kW/m^2*, compared to the diabatic friction factor results for the single-tube test section heated at* 2 kW/m^2*.*

6.3 Diabatic friction factors for a uniform heat flux of 3 kW/m^2

The multi-tube diabatic friction factors for a constant heat flux of 3 kW/m^2 are presented per the convention established in Section 3.4. Included in the figures are results for the single-tube test section heated uniformly with the same heat flux of 3 kW/m^2.

6.3.1 Diabatic friction factors for a pitch of 1.25

The results for the multi-tube setup, spaced horizontally at a pitch of 1.25 times the outer diameter, or 7.5 mm, heated uniformly at a heat flux of 3 kW/m^2,are shown in Figure 32.

6.3.1.1 Laminar diabatic friction factors for the pitch of 1.25

The measurements that fell between Reynolds numbers of 1 000 and 2 000 were once again taken as laminar. The laminar centre tube results deviated from the single tube data by an average of -1.7%, and a maximum deviation of -2.3% occurred at a Reynolds number of 1 998. The right tube correlated to within an average of +0.8% of the single tube results, with a maximum deviation of +1.2% occurring at a Reynolds number of 1 001. The left tube deviated from the single tube data by an average of -3.5%, with a maximum deviation of -9.6% occurring at a Reynolds number of 1 216.

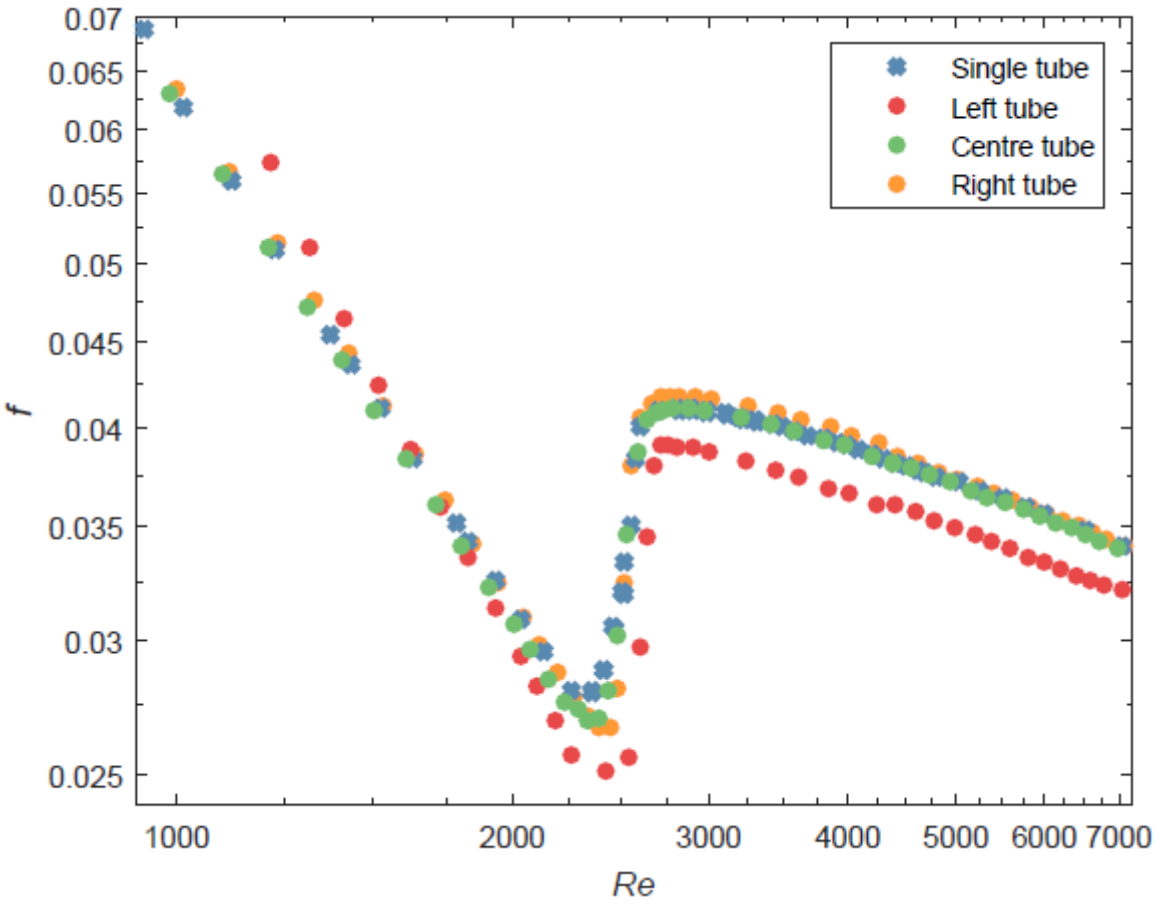

Figure 32: Multi-tube diabatic friction factors as a function of Reynolds number, for a horizontal pitch of 1.25 and a heat flux of 3 kW/m^2, *compared to the diabatic friction factor results for the single-tube test section heated at* 3 kW/m^2.

6.3.1.2 Turbulent diabatic friction factors for the pitch of 1.25

The data used in the turbulent analysis consisted of friction factor measurements for Reynolds numbers ranging from 3 600 to 7 000. Once again, the diabatic friction factors collected for the left tube deviated significantly more, with an average deviation of -6.6%, and a maximum deviation of -7.0% occurring at a Reynolds number of 4 234. The centre tube had an average deviation of -0.4%, and a maximum deviation of -0.6%, which occurred at a Reynolds number of 6 727. The right tube correlated to within an average of +0.8% of the single tube results, with a maximum deviation of +2.2% occurring at a Reynolds number of 4 441.

6.3.1.3 Transitional diabatic friction factors for the pitch of 1.25

The diabatic friction factors, for a heat flux of 3 kW/m^2 and a pitch of 1.25, that fall within the transitional flow regime are plotted in Figure 33, for both the single-tube and multi-tube setup. The critical Reynolds numbers, or the point at which transition starts, are once again highlighted in Figure 33. Transition occurred at a Reynolds number of 2 353 for the single-tube test section.

The three tubes of the multi-tube setup experienced a slight delay in transition, when compared to the single tube, with transition occurring at Reynolds numbers of 2 392, 2 421, and 2 444 for the centre, right, and left tubes respectively. Transition gradients, illustrated by the trend lines plotted through transitional friction factors, show that a slightly sharper transition is experienced by the tubes of the multi-tube test section. The values of transitional gradients are summarized in Table 14.

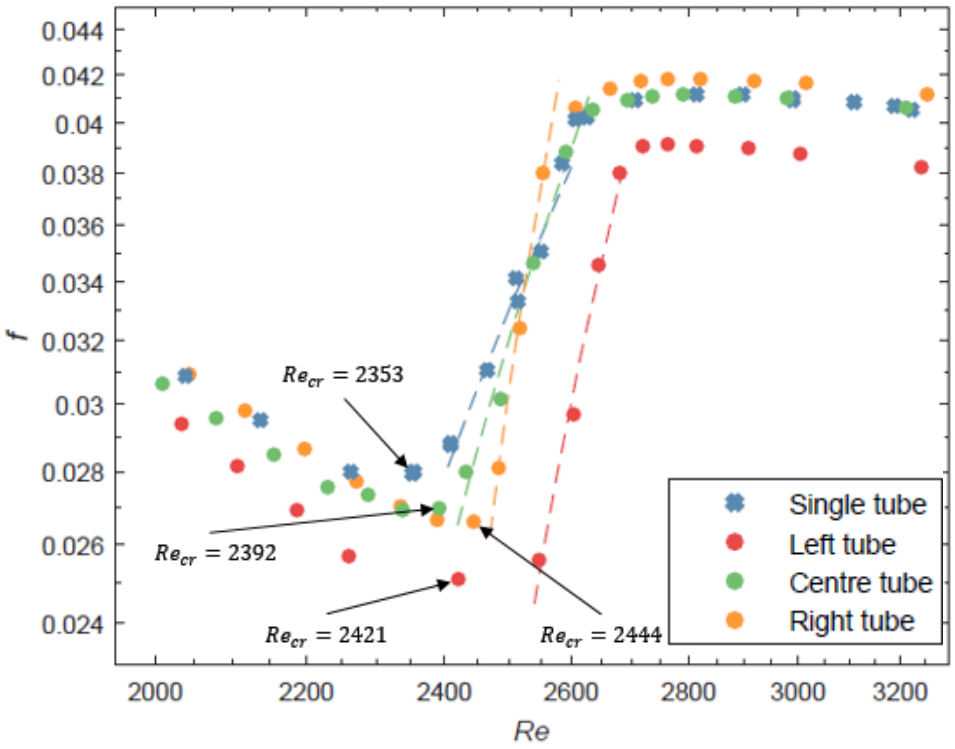

Figure 33: Multi-tube diabatic friction factors in the transitional flow regime, as a function of Reynolds number, for a horizontal pitch of 1.25 and a heat flux of 3 kW/m^2*, compared to the diabatic friction factor results for the single-tube test section heated at* 3 kW/m^2*.*

6.3.2 Diabatic friction factors for a pitch of 1.5

The results for the multi-tube setup, spaced horizontally at a pitch of 1.5 times the outer diameter, or 9 mm, heated uniformly at a heat flux of 3 kW/m^2, are shown in Figure 34.

6.3.2.1 Laminar diabatic friction factors for the pitch of 1.5

For the results between Reynolds numbers of 1 000 to 2 000, the left tube deviated from the single tube data by an average of -6.9%, with a maximum deviation of -8.7% occurring at a Reynolds number of 1 329. The centre tube had an average deviation of -1.2%, and a maximum deviation of -2.2%, which occurred at a Reynolds number of 1 782. The right tube correlated to within an average of -1.5% of the single tube results, with a maximum deviation of -2.8% occurring at a Reynolds number of 1 074.

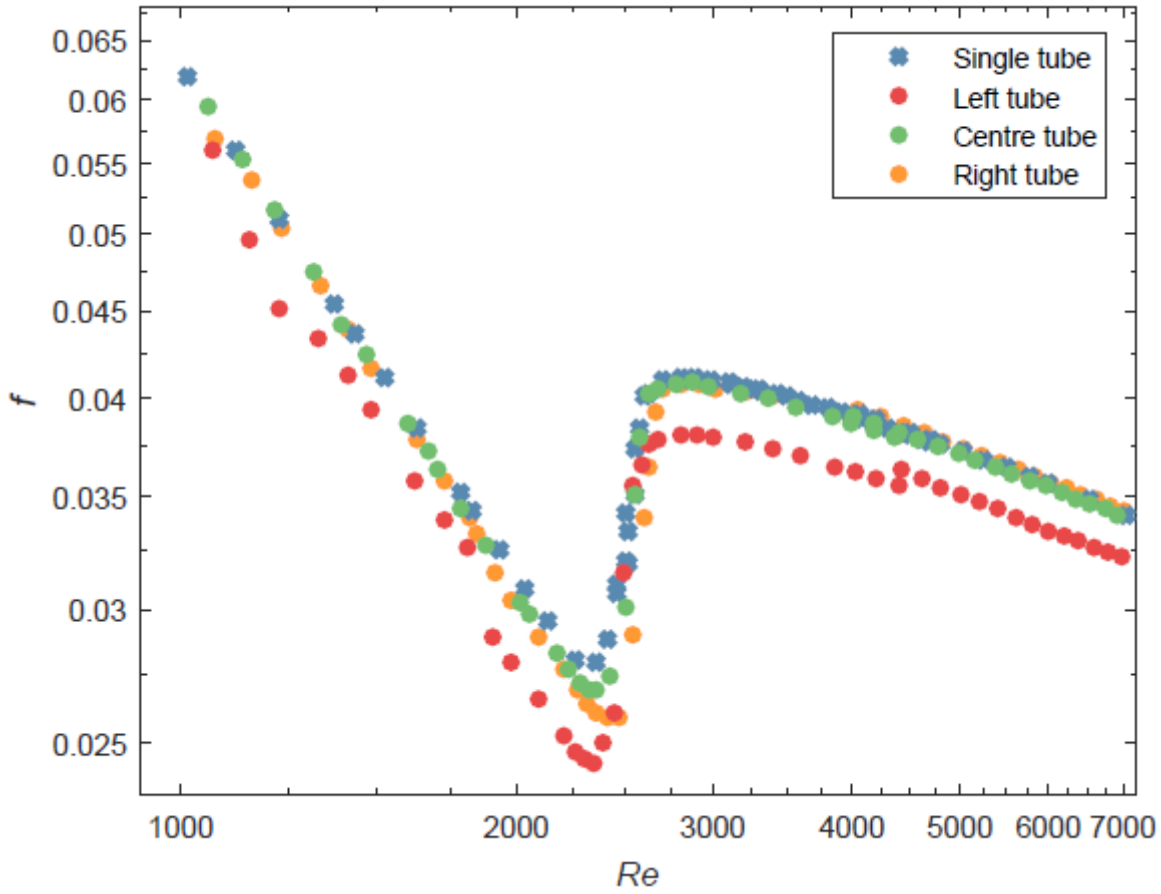

Figure 34: Multi-tube diabatic friction factors as a function of Reynolds number, for a horizontal pitch of 1.5 and a heat flux of 3 kW/m^2, *compared to the diabatic friction factor results for the single-tube test section heated at* 3 kW/m^2.

6.3.2.2 Turbulent diabatic friction factors for the pitch of 1.5

The left tube deviated from the single tube data by an average of -6.5%, with a maximum deviation of -7.9% occurring at a Reynolds number of 4 210. The data collected for right and centre tubes were very similar to that of single-tube setup, with the centre tube correlating to an average of -0.5%. A maximum deviation of -1.1% occurred at a Reynolds number of 3 836.

The right tube correlated to within an average of +0.4% of the single tube results, with a maximum deviation of +0.7% occurring at a Reynolds number of 4 639.

6.3.2.3 Transitional diabatic friction factors for the pitch of 1.5

The diabatic friction factors, for a heat flux of 3 kW/m^2 and a pitch of 1.5, that fall within the transitional flow regime, are plotted in Figure 35 for both the single-tube and multi-tube setup. The critical Reynolds numbers are indicated for comparative purposes. As previously mentioned, transition occurred at a Reynolds number of 2 353 for the single-tube test section heated uniformly with a heat flux of 3 kW/m^2.

The three tubes of the multi-tube setup started transition at Reynolds numbers close to that of the single tube, with transition occurring at Reynolds numbers of 2 362, 2 410, and 2 351 for the centre, right, and left tubes respectively. No clear delay in transition, like the one experienced by the 1.25 pitch setup, is evident for the pitch of 1.5 and a heat flux of 3 kW/m^2.

Transitional gradients, illustrated by the trend lines plotted through transitional friction factors, experienced by the multi-tube setup with a pitch of 1.5 are almost identical to that of the single tube, indicating that the pitch of 1.5 has far less of an influence than the pitch of 1.25, with respect to the sharpness of transition.

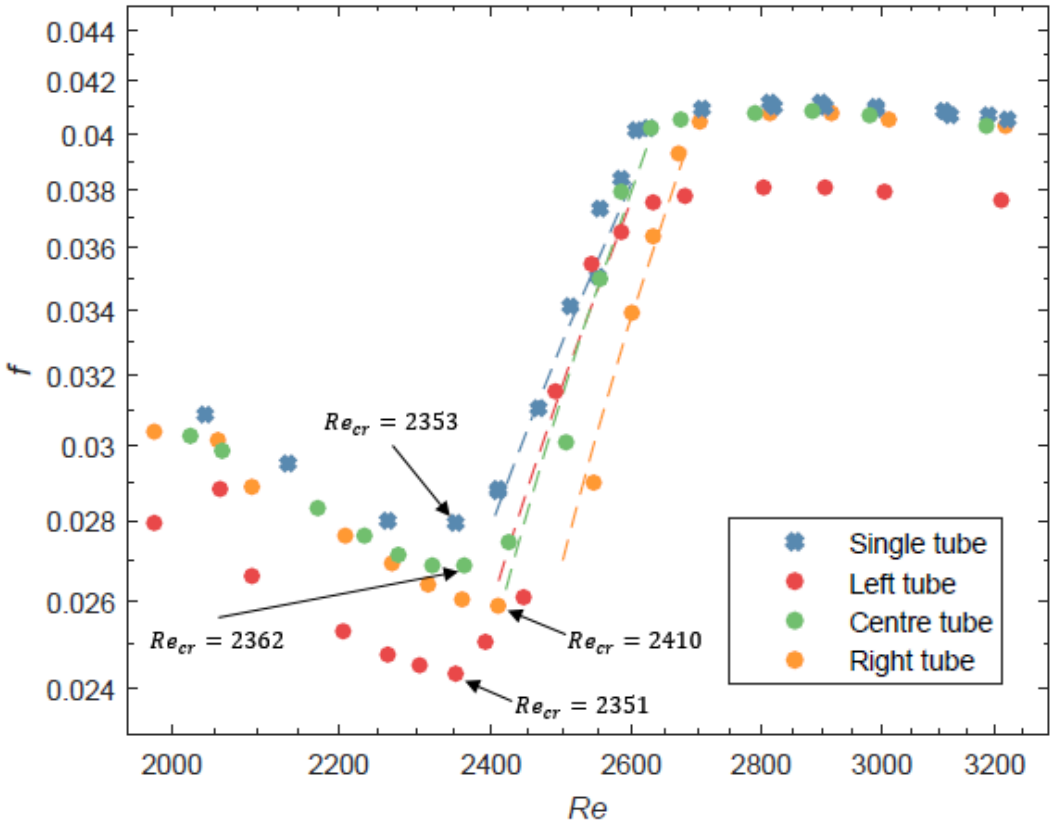

Figure 35: Multi-tube diabatic friction factors in the transitional flow regime, as a function of Reynolds number, for a horizontal pitch of 1.5 and a heat flux of 3 kW/m^2*, compared to the diabatic friction factor results for the single-tube test section heated at* 3 kW/m^2.

6.4 Diabatic friction factors for a uniform heat flux of 4 kW/m^2

The multi-tube diabatic friction factors for a constant heat flux of 4 kW/m^2 are presented per the convention established in Section 3.4. Included in the figures are results for the single-tube test section heated uniformly with the same heat flux of 4 kW/m^2.

6.4.1 Diabatic friction factors for a pitch of 1.25

The results for the multi-tube setup, spaced horizontally at a pitch of 1.25 times the outer diameter, or 7.5 mm, heated uniformly at a heat flux of 4 kW/m^2,are shown in Figure 36.

6.4.1.1 Laminar diabatic friction factors for the pitch of 1.25

The laminar data for the heat flux of 4 kW/m^2 and a pitch of 1.25 followed previous trends, with the left tube deviating significantly more than the right and centre tubes. The left tube deviated from the single tube data by an average of -5.4%, with a maximum deviation of -10% occurring at a Reynolds number of 1 233. The centre tube had an average deviation of only +0.7%, and a maximum deviation of +1.5%, which occurred at a Reynolds number of 1 302. The right tube correlated to within an average of +0.9% of the single tube results, with a maximum deviation of -1.7% occurring at a Reynolds number of 1 319.

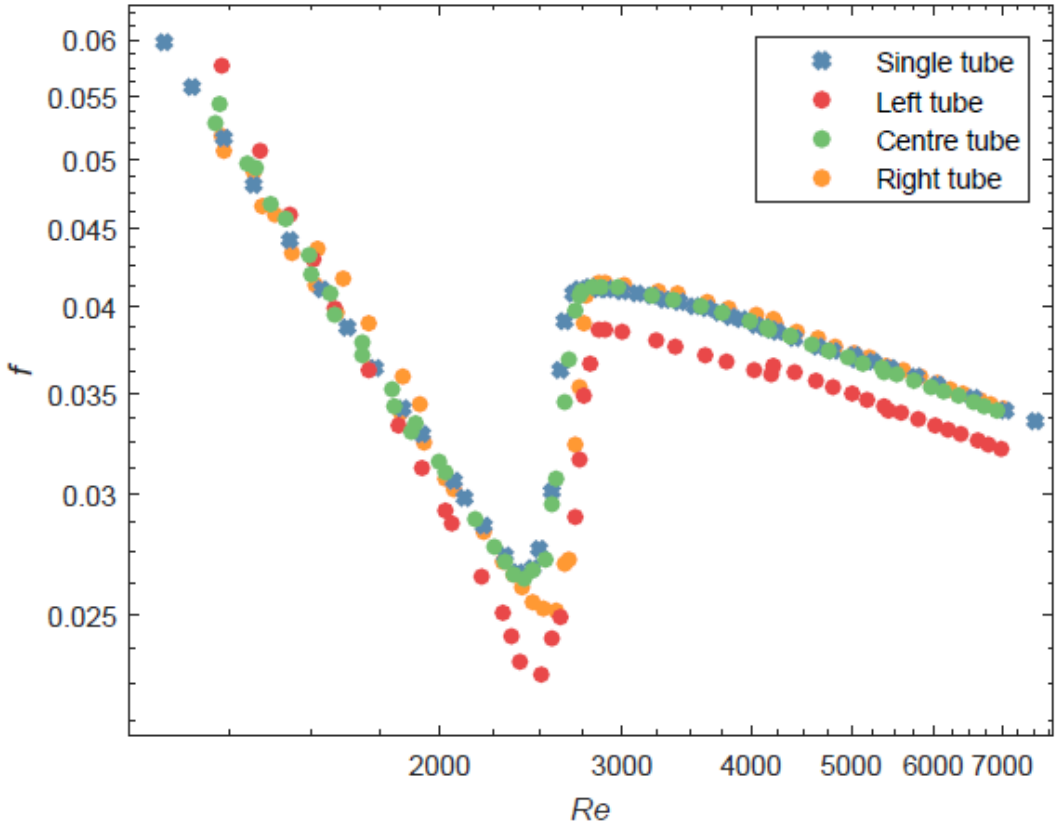

Figure 36: Multi-tube diabatic friction factors as a function of Reynolds number, for a horizontal pitch of 1.25 and a heat flux of 4 kW/m^2, *compared to the diabatic friction factor results for the single-tube test section heated at* 4 kW/m^2.

6.4.1.2 Turbulent diabatic friction factors for the pitch of 1.25

The left tube deviated from the single tube data by an average of -6.5%, with a maximum deviation of -7.2% occurring at a Reynolds number of 4 022. The centre tube had an average deviation of -0.4%, and a maximum deviation of -0.7%, which occurred at a Reynolds number of 6 335. The right tube correlated to within an average of +0.6% of the single tube results, with a maximum deviation of +1.6% occurring at a Reynolds number of 4 201.

6.4.1.3 Transitional diabatic friction factors for the pitch of 1.25

The diabatic friction factors, for a heat flux of 4 kW/m^2 and a pitch of 1.25, that fall within the transitional flow regime are plotted in Figure 37, for both the single-tube and multi-tube setup. Also shown in this figure, are the critical Reynolds numbers for the single- and multi-tube test sections.

Transition occurred at a Reynolds number of 2 459 for the single-tube test section heated at a uniform heat flux of 4 kW/m^2. The start of transition in the centre tube of the multi-tube test occurred at a Reynolds number of 2 455, which closely matched that of the single tube.

The two remaining tubes of the multi-tube setup experienced a slight delay in transition, when compared to the single tube, with transition occurring at Reynolds numbers of 2 594, and 2 502 for the right, and left tubes respectively. Transition gradients illustrated by the trend lines plotted through transitional friction factors, showed no clear difference between the single- and multi-tube test sections. The values of transitional gradients are summarized in Table 15.

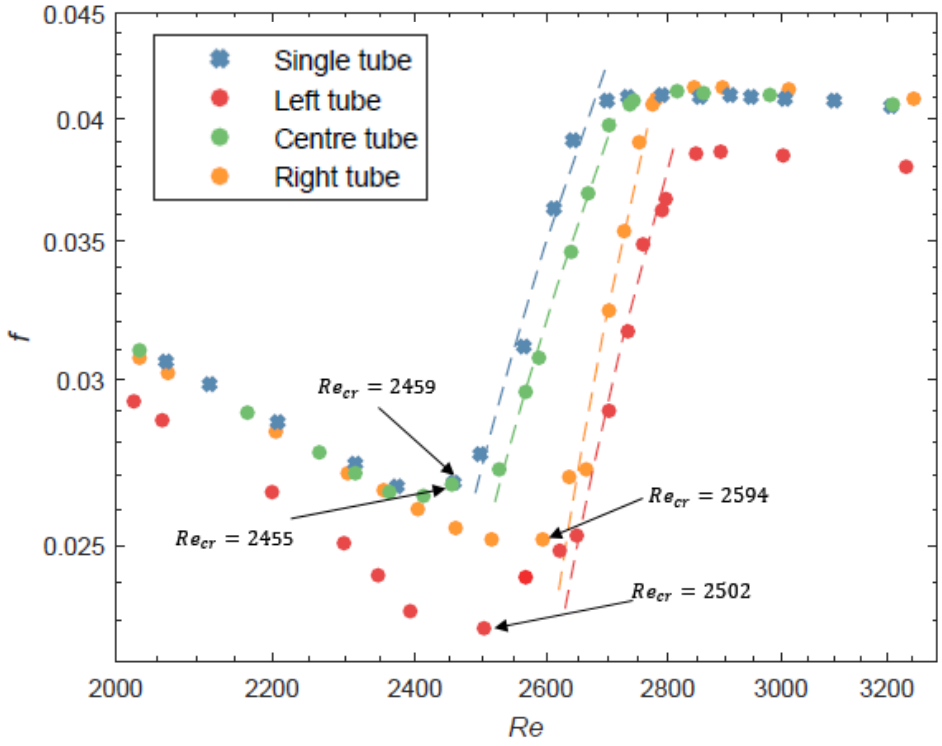

Figure 37: Multi-tube diabatic friction factors in the transitional flow regime, as a function of Reynolds number, for a horizontal pitch of 1.25 and a heat flux of 4 kW/m^2*, compared to the diabatic friction factor results for the single-tube test section heated at* 4 kW/m^2.

6.4.2 Diabatic friction factors for a pitch of 1.5

The results for the multi-tube setup, spaced horizontally at a pitch of 1.5 times the outer diameter, or 9mm, heated uniformly at a heat flux of 4 kW/m^2,are shown in Figure 38.

6.4.2.1 Laminar diabatic friction factors for the pitch of 1.5

For the results between Reynolds numbers of 1 000 to 2 000, the left tube deviated from the single tube data by an average of -9.5%, with a maximum deviation of -14.4% occurring at a Reynolds number of 1 128. The centre tube had an average deviation of -3.5%, and a maximum deviation of -4.0%, which occurred at a Reynolds number of 1 204. The right tube correlated to within an average of -3.4% of the single tube results, with a maximum deviation of -3.8% occurring at a Reynolds number of 1 134.

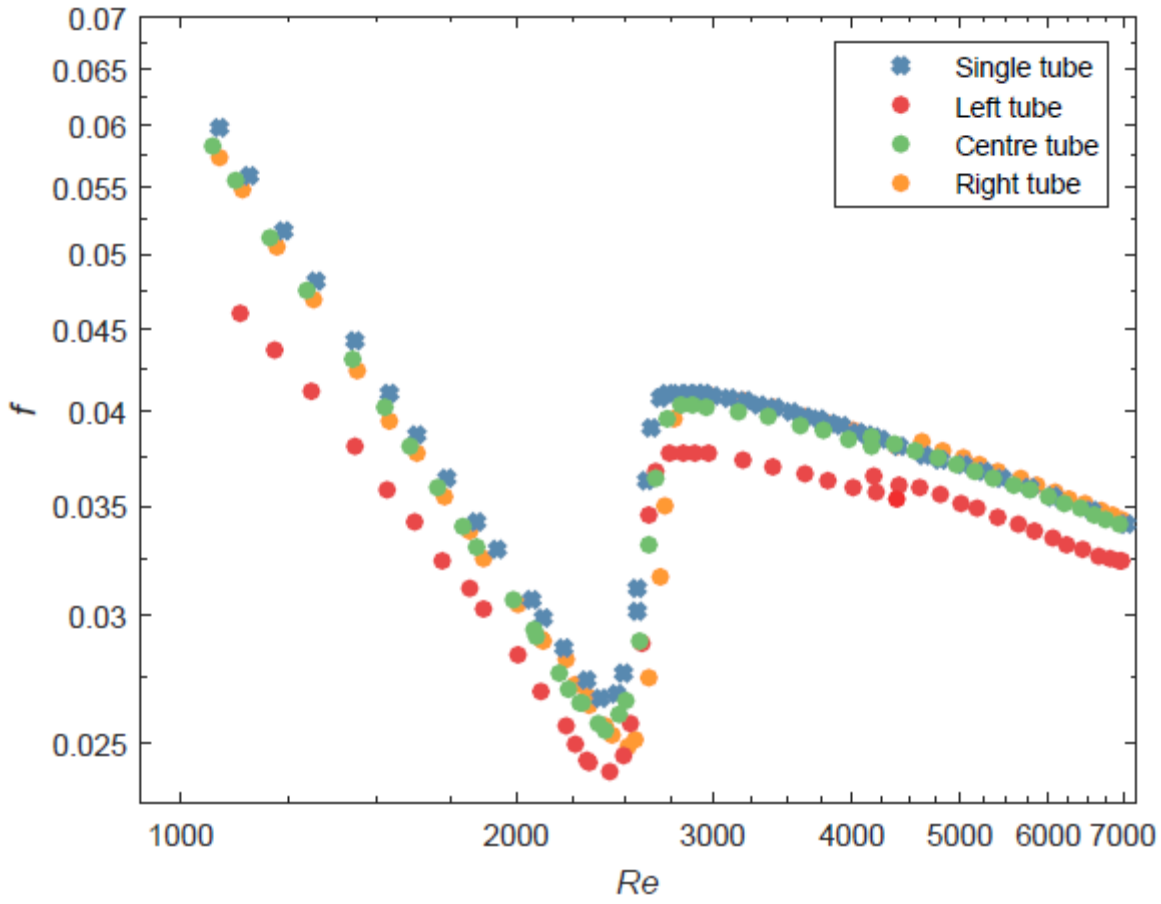

Figure 38: Multi-tube diabatic friction factors as a function of Reynolds number, for a horizontal pitch of 1.5 and a heat flux of 4 kW/m^2*, compared to the diabatic friction factor results for the single-tube test section heated at* 4 kW/m^2*.*

6.4.2.2 Turbulent diabatic friction factors for the pitch of 1.5

The left tube deviated from the single tube data by an average of -6.4%, with a maximum deviation of -8.7% occurring at a Reynolds number of 3 621. The centre tube had an average deviation of -0.6%, and a maximum deviation of -1.4%, which occurred at a Reynolds number of 3 768. The right tube correlated to within an average of +0.7% of the single tube results, with a maximum deviation of +1.6% occurring at a Reynolds number of 4 212.

6.4.2.3 Transitional diabatic friction factors for the pitch of 1.5

The diabatic friction factors, for a heat flux of 4 kW/m^2 and a pitch of 1.5, that fall within the transitional flow regime, are plotted in Figure 39 for both the single-tube and multi-tube setup. The critical Reynolds numbers are indicated for comparative purposes. As discussed in Section 6.4.1.3, transition occurred at a Reynolds number of 2 459 for the single-tube test section heated uniformly with a heat flux of 4 kW/m^2.

For the multi-tube setup, transition started within roughly 50 Reynolds number values of the critical Reynolds number for the single-tube test section, with critical Reynolds numbers of 2 405, 2 514, and 2 431 for the centre, right, and left tubes respectively. As with the pitch of

1.25 heated uniformly at 4 kW/m^2,there are no clear differences between transition gradients summarized in Table 15.

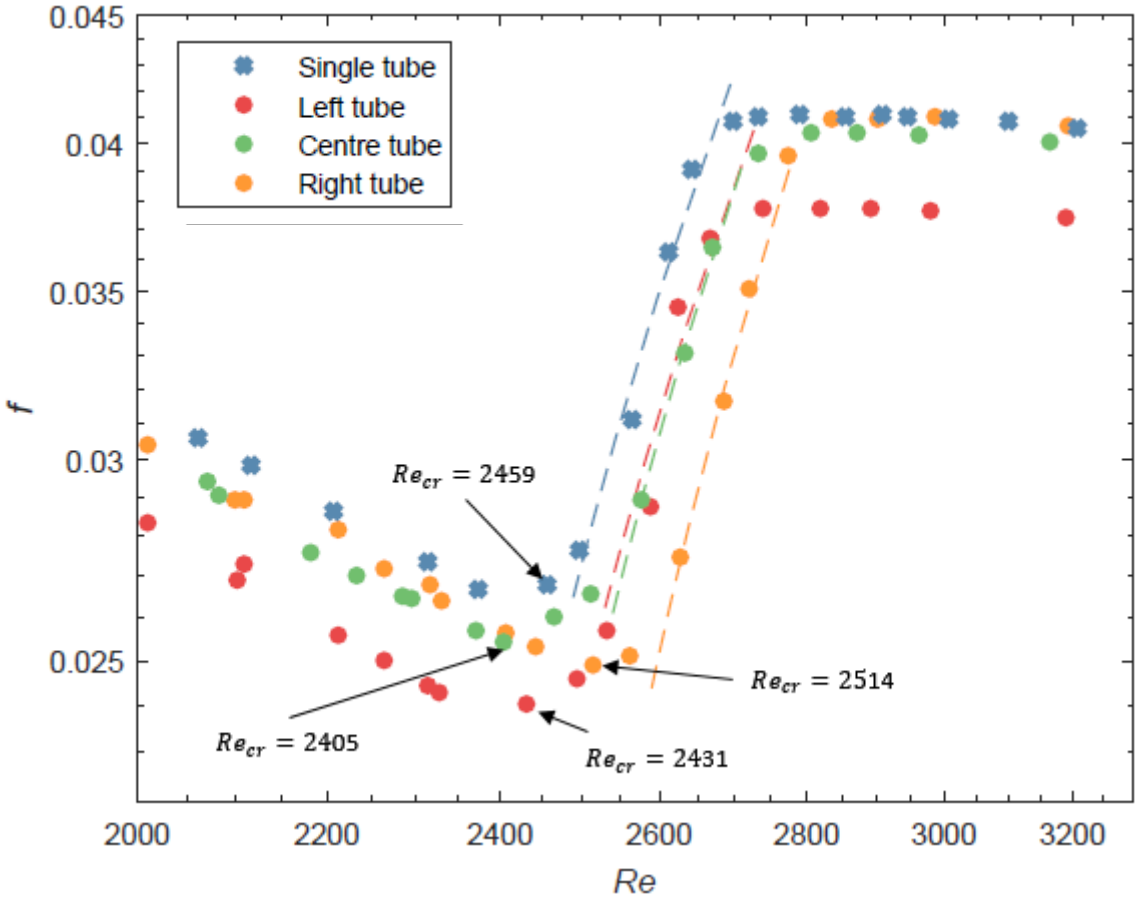

Figure 39: Multi-tube diabatic friction factors in the transitional flow regime, as a function of Reynolds number, for a horizontal pitch of 1.5 and a heat flux of 4 kW/m^2*, compared to the diabatic friction factor results for the single-tube test section heated at* 4 kW/m^2.

6.5 Summary

6.5.1 Laminar and turbulent results

The diabatic results that fall within the laminar, and turbulent flow regimes are summarized in Table 12. The laminar data produced for all three tubes of the multi-tube setup followed the same trend as the single tube results, for both the 1.25 and 1.5 pitch ratio, but did not correlate as well as the isothermal data. The left tube correlated consistently worse than the centre and right tubes, pointing to minor geometrical variations in this tube. However, all the laminar results were still within the uncertainties calculated in Section 3.10, suggesting that the slight difference in the inner diameter of the left tube was still within the tolerance guaranteed by the manufacturer.

The turbulent results for the two pitch ratios also showed similar trends, when compared to that of the single tube setup. As with the isothermal case, a sudden jump in friction factor can be observed in the data collected for each tube, at a Reynolds number of roughly 4000. This abrupt change can once again be attributed to the changing of diaphragms in the variable

reluctance pressure transducer. At this point, the low-pressure diaphragm is exchanged for a high-pressure diaphragm, resulting in reduced measurement accuracy, which is dependent on the full-scale pressure value of each diaphragm. The turbulent results, for all heat fluxes, fell within the calculated friction factor uncertainty of roughly 9.2%. From the summary presented in Table 12, it is evident that both the laminar and turbulent isothermal friction factors are hardly influenced by the different inlet pitch ratios, since the average deviation stays within the same order of magnitude. This coincides with the findings of Meyer and Olivier (2010), Ghajar and Tam (1994) and Tam and Ghajar (1997).

		Pitch 1.25			Pitch 1.5		
		Left tube	Centre tube	Right tube	Left tube	Centre tube	Right tube
2 kW/m²	Laminar	-8.4%	-1.6%	+2.6%	-7.9%	-2.1%	-1.7%
	Turbulent	-6.6%	-0.3%	+0.4%	-6.2%	-0.7%	+0.6%
3 kW/m²	Laminar	+3.5%	-1.7%	+0.8%	-6.9%	-1.2%	-1.5%
	Turbulent	-6.6%	-0.4%	+0.8%	-6.5%	-0.5%	+0.4%
4 kW/m²	Laminar	-5.4%	+0.7%	+0.9%	-9.5%	-3.5%	-3.4%
	Turbulent	-6.5%	-0.4%	+0.6%	-6.4%	-1.4%	+0.7%

Table 12: Comparison of the average deviation of laminar and turbulent diabatic friction factors for the multi-tube test setup, for pitch ratios of 1.25 and 1.5, compared to the single-tube setup.

6.5.2 Transitional results

The transitional diabatic friction factor results from the single- and multi-tube setups are summarised in Tables 13 – 15. By looking at the single-tube critical Reynolds numbers where uniform heat fluxes of 2 kW/m^2, 3 kW/m^2, and 4 kW/m^2 were applied, it is evident that transition was delayed for increasing heat fluxes. This coincides with the findings of Ghajar and Tam (1997), and Meyer and Olivier (2011). Furthermore, it can be concluded that the transition gradient increased for increasing heat fluxes, as was the case with the study performed by Everts (2014). These trends are also evident in the multi-tube data, with transition of each individual tube being delayed, and the transition gradients becoming steeper for increasing heat fluxes.

A delay in transition from laminar to turbulent flow is evident when comparing the multi-tube results to that of the single-tube setup, for the case where a uniform heat flux of 2 kW/m^2. This delay was more significant for the pitch of 1.25 than for the tube pitch of 1.5. The three tubes spaced at a pitch of 1.25, heated at a constant heat flux of 2 kW/m^2, underwent a more abrupt transition from laminar to turbulent flow, leading to sharper transition gradients. However, this was not the case for the pitch of 1.5, as the transitional gradients were close to that of single-tube setup.

The delay in transition became less significant with the addition of a 3 kW/m^2 heat flux, with the delay caused by the pitch of 1.25 being more notable than that of the 1.5 pitch. The multi-

tube setup with a pitch of 1.25 again experienced a sharper transition, evident from the transitional gradients.

The delay in transition of the multi-tube inlet condition became negligible for the 4 kW/m^2 case, for both pitch ratios. At this heat flux, transitional gradients were unaffected by the multi-tube inlet and were almost identical to that of the single tube data.

Any disturbance caused at the inlet due to the presence of adjacent tubes seems to be damped out by buoyancy induced secondary flow effects, resulting from the addition of heat. This dampening effect becomes more significant for increasing heat fluxes.

The end of transition appeared to remain largely unaffected for both tube pitch ratios, as transition ended in a relatively small band of Reynolds numbers, close to that of the single tube. The end of transition for each individual tube, was however, delayed for increasing heat fluxes.

Setup configuration		Start of transition	End of transition	Transition gradient
Single tube		Re = 2 235	Re = 3 033	4.7×10^{-5}
Pitch 1.25	Left tube	Re = 2 416	Re = 3 002	7.9×10^{-5}
	Centre tube	Re = 2 315	Re = 2 973	6.6×10^{-5}
	Right tube	Re = 2 330	Re = 3 014	9.1×10^{-5}
Pitch 1.5	Left tube	Re = 2 300	Re = 3 074	4.7×10^{-5}
	Centre tube	Re = 2 276	Re = 3 047	4.1×10^{-5}
	Right tube	Re = 2 326	Re = 3 080	5.3×10^{-5}

Table 13: Comparison of critical Reynolds numbers and transitional gradients for the single-tube setup and the multi-tube setup, heated uniformly at 2 kW/m^2.

Setup configuration		Start of transition	End of transition	Transition gradient
Single tube		Re = 2 353	Re = 3 120	5.2×10^{-5}
Pitch 1.25	Left tube	Re = 2 421	Re = 3 242	9.4×10^{-5}
	Centre tube	Re = 2 392	Re = 3 213	7.0×10^{-5}
	Right tube	Re = 2 444	Re = 3 255	1.4×10^{-4}
Pitch 1.5	Left tube	Re = 2 351	Re = 3 211	5.8×10^{-5}
	Centre tube	Re = 2 362	Re = 3 184	6.5×10^{-5}
	Right tube	Re = 2 410	Re = 3 218	6.8×10^{-5}

Table 14: Comparison of critical Reynolds numbers and transitional gradients for the single-tube setup and the multi-tube setup, heated uniformly at 3 kW/m^2.

		Start of transition	End of transition	Transition gradient
Single tube		Re = 2 459	Re = 3 209	7.7×10^{-5}
Pitch 1.25	left tube	Re = 2 502	Re = 3 239	8.6×10^{-5}
	centre tube	Re = 2 455	Re = 3 212	7.2×10^{-5}
	right tube	Re = 2 594	Re = 3 252	1.0×10^{-4}
Pitch 1.5	left tube	Re = 2 431	Re = 3 191	7.3×10^{-5}
	centre tube	Re = 2 405	Re = 3 165	7.6×10^{-5}
	right tube	Re = 2 514	Re = 3 193	7.9×10^{-5}

Table 15: Comparison of critical Reynolds numbers and transitional gradients for the single-tube setup and the multi-tube setup, heated uniformly at 4 kW/m^2.

A summary of all the transitional friction factors obtained for the centre tube is shown in Figure 40. The influence of adjacent tubes is evident in the delay in transition from laminar to turbulent flow, experienced by the centre tube in the multi-tube setup compared to that of the single tube configuration. Transition is delayed further as the tube pitch ratio is increased from 1.25 to 1.5.

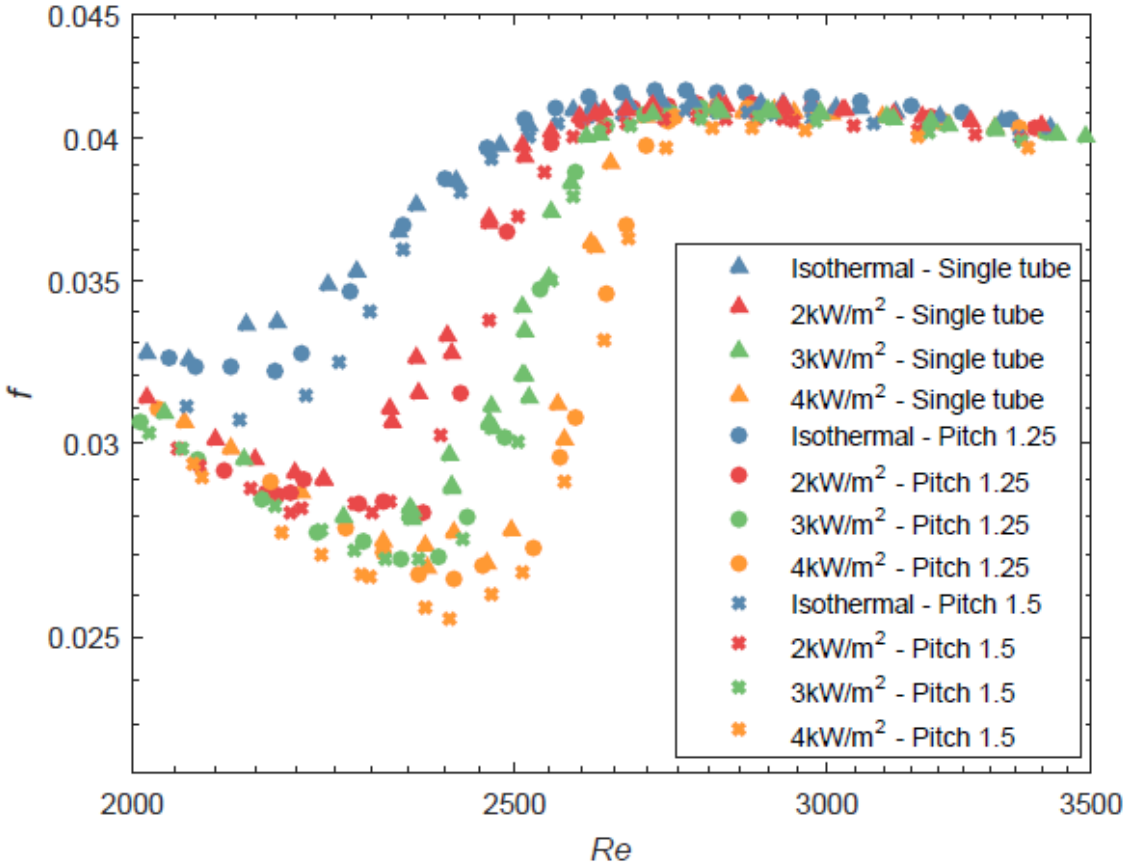

Figure 40: Comparison of isothermal and diabatic friction factors in the transitional flow regime, for the centre tube.

6.6 Conclusion

This chapter discussed the results from an investigation into the effect of the inlet tube pitch ratio on diabatic friction factors in the transitional flow regime. For this study, three identical stainless steel tubes with square-edged inlets, as presented in Chapter 3, were spaced horizontally at pitches of 1.25 and 1.5 times the outer diameter of the tubes. Diabatic friction factor data were produced from fully developed pressure drop measurements, taken for Reynolds numbers ranging from 1 000 to 7 000, and heat fluxes of 2 kW/m^2, 3 kW/m^2, and 4 kW/m^2. The results for the two different pitch ratios were plotted against Reynolds numbers, and compared against diabatic friction factor data for the single-tube setup.

It was concluded that both the laminar and turbulent diabatic friction factors were not influenced by the different inlet pitch ratios. A delay in transition from laminar to turbulent flow was evident, when comparing the multi-tube results to that of the single-tube setup, for the heat flux of 2 kW/m^2. This delay was more significant for the pitch of 1.25 than for the tube pitch of 1.5.

The delay in transition became less significant for the 3 kW/m^2 heat flux and almost negligible for the 4 kW/m^2 heat flux, for both the 1.25 and 1.5 pitch ratio. It was concluded that any disturbance caused at the inlet due to the presence of adjacent tubes seems to be damped out by buoyancy induced secondary flow effects, resulting from the addition of heat. This dampening effect becomes more significant for increasing heat fluxes.

Chapter 7:
Summaries, conclusions and recommendations

7.1 Summary

Intensive research has been conducted in order to investigate characteristics of convective heat transfer in the transitional region. These studies include the effect of different types of inlet geometries, different heating methods, as well as surface roughness. However, all these studies were limited to single-tube heat exchangers. It was evident that this gap in literature had to be addressed, and a study focussing on multiple tubes spaced at different pitch ratios was required in order to gain further understanding of the transitional flow regime, which would ultimately lead to more efficient shell-and-tube heat exchangers.

The experimental setup was developed and validated by comparing the measured single-tube data to theoretical predictions and results obtained from previous investigations. The multi-tube test section consisted of three smooth stainless steel circular tubes, with an inner diameter and length of 4 mm and 6 m, respectively. The effects of the two pitch ratios, equal to 1.25 and 1.5 times the tube outer diameter, were investigated whilst being heated at constant heat fluxes of 2 kW/m^2, 3 kW/m^2, and 4 kW/m^2. Water, with relatively low Prandtl numbers ranging from approximately 3 to 7, was used as the test fluid.

A calming section was built to dampen out any pulsations created by the pump and to ensure a uniform velocity profile is achieved at the square-edged inlet of each tube. A mixer and mass flow meter was placed downstream of each tube to accurately measure bulk fluid temperature and flow rate.

An uncertainty analysis was performed in order to quantify the accuracies of the instruments used in the study, and ultimately determine the uncertainties associated with the calculated results. The Reynolds number uncertainties were found to be independent of temperature, and remained below 1.4% for all heat fluxes and pitch ratios. However, the friction factor uncertainties were found to increase significantly, for increasing heat fluxes, with uncertainties peaking close to 14% at the lowest Reynolds number and a heat flux of 4 kW/m^2.

7.2 Conclusion

For the isothermal study, three identical stainless steel tubes with square-edged inlets, were spaced horizontally at pitches of 1.25 and 1.5 times the outer diameter of the tubes. Isothermal friction factor data were produced from fully developed pressure drop measurements, taken for Reynolds numbers ranging from 1 000 to 7 000. From the results, it is evident that both the laminar and turbulent isothermal friction factors are hardly influenced by the different inlet pitch ratios, since the results are nearly identical to that of the single tube.

The isothermal friction factor results for the three tubes of the multi-tube setup exhibits a significant delay in transition, compared to the singe-tube setup. The delay in transition from laminar to turbulent flow experienced by the multi-tube setup, was more significant for the pitch of 1.25, where the tubes are spaced closer together, than for the pitch of 1.5.

The three tubes of the multi-tube setup also underwent a more abrupt transition from laminar to turbulent flow, leading to sharper transition gradients. The test section with a pitch of 1.25 experienced a sharper transition than the setup where the tubes were spaced further apart, at a pitch of 1.5. The end of transition appeared to remain largely unaffected for both tube inlet pitch ratios, as transition ended in a relatively small band of Reynolds numbers, close to that of the single tube.

The diabatic laminar data produced for all three tubes of the multi-tube setup followed the same trend as the single tube results, for both the 1.25 and 1.5 pitch ratio. However, the left tube correlated consistently worse than the centre and right tubes, pointing to minor geometrical variations in this tube. The turbulent results for the two pitch ratios also showed similar trends, when compared to that of the single tube setup. The laminar and turbulent results, for all heat fluxes, fell within the calculated friction factor uncertainty. It was concluded that both the laminar and turbulent diabatic friction factors are not influenced by the different inlet pitch ratios, since the average deviation stays within the same order of magnitude. A jump in friction factor can be observed at a Reynolds number of roughly 4000. This abrupt change can be attributed to the changing of diaphragms in the variable reluctance pressure transducer. At this point, the low-pressure diaphragm is exchanged for a high-pressure diaphragm, resulting in reduced measurement accuracy, which is dependent on the full-scale pressure value of each diaphragm.

Single tube results from the diabatic study showed that transition was delayed for increasing heat fluxes. Furthermore, it was concluded that the transition gradient increased for increasing heat fluxes. These trends were also evident in the multi-tube data, with transition of each individual tube being delayed, and the transition gradients becoming steeper for increasing heat fluxes.

The three tubes spaced at a pitch of 1.25, heated at a constant heat flux of 2 kW/m^2, underwent a more abrupt transition from laminar to turbulent flow, leading to sharper transition gradients. However, this was not the case for the pitch of 1.5, as the transitional gradients were close to that of single-tube setup. The delay in transition became less significant with the addition of a 3 kW/m^2 heat flux, with the delay caused by the pitch of 1.25 being more notable than that of the 1.5 pitch. The multi-tube setup with a pitch of 1.25 again experienced a sharper transition. The delay in transition of the multi-tube inlet condition became negligible for the 4 kW/m^2 case, for both pitch ratios. At this heat flux, transitional gradients were unaffected by the multi-tube inlet and were almost identical to that of the single tube data.

The end of transition appeared to remain largely unaffected for both tube pitch ratios, as transition ended in a relatively small band of Reynolds numbers, close to that of the single tube. The end of transition for each individual tube, was however, delayed for increasing heat fluxes.

It can be concluded that the presence of adjacent tubes had a significant effect under isothermal conditions, causing delayed and more abrupt transition from laminar to turbulent flow. This effect was more significant for the pitch spacing of 1.25 than for the pitch of 1.5. However, the disturbance caused at the inlet due to the presence of adjacent tubes seems to be damped out by buoyancy induced secondary flow effects with the addition of heat. This dampening effect becomes for significant for increasing heat fluxes.

7.3 Recommendations

- Larger diameter tubes will result in a better ratio of inner diameter and tube tolerance, which will reduce friction factor uncertainties. However, this will increase the length required to achieve fully-developed flow. The trade-off in these quantities should be carefully considered in any follow-up projects. The most common tube sizes used in shell-and-tube heat exchangers are 15.88, 19.05, and 25.40 mm, based on tube outside diameters.
- Most of the inlet disturbance caused by the adjacent tubes could be damped out before flow becomes fully developed. It would be beneficial to investigate the effect of adjacent tubes and different tube pitch ratios on friction factor characteristics in the developing portion of flow.
- The rolling of the tubes during the manufacturing of shell-and-tube heat exchangers result in small indentations at the inlet, shown in Figure 8. These imperfections could be replicated and investigated experimentally.
- Testing with different working fluids will lead to better understanding of transitional behaviour.

References

Allen, R.W. and Eckert, E.R.G., 1964. Friction and heat transfer measurements to turbulent pipe flow of water (Pr = 7 and 8) at uniform wall heat flux.. *J. Heat transfer 86,* pp. 301-310.

ASHRAE, 2009. *ASHRAE handbook - Fundamentals.* Atlanta: American Society of Heating, Refrigerating and Air-Conditioning Engineers, Inc.

Bakker, A., LaRouche, R.D. and Marshall, E.M., n.d. *Laminar flow in static mixers with helical elements.* [Online]
Available at: www.bakker.org/cfmbook/lamstat.pdf
[Accessed 21 October 2016].

Cengel and Ghajar, 2011. *Heat and Mass Transfer: Fundamentals and Applications.* 4th ed. Singapore: McGraw-Hill.

Chang, 2014. Experimental and numerical study of heat transfer characteristics in solar thermal absorber tubes with circumferentially non-uniform heat flux. *Energy Procedia 49, pp. 305-313.*

Dunn, P., 2010. *Measurement and data analysis for Engineering and science.* 2nd ed. Boca Raton: CRC Press.

Everts, M., 2014. *Heat transfer and pressure drop of developing flow in smooth tubes in the transitional flow regime.* University of Pretoria.

George, W.K., Beuther, P.D. and Shabbir, A., 1989. Polynomial Calibrations for Hot Wires in Thermally Varying Flows.. *Experimental Thermal and Fluid Science,* pp. 230-235.

Ghajar, A.J. and Madon, A.J., 1992. Pressure drop measurements in the transition region for a circular tube with three different inlet configurations. *Experimental Thermal and Fluid Science 5(1),* pp. 129-135.

Ghajar, A.J. and Tam, L.M., 1994. Heat transfer measurements and correlations in the transition region for a circular tube with three different inlet configurations. *Experimental Thermal and Fluid Science 8(1),* pp. 79-90.

Ghajar, A.J., Tang, C.C. and Cook, W.L., 2010. Experimental investigation of friction factor in the transition region for water flow in minitubes and microtubes. *Heat Transfer Engineering 31(8),* pp. 646-657.

Meyer and Olivier, 2014. Heat Transfer in the Transitional Flow Regime. *Evaporation, Condensation and Heat Transfer 35(14-15),* pp. 245-260.

Meyer, J.P. and Olivier, J.A., 2011. Transitional flow inside enhanced tubes for fully developed and developing flow with different types of inlet disturbances: Part 1- Adiabatic pressure drops. *International Journal of Heat and Mass Transfer 54(7-8),* pp. 1587-1597.

Meyer, J.P. and Olivier, J.A., 2011. Transitional flow inside enhanced tubes for fully developed and developing flow with different types of inlet disturbances: Part 2 - Heat transfer. *Internatio[redacted]8),* pp. 1598-1607.

Meyer, J.P., McKrell, T.J. and Grote, K., 2013. The influence of multi-walled carbon nanotubes on single-[redacted] flow regime of smooth tubes. *International Journal of Heat and Mass Transfer 58(1-2).*

Mulock-Houwer, F., 2015. *The Effect of Adjacent tubes on the diabatic friction factors in the transitional flow regime.* University of Pretoria.

Nellis, G. and Sanford, K., 2009. *Heat Transfer.* 1st ed. New York: Cambridge University [redacted]

[redacted]

Jersey: John Wiley & Sons, Inc..

Sengers, J.V. and Watson, J.T.R., 1986. Improved international formulations for the viscosity and thermal conductivity of water substance. *Journal of Physical and Chemical Reference Data 23,* pp. 1291-1312.

Shokouhmand, H. and Salimpour, M.R., 2007. Optimal Reynolds number of Laminar Forced Convection in a Helical Tube Subject to Uniform Wall Temperature. [redacted]

[redacted]

Tam, H.K., Tam, L.M., Ghajar, A.J., Tam, S.C. and Zhang, T., 2012. Experimental investigation of heat transfer, friction factor, and optimal fin geometries for the internally microfin tubes in the transition and turbulent regions. *Journal of Enhanced Heat Transfer 19(5),* pp. 457-576.

Tam, L.M. and Ghajar, A.J, 1997. Effect of inlet geometry and heating on the fully developed friction factor in the transition region of a horizontal tube. *Experimental Thermal and Fluid Science 15(1)*[redacted]pp. 52-64.

TEMA, 1999. *Standards of the Tubular Exchanger Manufacturers Association.* New York: s.n.

[redacted]

International Journal of Heat and Mass Transfer 8[redacted]pp. 1229-1242.

White, F., 2011. *Fluid Mechanics.* 6th ed. Singapore: McGraw-Hill.

[redacted]

Appendix A: Calibration

A.1 Introduction

Instrument calibration is an essential step in most experimental work. This appendix covers the calibration process for the various sensors used in this experimental study. Firstly, the procedure used for the calibration of all sensors is discussed, followed by a summary of the results obtained from this calibration process for each sensor.

A.2 Calibration procedure

Ideally the calibration range should be chosen so that the majority of the expected test samples fall towards the centre of the range, as this is the area of the calibration range where the uncertainty associated with the predicted response is at a minimum. Most calibration guides and standards recommend that a duplicate run be performed in order to evaluate the precision of the calibration process and confirm repeatability.

Since the response of the PT100 probes, thermocouples, and pressure transducers are all linear, a linear regression analysis can be performed to determine a calibration equation. This process involves plotting the sensor response (y-axis) against a reference measurement(x-axis), and then determining the gradient and intercept of the line of best fit through data points:

The gradient of the least squares line, m is given by

$$m = \frac{\sum_{i=1}^{n}\{(x_i - \bar{x})(y_i - \bar{y})\}}{\sum_{i=1}^{n}(x_i - \bar{x})^2} \tag{A.1}$$

whilst the intercept of the least squares line, c is given by

$$c = \bar{y} - m\bar{x} \tag{A.2}$$

A.3 PT100 calibration

The four PT100 probes used in the study were calibrated in a LAUDA PROLINE AP1940 thermal bath, that can maintain a set temperature to within 0.03°C. The temperature measured by a LAUDA DIGICAL DCS 2 temperature probe, factory calibrated to an accuracy of 0.05°C, was used as the reference to which the response of the PT100 probes were calibrated.

The PT100 probes, connected to a data acquisition system, were calibrated between 15°C and 67.5°C in +2.5°C intervals, as most of the experimental results were estimated to fall in the middle of this chosen range. Once the thermal bath reached a set temperature and all four the PT100 probes, together with the reference probe, measured roughly the same temperature, a measurement consisting of 100 samples was taken. This process was repeated for decreasing intervals of −2.5°C, from 67.5°C down to 15°C. A duplicate calibration run was then performed, resulting in two independent up- and down-calibration experiments, to investigate repeatability.

The 100 samples taken at each measurement point were then averaged for each PT100 probe and plotted against the reference DigiCal probe temperature, shown in Figure A1 for the inlet PT100. Using the least squares method, a regression analysis is then performed to obtain a calibration curve for each individual PT100 probe. The calibrated residuals are then compared to the uncalibrated residuals, as shown in Figure A1(c), as a measure of the accuracy of the calibration process. The calibration constants obtained from the regression analysis are summarized in Table A1.

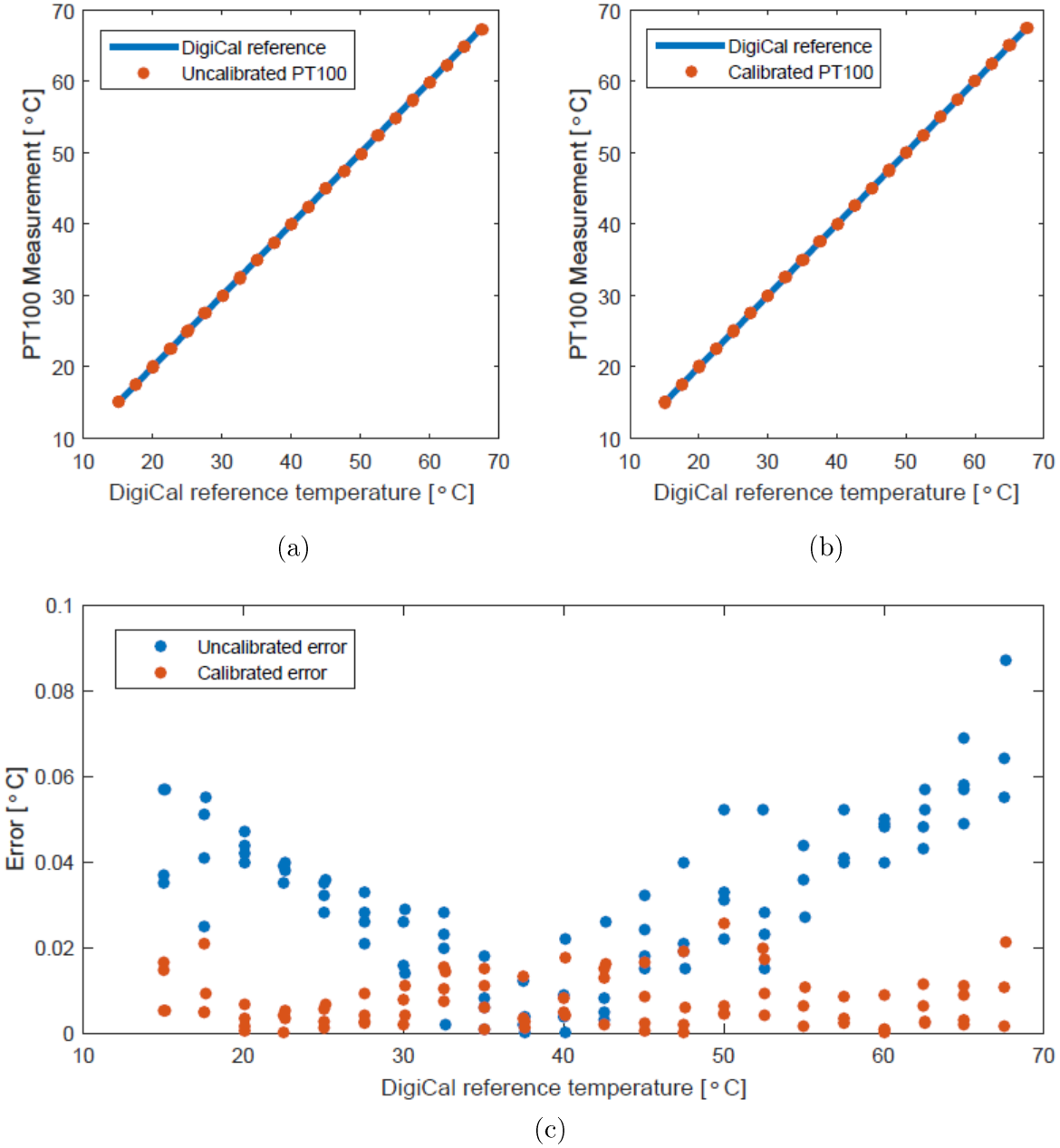

Figure A1: Measured response of the inlet PT100 plotted against the reference DigiCal temperature. (a) before calibration and (b) after calibration (c) residuals compared before and after calibration.

PT100	m	c
Inlet	0.9996	+0.0126
Left tube outlet	1.0022	-0.0861
Middle tube outlet	1.0014	-0.0337
Right tube outlet	1.0042	-0.0673

Table A1: Calibration constants for PT100 sensors.

A.4 Thermocouple calibration

Thermocouples are simple, inexpensive temperature sensors that are reasonably linear in behaviour. These sensors consist of two electrical conductors, made from dissimilar metals, that output a small electromotive force, either a voltage or electromagnetic field, proportional to the temperature difference across a junction (Figiola and Beasly, 2011).

The T-type thermocouple junctions used in this study were made by soldering a copper and a constantan conductor together, to ensure good electrical contact between the two wires. The thermocouples were connected to the stainless steel tubes by using a thermally conductive epoxy, as explained in Chapter 3. A total of 117 thermocouples were attached to the three tubes. Each of the three tubes of the multi-tube test section had 13 thermocouple stations, numbered A to M, consisting of 3 thermocouples each.

The supply and return lines of the completed test section were connected directly to the LAUDA ECO RE1225 thermal bath. The four calibrated PT100 sensors were placed in the calming section and at the outlet of each tube. The thermocouples, connected to a data acquisition system, were calibrated between $15°C$ and $65°C$ in $+2.5°C$ intervals, as most of the experimental results were estimated to fall in the middle of this chosen range. Once the thermal bath reached a set temperature and all four the PT100 probes, measured roughly the same temperature, a measurement consisting of 100 samples was taken.

This process was repeated for decreasing intervals of $-2.5°C$, from $65°C$ down to $15°C$. A duplicate calibration run was then performed, resulting in two independent up- and down-calibration experiments, to investigate repeatability. The 100 samples taken at each measurement point were then averaged for each thermocouple and plotted against the average of the inlet and outlet PT100 temperature, shown in Figure A2 for a single thermocouple attached to the middle tube.

Using the least squares method, a regression analysis is then performed to obtain a calibration curve for each individual thermocouple. The calibrated residuals are then compared to the uncalibrated residuals, as shown in Figure A2(c), as a measure of the accuracy of the calibration process. The calibration constants obtained from the regression analysis are summarized in Table A2.

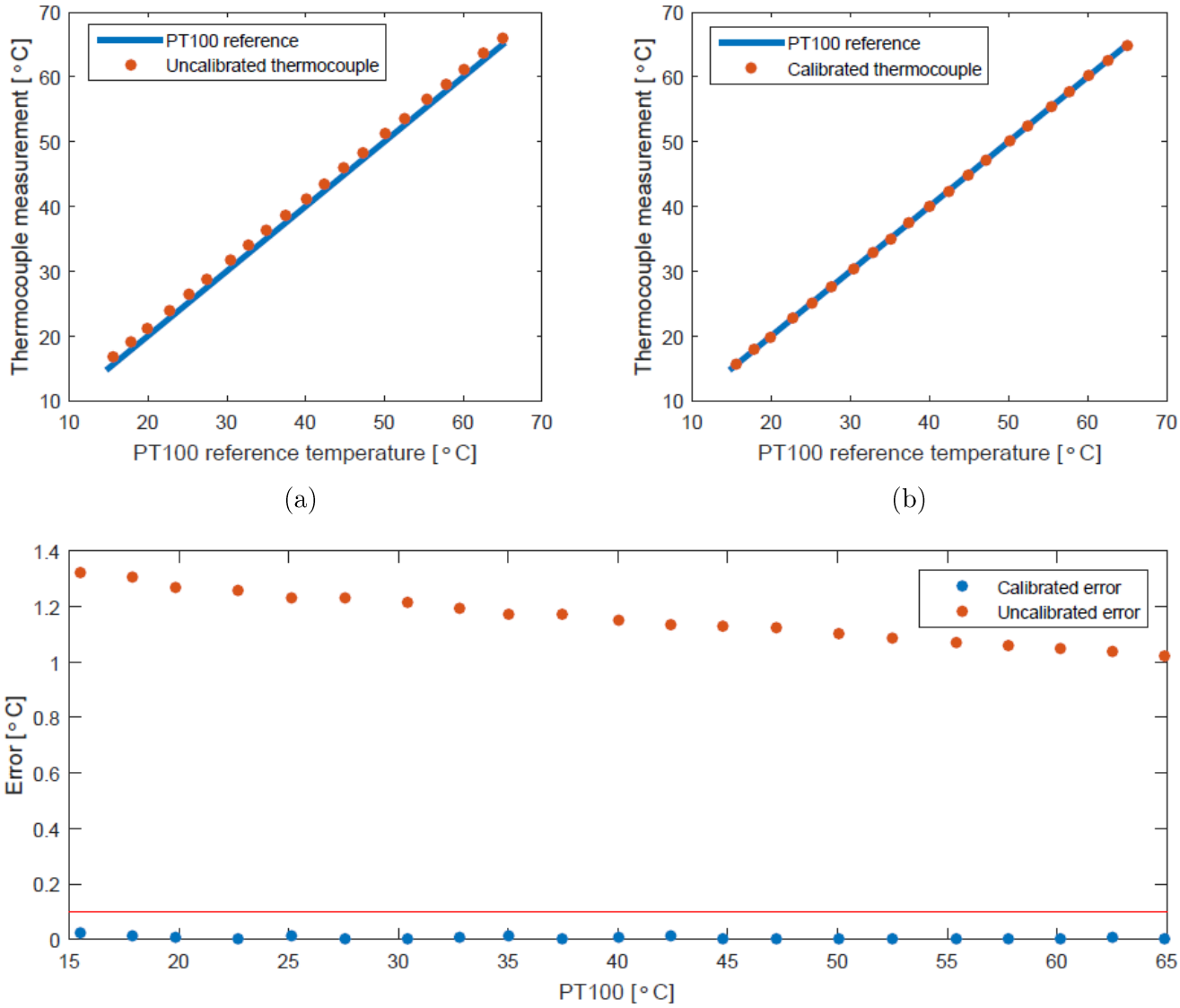

Figure A2: Measured response of a thermocouple plotted against the reference PT100 temperature. (a) before calibration and (b) after calibration (c) residuals compared before and after calibration.

Station name	Left tube		Centre tube		Right tube	
	m	c	m	c	m	c
T1	1.0082	-0.91635	1.0075	-1.2079	1.0093	-1.3122
	1.0071	-1.1743	1.0064	-1.4608	1.0102	-1.364
	1.0084	-1.6181	1.0041	-1.1869	1.0045	-1.2509
T2	1.0098	-1.0448	1.0095	-1.3846	1.011	-1.2609
	1.0051	-0.80314	1.006	-1.4263	1.0105	-1.5336
	1.01	-1.0477	1.0093	-1.6885	1.0155	-2.0683
T3	1.0094	-1.1484	1.0071	-1.5136	1.0077	-1.2627
	1.0088	-0.93349	1.0077	-1.4698	1.012	-1.9454
	1.0105	-1.4208	1.0031	-1.4016	1.005	-1.4756
T4	1.0104	-1.437	1.0001	-0.99537	1.0089	-1.2644
	1.0044	-1.6974	1.0027	-1.1602	1.0137	-1.1121
	1.0126	-1.5281	1.0089	-1.8232	1.008	-0.68683
T5	1.0096	-1.0782	1.0058	-1.4665	1.0098	-0.68197
	1.0118	-1.615	1.0104	-1.6122	1.0091	-0.76474
	1.0067	-1.1062	1.0038	-1.7542	1.0069	-0.75868
T6	1.0129	-1.6727	1.0124	-1.6121	1.0144	-1.1315
	1.0078	-1.1878	1.0052	-0.97934	1.0143	-1.4001
	1.0139	-1.7093	1.0062	-0.69602	1.016	-1.0882
T7	1.0144	-1.6304	1.0067	-0.67965	1.011	-1.407
	1.0145	-1.7079	1.0073	-0.83949	1.0122	-1.4267
	1.0126	-1.3092	1.0036	-0.70482	1.0079	-1.2782
T8	1.0097	-1.6685	1.0055	-1.245	1.0121	-1.0367
	1.0053	-0.64251	1.0061	-0.94331	1.0161	-1.5048
	1.0093	-1.2796	1.0085	-1.3187	1.0168	-1.8402
T9	1.0105	-0.85141	1.0074	-0.67123	1.0103	-1.0651
	1.0105	-0.61257	1.0093	-1.2094	1.0147	-1.5347
	1.0125	-1.0709	1.0055	-0.67578	1.0082	-1.4857
T11	1.0098	-0.71691	1.008	-1.0124	1.0147	-1.976
	1.0086	-0.72826	1.0036	-0.4405	1.0125	-1.3991
	1.0155	-1.2589	1.0078	-0.84311	1.017	-1.72
T12	1.0114	-1.0921	1.0075	-0.9201	1.0115	-1.5936
	1.0154	-1.2406	1.0075	-1.1442	1.013	-1.5913
	1.0107	-1.0963	1.0034	-0.65788	1.0081	-1.1333
T13	1.0103	-1.1114	1.0137	-1.433	1.0149	-1.8217
	1.0061	-0.77263	1.0052	-0.95173	1.0171	-1.7253
	1.0139	-1.1939	1.008	-0.81997	1.0152	-1.4776
T14	1.0073	-0.82641	1.0065	-1.3327	1.0137	-1.6574
	1.012	-0.89859	1.0091	-1.0748	1.0141	-1.5753
	1.0131	-0.93471	1.0052	-0.96696	1.0086	-1.2156

Table A2: Calibration constants for all thermocouples.

A.5 Pressure transducer calibration

Friction factor results were obtained by taking differential pressure measurements over 1.5 m in the fully developed portion of each test section, by using Validyne DP15 variable reluctance pressure transducers with interchangeable diaphragms.

The small diaphragm, with a full-scale value of 8.6 kPa, was used for Reynolds numbers ranging from 1 000 to 4 400, while the large diaphragm, with a full-scale value of 22 kPa, was used for all Reynolds numbers larger than 4 400. The accuracy of the diaphragms is 0.25% of the full-scale value, which translates to 21.5 Pa and 55 Pa respectively.

The diaphragms were calibrated with a water column, by connecting a Beta T-140 manometer in parallel with the DP15 sensor. The manometer had a full-scale value of 50 kPa and an accuracy of 50 Pa.

A system zero value was obtained by connecting the two tubes of the water column, using copper pipe. Water flowed through the connecting tube until the level in both columns equalized. The pressure readings on the manometer was zeroed, and the pressure transducer gain was adjusted to 4 mA. The span of the pressure transducer was set equal to 20 mA, for the corresponding full-scale pressure value of the diaphragm.

The output signal, logged by the data acquisition system, could then converted to a pressure value via linear interpolation. The water column was then used to compare the output of each sensor to the reading on the manometer, at intervals of 1 kPa, to ensure successful calibration, as shown in Figure A3. Air was bled out of the system and a new zero-pressure measurement was taken at the start of each day, and used as an offset in the calculations.

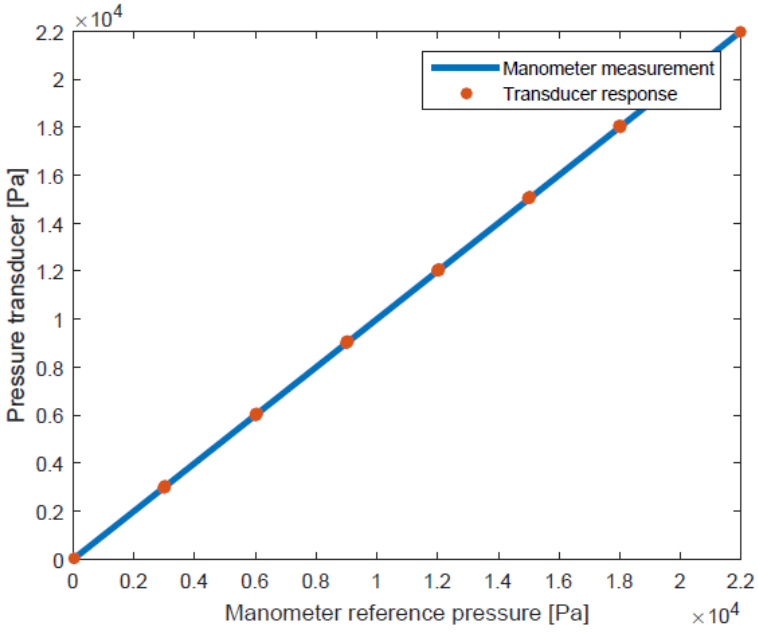

Figure A3: Calibration curve produced for the 22 kPa pressure diaphragm.

A.6 Conclusion

This appendix covered the calibration process for the various sensors used in this experimental study. Firstly, the procedure used for the calibration of all sensors is discussed, followed by a summary of the PT100 and thermocouple calibration process. Lastly, the process with which the pressure sensors were calibrated and checked were briefly covered. Data collected from this study can be corrected using the appropriate calibration factors, summarised in this appendix.

A7. Nomenclature

Parameter	Nomenclature
Value on the *x*-axis	x_i
Observed value on the *y*-axis	y_i
Mean of x_i values	$\bar{x}$
Mean of y_i values	$\bar{y}$
Number of calibration points	n
Gradient of least squares line	m
Intercept of least squares line	c

A.8 References

Figiola, R.R and Beasly, D.E. (2011). *Mechanical measurements.* Hoboken: John Wiley & Sons, Inc.